NASA CONTRACTOR REPORT
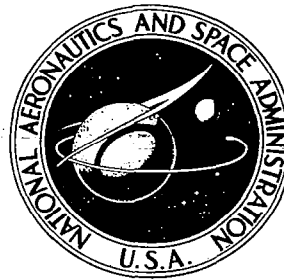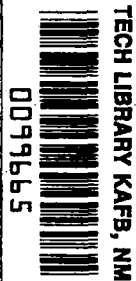
NASA CR-325

HEAT TRANSFER TO A GAS CONTAINING A CLOUD OF PARTICLES

by J. Andrew McAlister, Edward Y. H. Keng,
and Clyde Orr, Jr.

NATIONAL AERONAUTICS AND SPACE ADMINISTRATION • WASHINGTON, D. C. • NOVEMBER 1965

HEAT TRANSFER TO A GAS CONTAINING A CLOUD OF PARTICLES

By J. Andrew McAlister, Edward Y. H. Keng, and Clyde Orr, Jr.

TABLE OF CONTENTS

Page

NOMENCLATURE

Symbol	Description	Units
A	cross sectional area of aerosol conduit	ft^2
A_c	total cross sectional area of particles representing a size distribution	ft^2
$(A_c)_{nd}$	cross sectional area of n particles with diameter d	ft^2
A_s	total surface area of particles representing a size distribution	ft^2
A_w	wall area of aerosol conduit	ft^2
a	subscript meaning air	-
a	particle radius	μ
a	constant for X	-
atm	atmosphere	-
b	constant for X	-
c	constant for X	-
C	particle concentration by volume, (ft^3 solids/ ft^3) of aerosol	dimensionless
C_n	particle number concentration	ft^{-3}
$\overline{C}$	average air heat capacity	Btu/lb $^{\circ}F$
CFM	cubic feet per minute	-
C_p	particle heat capacity	Btu/lb $^{\circ}F$
$\overline{C}_p$	average particle heat capacity	Btu/lb $^{\circ}F$
dA_w	differential area of conduit wall positioned with respect to dV	ft

d_p	particle diameter	ft
dV	differential volume of aerosol arbitrarily positioned and receiving radiation from dA_w	ft^3
E_b	ordinate for figures 32 through 37; heat absorbed per unit wall radiation intensity per unit cross sectional area of enclosure	dimensionless
H	enthalpy per unit time	Btu/min
h_a	convection heat transfer coefficient for air, and from a particle to its surroundings	Btu/hr ft^2 ^oF
h_p	convection heat transfer coefficient for a particle suspension	Btu/hr ft^2 ^oF
I	denotes integral of equation (2.19)	dimensionless
I_α	alpha series of I	dimensionless
$I_{\alpha 1}$	first term of alpha series	dimensionless
$I_{\alpha 2}$	second term of alpha series	dimensionless
$I_{\alpha 3}$	all odd terms of alpha series for n > 1	dimensionless
$I_{\alpha 4}$	all even terms of alpha series for n > 2	dimensionless
I_β	beta series of I	dimensionless
$I_{\beta 1}$	first term of beta series	dimensionless
$I_{\beta 2}$	second term of beta series	dimensionless
$I_{\beta, n > 2}$	all terms of beta series for n > 2	dimensionless
i	summation index	-
i_{bn}	black body radiation intensity normal to an emitting surface	Btu/hr ft^2 ω
i_{bn1}	black body radiation intensity normal to surface 1	Btu/hr ft^2 ω
i_{bn2}	black body radiation intensity normal to surface 2	Btu/hr ft^2 ω
i_{bnw}	black body radiation intensity emitted radially inward from a cylindrical wall	Btu/hr ft^2 ω

$i_{b\beta w}$	black body radiation emitted from a cylinder wall at an angle with the radial direction at the point of emission	Btu/hr ft^2 ω
i_o	directional radiation intensity at reference point	Btu/hr ft^2 ω
i_x	radiation intensity at point x in the x direction	Btu/hr ft^2 ω
J	integral term defined by equation (2.43)	dimensionless
J_1	J-terms not having a k coefficient; equation (2.43).	dimensionless
J_Σ	sum of J-terms having a k coefficient; equation (2.43)	dimensionless
j	summation index	
k	constant for the relation $k/\lambda^{1.39}$	-
k	attenuation coefficient	ft^{-1}
k_g	attenuation coefficient for gases, negative number	ft^{-1}
k_p	thermal conductivity of particle	Btu/hr ft ^oF
k_t	thermal conductivity of air	Btu/hr ft ^oF
L	heated length of radiating aerosol conduit, and mean beam length in equation (1.3)	ft.
m	geometric variable defined by equation (2.10) and described in Figure 6.	ft.
n	general term number of series expansion, number of particles having same diameter, and number of moles of air in aerosol conduit	-
P	exponent	-
q	isotropic radiation flux	Btu/hr ft^2
p	subscript indicating particle	-
Q_b'	black body radiant heat transfer between two surfaces without an intervening absorbing medium	Btu/min

Q'_{b12}	black body radiation emitted from surface 1 and absorbed by surface 2 with no intervening absorbing medium	Btu/min
Q'_{b21}	black body radiation emitted from surface 2 and absorbed by surface 1 with no intervening absorbing medium	Btu/min
Q_b	black body energy absorbed per unit time accounting for attenuation	Btu/min
Q_{b1}	black body energy absorbed per unit time with attenuation not considered	Btu/min
$Q_{b\Sigma}$	black body radiation attenuated from Q_{b1}	Btu/min
$(Q_c)_a$	heat transferred by convection to particle free air	Btu/min
$(Q_c)_p$	heat transferred by convection to particle suspension	Btu/min
R	radius of cylinder and sphere and 1/2 distance between parallel plates	ft
r	variable radius	ft
S	distance between an elemental area emitting to a differential volume of aerosol	ft
S_v	ratio of total cross sectional area of particles to the total volume of particles composing a complete distribution	ft^{-1}
T	temperature	^oR
t_a	temperature of air	^oF
t_p	temperature of particle suspension	^oF
t_θ	temperature at time θ	^oF
t_o	temperature at time $\theta = 0$	^oF
U	overall heat transfer coefficient	Btu/hr ft^2 ^oF
u	substitution variable of integration	-
V	total volume of particles composing a distribution, and volume of heated aerosol conduit	ft^3

$(V)_{nd}$	volume of n particles of diameter d	ft^3
v	substitution variable of integration	-
W	mass flow rate	lbs/min
W_g	mass flow rate of air	lbs/min
W_p	mass flow rate of particles	lbs/min
X	General quadratic function: $X = cx^2 + bx + a$	-
x	length of radiating enclosure or length equal to it; also length-to-radius ratio for these to quantities	dimensionless
x_g	geometric mean diameter	μ
y	axial distance separating differential aerosol volume, dV, receiving radiation from emitting wall element, dAw. See Figure 6	ft
y	functional notation in Newton-Cotes formulae	-
y_n	ordinates employed in Newton-Cotes formulae	-
Z	dummy variable of integration, equation (1.4)	-
z	axial distance between differential aerosol volume and beginning of radiating aerosol conduit	ft

GREEK LETTERS

α	particle absorptivity	
β_s	angle between direction of a radiant beam and the normal direction to the surface s	radians
β_w	angle between direction of a radiant beam and the normal direction to dAw	radians
γ	adsorption efficiency, heat absorbed divided by total heat emitted	dimensionless
Δ	difference operator	-
ΔE_x^{nx}	change in E_b when a length nx emits to an adjacent length x. ΔE_{nx}^{x} is the converse for the emitting and receiving length.	dimensionless

ϵ	particle emissivity	dimensionless
ϵ_λ	spectral particle emissivity	dimensionless
θ	time	sec
λ	radiation wave length	micron
μ	unit of length	micron
ρ	density of air	lb/ft^3
ρ_p	particle density	lb/ft^3
σ_g	standard geometric deviation	dimensionless
Φ	$\rho_p C_p / \rho_c$	dimensionless
Ψ	plane angle between plane containing dV and conduit axis and the plane containing dAw and conduit axis	radians
Ψ_m	value of Ψ giving minimum attenuation	radians
Ψ'_m	value of Ψ as determined only by Lambert's cosine law	radians
ω	solid angle	steradian

Special notations for energy balance calculations:

Superscripts	description
0	no particle flow
1	particle flow

Subscripts

0	property evaluated at furnace inlet
1	property evaluated at heat exchanger inlet
3	property evaluated at heat exchanger exit
A	air
c	heat exchanger coolant
p	particles

LIST OF TABLES

LIST OF FIGURES

SUMMARY

The principles describing the transfer of heat by radiation were formulated in the latter part of the previous century and their application to practical problems has been the subject of much study since that time. The resulting analyses are mostly of limited applicability, however, because of the lengthy calculations involved and the numerous empirical assumptions required to obtain them. Now space exploration, nuclear technology, and plasma research, to name a few, require more nearly exact solutions, since the temperatures encountered in these fields may be much above those in conventional equipment and radiation is likely the dominant mode of heat transfer. Fortunately, solutions are attainable now that high-speed electronic computers can be employed to solve problems that before were hopelessly involved.

A specific problem of timely concern is the absorption of radiant energy by particles suspended in weakly absorbing or transparent gases. This investigation undertook to examine both theoretically and experimentally the transference of energy by radiation from a cylindrical enclosure to a particle cloud contained within. Specifically, the study employed a non-reflective wall radiating to essentially non-reflective particles. The result was not intended to be inclusive; rather it was to be a new approach using modern computational methods, which could be modified to describe successively more complex processes and still be reliably related to basic radiation principles.

The net black body radiant interchange between two surfaces may be described by

$$Q_b' = \int_{A_2} \int_{A_1} (i_{bn2} - i_{bn1}) \left(\frac{\cos \beta_1 \cos \beta_2}{S^2} \right) dA_1 dA_2$$

where i_{bn1} and i_{bn2} are the black body radiation intensities normal to the differential area dA_1 and dA_2, β_1 and β_2 are the angles between the normal direction to the surfaces and the line segment S connecting them. For the particular problem investigated here, this expression becomes

$$Q_b = k \int_0^{2\pi} \int_0^{2\pi} \int_0^R \int_0^L \int_{-z}^{L-z} (i_{bnw}) \left(\frac{e^{-kS}}{S^2} \right) \left(\frac{S^2 + R^2 - r^2 - y^2}{2RS} \right) r \, dy \, dz \, dr \, d\Psi \, d\theta$$

where the radiation intensity is attenuated exponentially with distance (e^{-kS}) and the particles were sufficiently low in temperature not to back radiate significantly to the wall, i.e., $i_{bnp} = 0$. The other terms are: i_{bnw}, the normal wall intensity; L, the cylinder length; R, its radius; y and z (distance); and Ψ and θ (angles) describing the geometric location of a differential wall element dA_w that radiates to a differential amount of aerosol surface dA_p. The integral heat transfer equation was rewritten as

$$Q_b = (2\pi R)(i_{bnw})(k) \int_0^R \int_0^{2\pi} Ir \, d\Psi \, dr$$

where

$$I = \int_0^L \int_{-z}^{L-z} \left(\frac{e^{-kS}}{S^2} \right) \left(\frac{S^2 + R^2 - r^2 - y^2}{2RS} \right) dy \, dz$$

and the θ integration was performed to give the coefficient 2π. The integral I was evaluated analytically by means of a series expansion of e^{-ks}. The subsequent integrations for Ψ and r were performed numerically by use of closed form Newton-Cotes quadrature formulae. The integral equation was solved first for a particular set of conditions applying to a concurrent experimental investigation; calculations were made later to apply to other systems.

A generalized correlation was produced for radiation systems of specific interest to this investigation that related the rate of heat absorption, radiation intensity, cylinder length and radius, and particle cloud attenuation constants. The results are presented graphically, and an interpolation procedure is described to obtain very nearly exact data points not specifically represented. Finally, equations were derived for evaluating the radiant heating a particle cloud experiences while in unheated entrance and exhaust sections adjacent to a heated length.

While the theoretical analysis for thermal radiation processes was treated, the results apply equally as well to other types of radiation such as X-rays. For example, the dose rate for aerosols in a cylindrical enclosure might be calculated.

The experimental investigation sought to measure the absorption of radiation by low temperature aerosol systems, absorption data for aerosols under these conditions not being available. An experimental method was developed so that a particle cloud could be exposed to a radiant field in which conductive and convective heat transfer were reduced to a minimum and the energy could be absorbed by the cloud in

such a way that its magnitude might be determined by enthalpy balances before and after exposure. The system exposed a particle cloud to a radiant heat flux by passing it through a quartz tube which transmitted to its interior a large portion of the radiation falling on it externally. The quartz was protected from extraneous heat effects other than radiation by enclosing it in an evacuated air space the outer surface of which was air cooled. The surrounding protective tube was also quartz. The particle cloud was generated at a constant rate and preconditioned to a constant, fixed temperature. Then after passing through the radiation field, the cloud was cooled calorimetrically to determine the heat absorbed. The apparatus was designed for continuous operation and a filter mechanism was developed to capture the aerosol particles and return them to the generator.

Experimental data were collected for aerosols of ferrous sulfide, cupric oxide, and zinc. Particle sizes were chiefly between 20 to 30, 30 to 44, 44 to 53, 53 to 88 microns for the ferrous sulfide and cupric oxide powders and 1 to 10 microns for the zinc. Particle clouds of these materials, when exposed to a radiant heat flux of 17,600 Btu/hr ft^2 in a 0.0526 foot diameter quartz conduit 1.014 feet long, absorbed up to fifteen per cent of the radiation transmitted through the enclosure wall.

The experimental data were employed in testing the theoretical calculations. Calculations of the type employed had been proposed in previous investigations and had been applied in certain experimental studies requiring their use. A direct test of their validity, however, had never before really been performed. The experimental results

confirmed the theoretical calculations and showed that accurate evalua-
tion of the absorption of radiant energy by particles suspended within
a cylindrical enclosure might be assessed if precise measurements of
the dispersion concentration and particle size and size distribution
data are available.

It is recommended that subsequent studies be conducted to extend
the theoretical development to include back-radiation and radiation
scattering from the particles, to investigate the effects of non-black
enclosure surfaces, and to consider aerosol temperature profiles.
Further experimental work is recommended with systems having other
length-to-radius ratios to test more completely the theoretical
development.

CHAPTER I

INTRODUCTION

Definition of the Problem

The principles describing the transfer of heat by radiation were formulated in the latter part of the previous century and their application to practical problems has been the subject of many investigations since that time. The majority of these, however, have related to furnace technology because here sufficiently high temperatures were first attained for thermal radiation processes to have commercial significance and to merit the scrutiny of engineers. The problems were primarily associated with the transfer of radiation between solid surfaces or between solid surfaces and absorbing gases such as carbon dioxide and water vapor. The resulting analyses were of limited applicability because of the numerous empirical assumptions about combustion rates, furnace shapes, fuel characteristics, stoichiometric relationships, etc., that were required. They were, nevertheless, valuable in the design of furnaces and aided immensely in evaluating furnace performance.

Radiation heat transfer is currently undergoing a renewal of interest, the advent of plasma generators, re-entry missiles, and novel concepts in nuclear technology having brought to the fore new and more challenging radiation problems. Solutions are needed to basic as well as practical problems in these new areas where temperatures are much above those in conventional equipment and where radiation is the

dominant mode of heat transfer.

A specific problem of timely concern is the absorption of radiant energy by particles suspended in weakly absorbing or transparent gases. In particular, one version of a nuclear rocket, as presently envisioned, requires the transfer of heat at an extremely high rate to the propellant, which for best performance should be hydrogen gas. Since the temperature of the source must be exceedingly high for reasons of efficiency, the transfer will be primarily by radiation. Many gases, including hydrogen below about $10,000^{\circ}$ F, are essentially transparent however. It has been proposed, therefore, that the gas be made absorptive below this temperature by the addition of small particles. This is the immediate problem that suggested this investigation.

Detailed information on the absorption of radiation by aerosols -- the technical name applied to a system consisting of a gas with particles dispersed therein -- has applications in other areas also. X-ray and nuclear radiations, for instance, are known to produce chemical reactions in dispersed systems; just how is of much interest to the process industries, for example. Particles can be subjected to thermal energy in plasma generating devices to produce spherical particles, crystal transformations, and size reductions. For protection in a time of national emergency, aerosols might be produced to absorb radiation, both nuclear and thermal, that could otherwise prove lethal.

Since high-speed electronic computers can be employed to solve problems that before were hopelessly without solution, this investigation undertook to examine both theoretically and experimentally the specific radiation process in which energy is transferred from a cylindrical

2

enclosure to a particle cloud within. The theoretical portion sought complementary analytical solutions which were sufficiently general to be employed in predicting the behavior of systems considerably different from the experimental one. The experimental study was made to produce direct basic, data about the process, unaffected as nearly as possible, by other heat transfer phenomena. Specifically, this study employed a non-reflective wall radiating to essentially non-reflective particles. The result was not expected to be inclusive; rather, it was to make use of a new approach, using modern computational methods, which could be modified to describe successively more complex processes and still be reliably related to basic radiation principles.

Background

Radiant heat transfer from a solid surface to a cloud of particles is similar to the problem of radiation to an absorbing gas. Since the amount of energy absorbed by a gaseous medium is a function of the distance traversed by a radiant beam, the problems here are the description of attenuation processes in such media and the derivation of equations from which to calculate the radiation properties of an absorbing or emitting gas as a function of its temperature, pressure, composition, and shape. The relationship

$$i_x = i_o \, e^{-kx} \tag{1.1}$$

describes the process mathematically in most cases, or at least can be modified to apply to them. i_o and i_x are the intensities at the surface and at a distance x from the surface. The exponential factor, k, is

the absorption coefficient which for gases is determined by the composition, temperature, and pressure of the medium, and the wave length of the radiation.

The use of the exponential attenuation function generally requires the solution of very complicated integral relationships to obtain the radiative properties of a given medium. A volume of gas participating in a radiant interchange emits from its surrounding envelope or absorbs within itself an amount of energy equal to the sum of the contributions from each differential volume element. Functions describing the location of differential elements within an absorbing region are generally complex and, when incorporated in radiation equations, are not readily integrated. One simple case, however, is that of a small surface at the center of the base of a gaseous hemisphere. The exchange of radiation between the surrounding gas and the surface element is readily calculated, since the distance to the hemispherical surface is constant and is independent of direction.

Hottel and co-workers[1,2,3] noted that a given system had an "equivalent" dimension (or mean beam length) such that a hemisphere of gas having this "equivalent" dimension for its diameter would radiate to a differential area at the center of its base at a rate equal to that of a small area on the surrounding surface of the real gas shape. Then, if the "equivalent" dimensions were known, practical problems involving the characteristics of the radiation could be calculated from the simplified case. Hottel selected the most frequently occurring furnace shapes and calculated the "equivalent" dimensions. The calculations, unfortunately, had to be further restricted to arbitrarily selected dimensions because

the results were dependent on the radiation attenuation coefficients of the absorbing medium. Results were obtained for certain cases where the coefficient could be approximated as being zero and for other instances where finite coefficients are frequently encountered in practice; other values not specifically evaluated were recommended as being around 85 per cent of the result for the zero coefficient. Although limited, these calculations sufficed until recently for the majority of the radiation calculations involving absorbing gases.

The next step was to extend the method to apply to particle clouds. Wollenberg and Morrow[4] and Haslam and Hottel[5] considered the case where energy was removed from a radiant beam by the screening effect of randomly oriented particles. Based on probability considerations, the relationship

$$i_x = i_o \, e^{-(S_v C) x} \qquad (1.2)$$

was derived which, except for the absorption coefficient k, was identical to the Beer's law function for gases. The constant for the modified equation was the sum of the particle cross-sectional areas divided by the sum of the particle volumes times the particle volume concentration; for monodispersed systems and for dispersions considered to be represented by an average particle size, the constant reduces to the average particle cross-section times the particle number concentration. This exponential relationship was applied in calculating the emissivity or absorptivity of a pulverized coal flame after assumptions were made about the particle size distribution and the rate of combustion of the individual particles. It was noted, however, that the

results were almost inevitably lower than measured flame emissivities. The discrepancy was attributed to the contribution of cracked hydrocarbons producing luminous as well as residual ash particles not considered in the theoretical derivation. The problem was not pursued further because most pulverized coal installations involved such large flames that the emissivities did not differ greatly from unity.[6]

Other calculation methods were devised by Johnstone, Pigford, and Chapin.[7] These dealt with the heat transfer to a cloud of particles falling through a heated pipe. The objective was to provide information for use in the "flash" heating of finely divided particles by passing them through a section of pipe at temperatures as high as 1050° F. The carbonization of pulverized coal, the briquetting of blast furnace dusts, and the production of soluble phosphates afforded practical applications for the results. Convection was the dominant mode of heat transfer. For wall temperatures near 1000° F, however, the particle clouds gained up to approximately 20 per cent of their energy by radiation. The small absorption of radiation was due to the large size of the particles employed, which were sand grains on the order of 500 to 1000 microns in diameter. To calculate the radiant heat transfer, the investigators took advantage of Hottel's basic attenuation relationship but used developments by Nusselt and Jakob to evaluate particle cloud emissivities.[8] Combined analytical and graphical procedures were employed to integrate modified relationships and to obtain results for a sphere, an infinite cylinder, and an infinite parallel plate. Generalized curves were then constructed as shown in Figure 1, and approximate radiation properties for particle
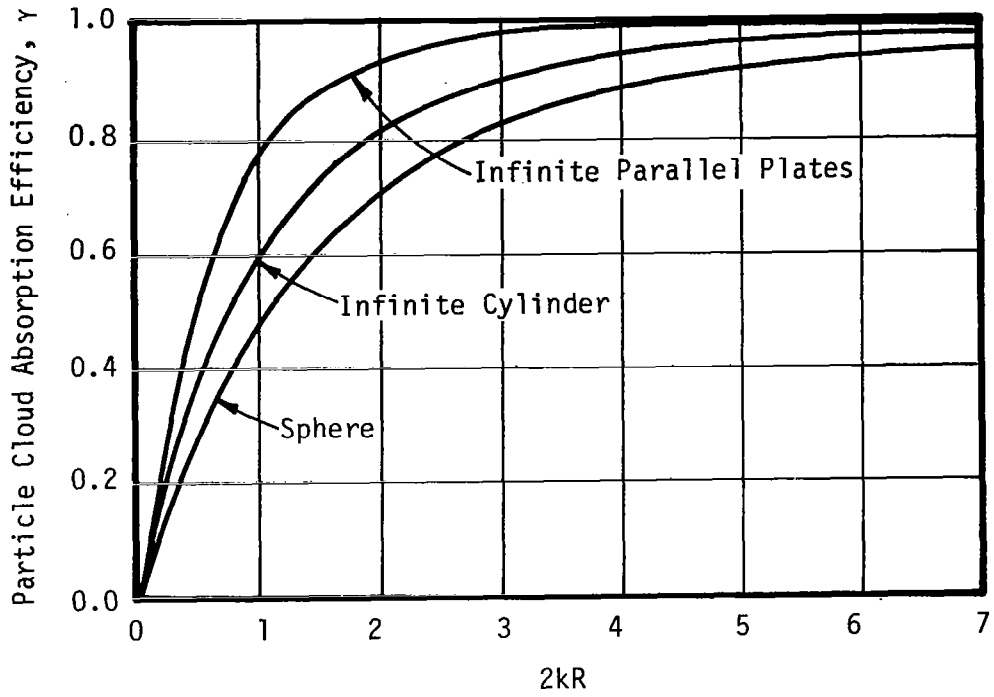
Figure 1. Absorptivity of Clouds of Particles in Furnaces
of Various Shapes.

clouds were estimated from qualitative deductions about the relative absorptance of the three different cloud configurations. For a given value of 2kR, a particle cloud between infinite parallel plates was noted to have the greatest absorptivity. Qualitatively this was expected since the average length of a radiant beam should be largest for infinite parallel plates because of the two infinite directions. The average beam length should be intermediate for a cylinder with one infinite direction and least for the sphere with no unlimited dimensions.

The investigation concluded that the absorptivities of cloud configurations encountered in practice could be estimated by interpolation between the curves of the idealized cases. For instance, a cubic cloud structure should have an emissivity between that of a cylinder and a sphere while a long rectangular enclosure should result in a value between the cylinder and parallel plates. The method thus afforded a means for estimating particle cloud emissivities; it was not intended to give precisely an evaluation of a cloud's shape.

In a later investigation, Oktay[9] extended this method of attack to include particles as small as 50 microns. As would be expected, the radiation contribution to the overall heat transfer increased rapidly with decreasing particle size. Shulderberg, et al.[10] made a similar investigation of the heat transfer characteristics of solid-gas suspensions for possible use as the working fluid of a nuclear power generation system. Again, high rates of heat transfer were obtained for very small particles. This latter investigation was exploratory in nature and did not emphasize basic analyses.

8

Hoffman and Gauvin[11] conducted a more fundamental study in which the evaporation of a spray contained in a high-temperature, cylindrical column was investigated. This analysis of radiant heat transfer to a cloud of particles amounted to an extension of the Hottel-Cohen[12] method in which the system was divided into zones, and the radiation between these zones, expressed as geometric interchange factors, was evaluated. Results for the total system were obtained from energy balances over each zone. The zones consisted of portions of the enclosing surface and of the absorbing medium that were small enough in size to be considered isothermal. To be exact, the zones must be of differential size, yet, because of the lengthy computations involved, the number of zones were restricted. Hoffman and Gauvin compromised by taking cylindrical aerosol volumes of height equal to diameter and by developing calculations for three such volumes. Mean beam lengths as previously outlined by Haslam and Hottel[13] are derivable from this work.

In a more recent analytical study, Einstein[14] continued the zone-type of calculation and made a computer analysis of the heat transfer to an absorbing medium within a black circular pipe under the combined influence of radiation, gas flow through the pipe, and thermal conduction from the wall to the gas. Here, the zones consisted of short lengths of cylindrical, concentric shells, and, at the outer boundary, of the enclosing portion of the emitting pipe surface. Specific results were obtained for a pipe with absorbing medium opacities of 1.0 to 10.0 [opacity being the absorption coefficient times the diameter of the pipe 2R].

Lanzo and Ragsdale[15] performed an experimental study of radiant heat transfer to a particle cloud flowing in a quartz annulus surrounding an electric arc. Very small, submicron (although only partially dispersed) were shown to attenuate considerable quantities of energy and to make excellent radiation absorbers. Even better results would undoubtedly have been obtained had good particle deagglomeration been obtained.

All the foregoing studies were similar in that the basic objective was to evaluate the net heat interchange between a solid surface and a particle cloud provided the absorption characteristics of the cloud were known. Unfortunately, many liquid sprays and particle dispersions may be highly reflective or, because of particle shape and dimensions and size distribution, exhibit very complicated radiation scattering phenomena and as a result possess uncertain radiation properties.

An entirely different approach is required to account for these parameters. Early work of the latter type attempting to define the emissive properties of luminous flames in furnaces is described in Heat Transmission by McAdams.[16] Semi-empirical results are represented by the equation

$$\epsilon_\lambda = 1 - e^{-C.L.f(\lambda)} \qquad (1.3)$$

where ϵ_λ is the spectral emissivity of a particle cloud of concentration C with a mean beam length L and the function $f(\lambda)$ is an absorption coefficient. The function is represented either by $(k/\lambda^{1.39})$, which is supposed to account for particle size variations, or by $[1 - 15(r/x)^2]/\lambda$, where r is the radius of a specific particle. The general validity of

10

these functions is uncertain, however. Stull and Plass[17] attacked the problem more fundamentally by using spectroscopic and electromagnetic data to solve the Mie equations[18] for the absorption and reflective characteristics of small luminous particles. Based on observed particle size distribution data, emissive properties of luminous carbon flames were obtained for a temperature of 2250° K and exposure to several appropriately selected radiation wave lengths. Thring, et al.[19] applied the data of Stull and Plass to practical cases and found that for flames two meters across (square tunnel) the emissivity could be predicted within ± 15 per cent, but for smaller flames of 0.5 meter across deviations of about ± 300 per cent were observed. Strangely, small laminar flames in the laboratory had emissivities in good agreement with the theoretical predictions.

Ordinarily, solid particles must be on the order of one micron or less to exhibit pronounced scattering, alumina, quartz, and other visually transparent minerals being exceptions.[20,21] Liquids, on the other hand, have significant transmissive and refractive properties. Because water and atomized fuel droplets occur frequently in high temperature processes, investigations of their radiation properties have been made. Thomas[22] determined the absorptivity of water droplets by use of geometric optics. Friedman and Churchill[23] produced similar absorptivity results for fuel droplets. The data in either case are only valid for droplets larger than the radiation's wave length. The error is uncertain if this condition is not met since the optical laws of reflection for large spheres do not hold for bodies smaller than the radiation wave length.[24]

Still another problem associated with the radiant heating of particle dispersions is the dissipation of the energy absorbed by the particles. Mathematical solutions have been obtained for the transfer of heat from submerged bodies to a surrounding medium, but, because of the many complicating factors, they were highly idealized. Heat transfer in the neighborhood of a particle is dependent upon the particle shape, size, distance to other particles, and the time-dependent hydrodynamic flow patterns in the surrounding space. Obtaining accurate descriptions of all the variables required for an exact analysis has not been feasible. With certain simplifications, however, guidelines have been established for estimating the heat transfer between suspended particles and their surroundings.

Notably, Sliecher and Churchill[25] investigated the problem for quiescent aerosols and derived limiting results where spherical, uniformly dispersed particles are heated by isotropic radiation and cooled by conduction. The development was made first for a single particle in an infinite medium and was then extended to apply to a dense dispersion of particles. For a single particle in a large medium, its temperature history was found to be expressed exactly by

$$t_\theta - t_o = \frac{\alpha q a}{k_t} \left[1 - \frac{2}{\pi} \int_0^\infty \frac{e^{-k_t \theta z^2 / \rho_p C_p a^2}}{1 - (2\Phi - 1)z^2 + \Phi^2 z^4} \, dz \right] \qquad (1.4)$$

and approximately by

$$t_\theta - t_o = \frac{\alpha q a}{k_t} \left[1 - e^{-3k_t \theta / \rho_p C_p a^2} \right] \qquad (1.5)$$

The former equation is a function of the parameter Φ ($= \rho_p C_p / 3\rho C$) while

the latter is not. At high values of Φ, however, the two become nearly identical. Since this number is usually large (over 400), both equations in practical applications were found to agree within ± 3 per cent. The functions were plotted in non-dimensional form as shown in Figure 2 for an arbitrary value of $\Phi = 500$, which corresponded to a particular case, viz., a 25 micron coal particle exposed to a 2000° F black-body heat source. For these conditions a dimensionless abscissa of 4 represents an exposure time of 16.1 milliseconds during which the coal particle attains over 95 per cent of its maximum possible temperature.

For a dense particle dispersion, the temperature rise of a single particle could be described by the function

$$t_\theta - t_o = \frac{\alpha q a}{k_t}\left(1 - e^{-3k_t\theta/c_p\rho_p a^2} + \frac{4\pi a n k_t \theta}{\rho C}\right) \qquad (1.6)$$

containing two linear terms and one exponential term. Initially the exponential term is controlling and a particle's temperature rises in a manner very nearly that of a single particle in an infinite medium. This characteristic is demonstrated graphically in Figure 3, where, below an abscissa of 1.0, the curves shown are very nearly exponential. For the coal particle, an abscissa of 1.0 again represents 16.1 milliseconds. At still greater times, the particle temperature establishes a pseudo-equilibrium condition such that the energy received by radiation equals the heat lost by conduction; the linear terms are then controlling as may be noted from its long term temperature history as shown in Figure 4.

The temperature difference at pseudo-equilibrium between the particles and the surrounding air is constant, and this difference for
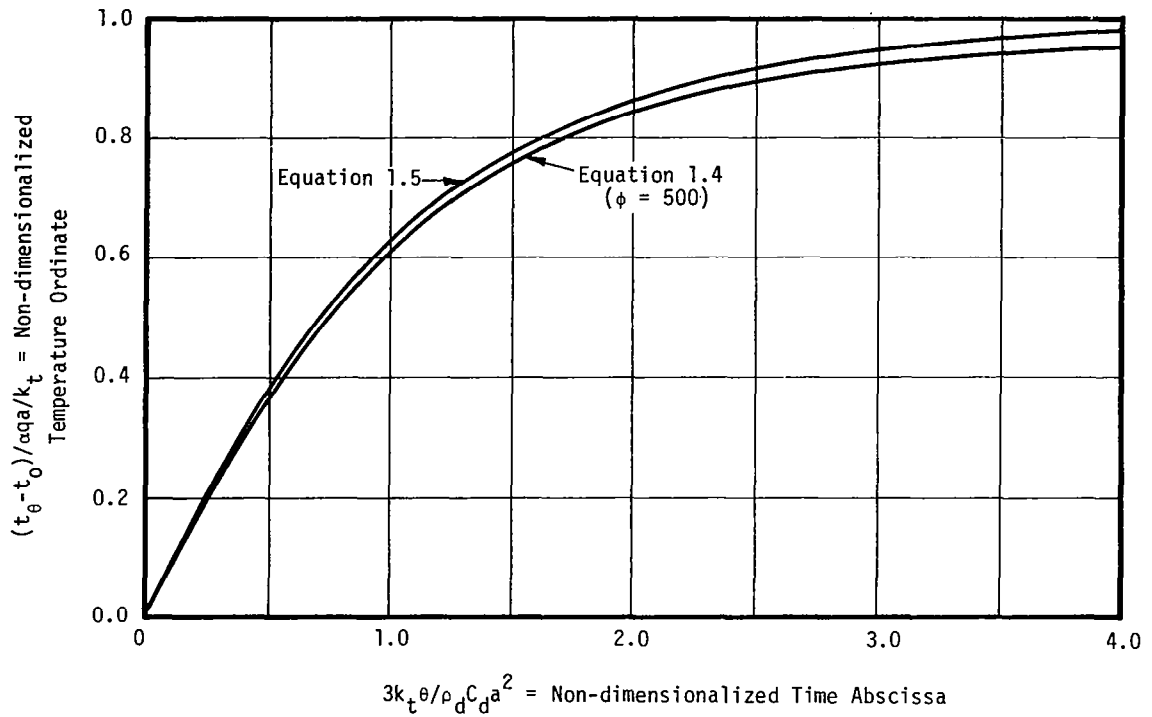
Figure 2. Temperature History of a Single Particle Exposed to Thermal Radiation.
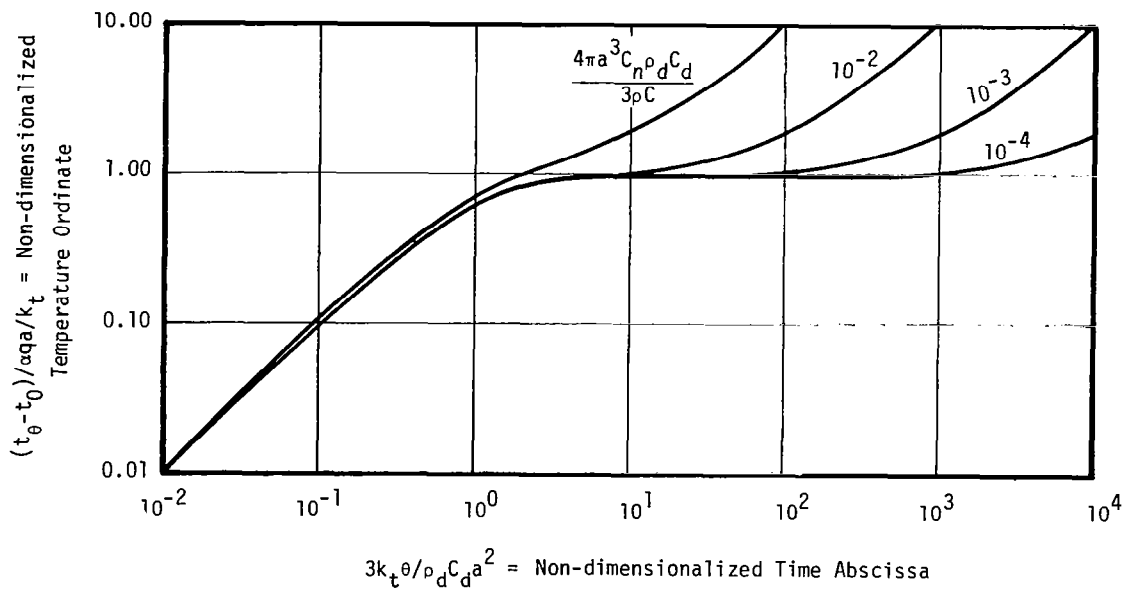
Figure 3. Initial Temperature History of a Dispersion Exposed to Thermal Radiation.
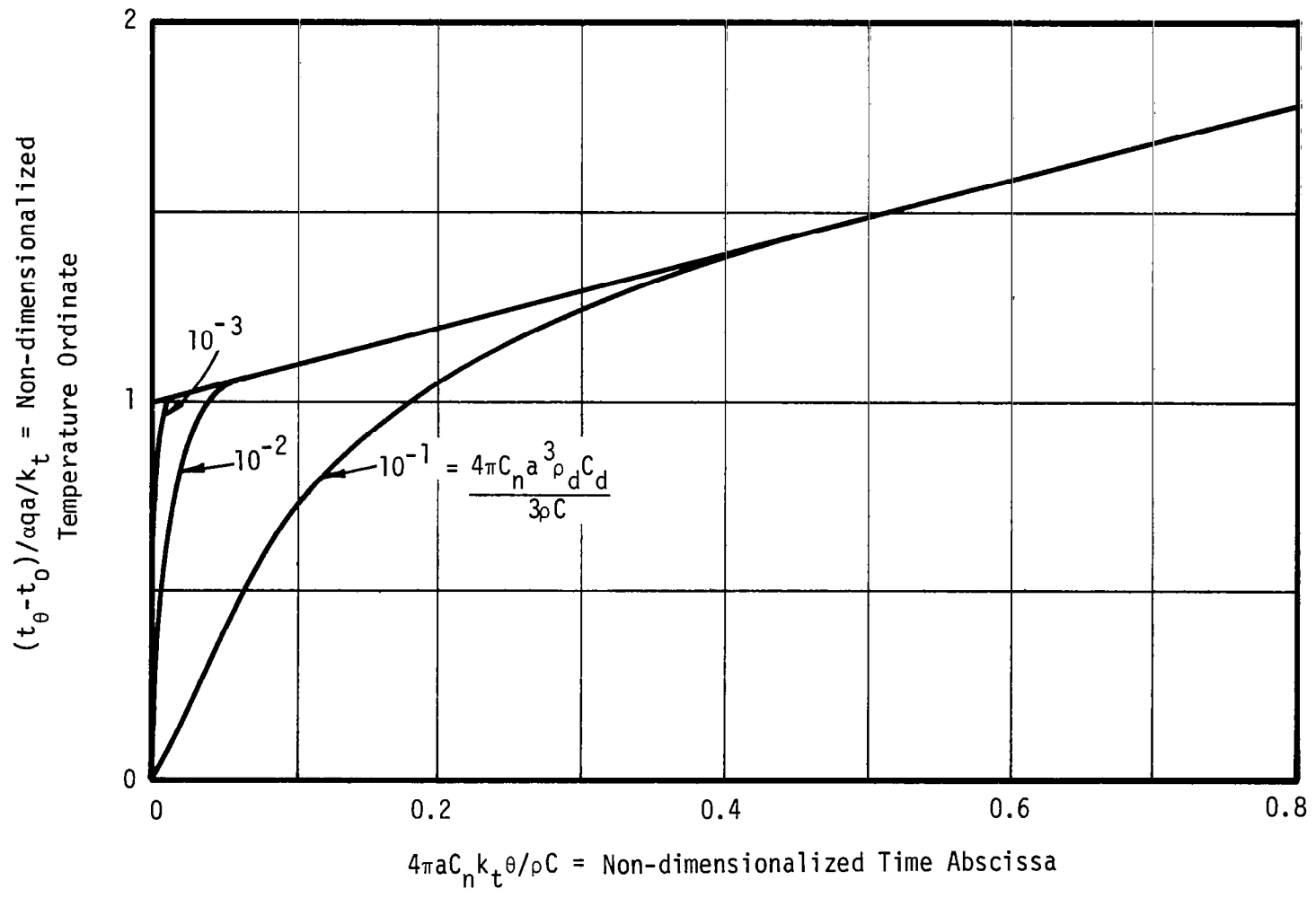
Figure 4. Long Term History of a Dispersion Exposed to Thermal Radiation.

the example is 318° F. Between the initial and pseudo-equilibrium conditions there is an intermediate range where all the terms are significant. This behavior is controlled, as shown in Figures 3 and 4, by the parameter, $4\pi^3 C_n \rho_p C_p / 3\rho C$, which represents the ratio of the particle heat capacity to that of the air associated with each particle.

The calculations of Sleicher and Churchill are important because they indicate limiting conditions and temperature differences that may be expected in an actual system. The significant finding is that time intervals of the order of milliseconds, and sometimes micro-seconds, are required for essentially complete transfer to occur. In flowing systems this means th t only very short distances are required for particle-gas interactions. For example, a gas-solid suspension flowing at 50 feet per second through a pipe and receiving 2000° F black body radiation would, if the particles were 50 microns or less, establish pseudo-equilibrium after only 6 inches of movement along the pipe, according to the predictions. After leaving the heated pipe, the suspended particles would in even less distance return very nearly to the ambient gas temperature.

Although the above type of thermal reaction is rapid, even less time than predicted is frequently required. Since the development was for quiescent aerosols, the particles were considered stationary relative to the gas, and conduction only was assumed to exist throughout the region among the particles. In flowing systems, however, there must be convective transfer and conduction can only exist in a small boundary layer surrounding a particle. Conduction due to the decreased thickness is actually faster and the temperature of a particle more quickly

adjusts to that of the surrounding air. Under highly accelerated particle-gas conditions, however, slippage,[26] i.e., the particle lagging in velocity behind that of the surrounding air because of momentum differences, can change a particle's environment. This would produce the opposite effect on the difference between particles and average air temperature. Carlson[27] measured spectroscopically the average air and particle temperatures in a rocket engine where severe acceleration was exhibited. There, magnesium oxide particles on the order of one micron lagged the gas temperature about 650° F when the rocket exhaust was about 4200° F. This temperature difference is considerably larger than would be expected from Sleicher and Churchill's calculations. Where large accelerations are expected, the effect must be investigated further, therefore.

That heat transfer from a particle to its surroundings is rapid may be readily demonstrated by considering the classical developments for heat transfer from a sphere submerged in a gas.[28] The limiting case is for a Nusselt number of 2 where only conduction prevails. Thus, the lowest heat transfer coefficient is

$$h_a = 2 \frac{k_t}{d_p} \tag{1.7}$$

If the macroscopic properties of the gaseous medium are not violated, a small diameter particle has associated with it a very high heat transfer coefficient, even for conduction. For a 100 micron particle in air, h_a is over 9000 Btu/hr ft^2 $^{\circ}$F as normally encountered in convective heat transfer. As may be seen from equation (1.7), the increased heat tranfer coefficient arises from its inverse variation with particle diameter. Use

has been made of this fact in measuring air temperatures in the presence of radiant fields.[29] When the air temperature is determined with several thermocouples of successively smaller size, the actual and indicated temperatures become more nearly equal. The results are extrapolated to zero diameter to obtain the actual gas temperature.

CHAPTER II

THEORETICAL INVESTIGATIONS

Method of Analysis

It is frequently expedient to approach radiation problems by first assuming black body behavior for all the bodies involved, then, if a solution is obtained, to seek progressively more accurate descriptions of the problem by modifying the basic result with the parameters necessary to account for the non-ideal characteristics of the system. The fundamental developments of classical radiative heat transfer theory have followed this procedure. Accordingly, the heat exchange between a particle cloud and a cylindrical enclosure was first investigated when both were perfect radiators. A combined analytical and numerical approach was employed to derive an accurate evaluation of the radiant heat transfer to a particle cloud within an enclosure having practically any length-to-diameter ratio. Calculated results are readily obtained by use of a digital computer.

Development of Equations

Radiation emitted from each of two black surfaces of differential size and received by the other is described by

$$dQ'_{b12} = i_{bn1} \cos \beta_1 \, d\omega_2 \, dA_1 \qquad (2.1)$$

and

$$dQ'_{b21} = i_{bn2} \cos \beta_2 \, d\omega_1 \, dA_2 \qquad (2.2)$$

for which

$$d\omega_2 = \frac{\cos \beta_2}{S^2} dA_2 \qquad (2.3)$$

$$d\omega_1 = \frac{\cos \beta_1}{S^2} dA_1 \qquad (2.4)$$

The subscript b indicates black body behavior and n specifies that the radiation intensity, i, is normal to the emitting surface. The number subscripts, 1 and 2, refer to the surfaces exchanging radiation. Figure 5 defines the geometry of the plane angles, β_1 and β_2, and the solid angles, $d\omega_1$ and $d\omega_2$.

Since the surfaces are black, all the impinging radiation is absorbed. The net exchange of energy, therefore, is

$$dQ'_b = dQ'_{b21} - dQ'_{b12} \qquad (2.5)$$

If equations (2.3) and (2.4) are substituted into (2.1) and (2.2) and the results applied to (2.5), the net heat transfer is

$$dQ'_b = (i_{bn2} - i_{bn1}) \left(\frac{\cos \beta_1 \cos \beta_2}{S^2} \right) dA_1 dA_2 \qquad (2.6)$$

or in integrated form

$$Q'_b = \int_{A_2} \int_{A_1} (i_{bn2} - i_{bn1}) \left(\frac{\cos \beta_1 \cos \beta_2}{S^2} \right) dA_1 \, dA_2 \qquad (2.7)$$

Equation (2.7) is a general expression that relates the radiant heat transfer between two finite surfaces. For a specific application, the spatial arrangement of dA_1 and dA_2 in the differential expression must be described with appropriate functions to permit the integration indicated in equation (2.7). For a particle cloud receiving radiation from
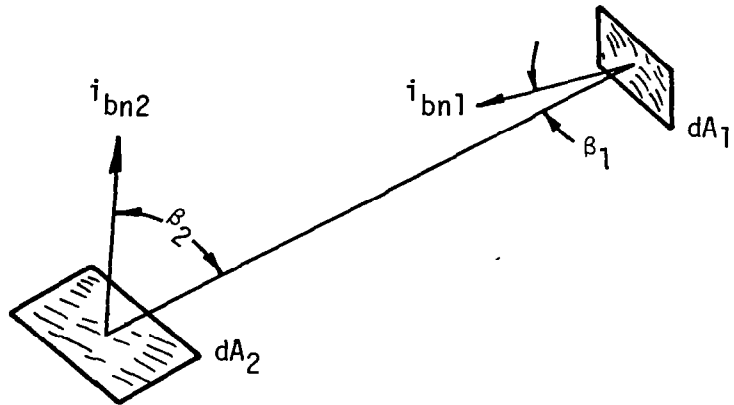
(a) Orientation and Separation of Differential Areas

(1) Solid Angle, $d\omega_1$
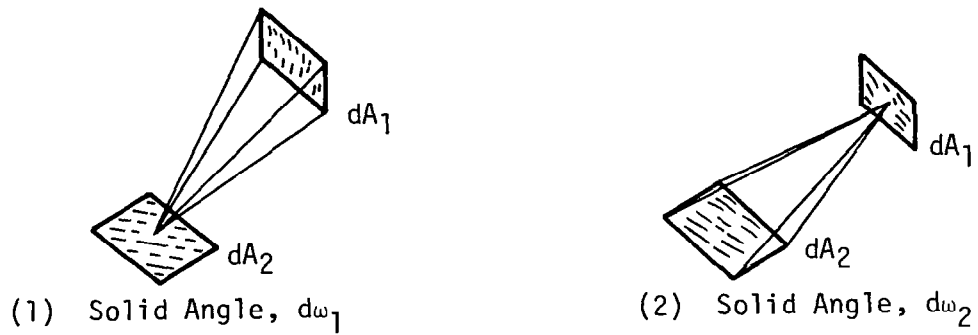
(2) Solid Angle, $d\omega_2$

(b) Solid Angle Relationships

Figure 5. Angular Functions Used in Defining Radiation Interchange
Between Two Areas of Differential Size.

a tubular enclosure, adaptation was made as indicated in Figure 6 where the system of coordinates is also defined. As shown, radiation leaves the tube wall with an intensity, i_w, and proceeds along the line segment, S, to a small elemental volume of aerosol. The location of dA_w is described by the variables y, z and Ψ, and the position of the elemental volume, by z and r. Other quantities of equation (2.7) in terms of these coordinate variables are:

$$dA_w = Rd\Psi dy \qquad (2.8)$$

$$S = \sqrt{m^2+y^2} \qquad (2.9)$$

$$m = \sqrt{R^2+r^2-(2Rr)\cos \Psi} \qquad (2.10)$$

and

$$\cos\beta_w = \frac{S^2+R^2-r^2-y^2}{2RS} \qquad (2.11)$$

Receiving the radiation is dA_s which is the surface area of the particles contained in the volume element. As shown in Figure 5a, however, the effectiveness of an area for intercepting radiation is determined by its projection perpendicular to the incoming radiation. This projection is obtained from multiplication of the area by $\cos \beta_s$ which is the cosine of the angle between the normal direction to the surface and the impinging radiation. When a particle is considered, the projection is its cross-sectional area, A_c. The effective particle area participating in a radiant interchange, then is given by

$$dA_c = CS_v dV \qquad (2.12)$$
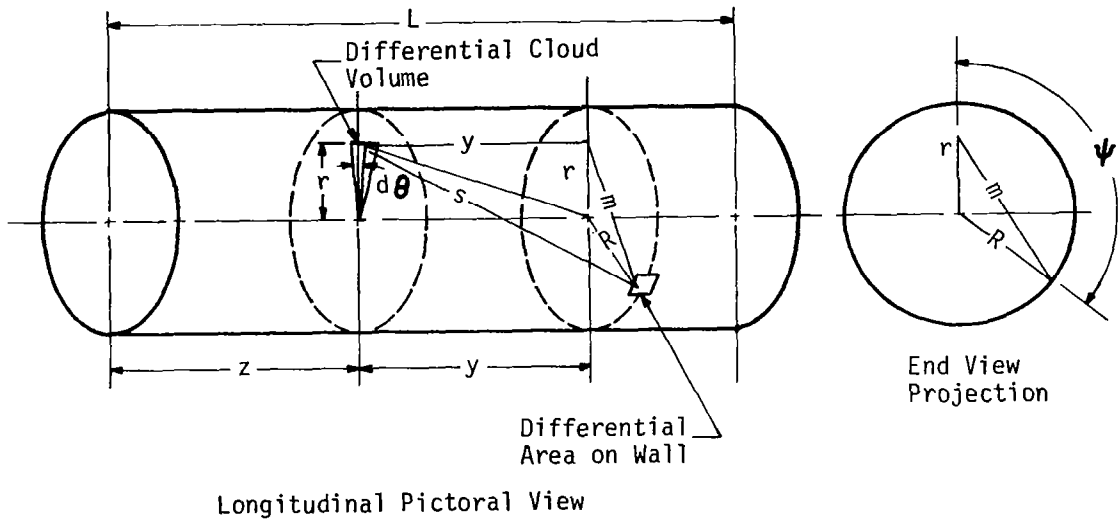
Figure 6. Definitions of Geometric Variables for Tube Radiating
to Enclosed Particle Cloud.

or

$$dA_c = CS_v\, r\, dr\, d\theta\, dz \qquad (2.13)$$

where S_v is the cross-sectional area per unit volume of powdered material (ft^2/ft^3), and C is the volume concentration of powder in the aerosol (ft^3 solids/ft^3 aerosol). The quantity S_v may be computed from statistical measurements of randomly oriented particles. If the surface area of a powder is known from other information, the required area is 0.25 times the envelope surface, or

$$dA_c = 0.25\, dA_s \qquad (2.14)$$

Equation (2.14) follows from the fact that the projected area of randomly oriented particles whose surfaces are everywhere positively curved is 0.25 times the surface area.[30]

Substitution of the required quantities into the radiation equation yields

$$Q_b' = R \int_o^{2\pi} \int_o^{R} \int_o^{2\pi} \int_o^{L} \int_{-z}^{L-z} (i_{bnw}-i_{bnp})(CS_v)(\frac{1}{S^2})(\frac{S^2+R^2-r^2-y^2}{2RS})(r)\,dy\,dz\,d\Psi\,dr\,d\theta \quad (2.15)$$

where the limits of integration are as shown.

The result, however, is still incomplete. Radiation passing through a cloud has its intensity attenuated. For black particles this reduction may be expressed as

$$i_s = i_w\, e^{-kS} \qquad (2.16)$$

where k, is a function of particle geometry and concentration;[31] the radiation intensity i_w at the wall is reduced to i_s after

penetrating a distance S into the particle cloud. Therefore, when radiation attenuation is considered, equation (2.15) becomes

$$Q_b = R \int_0^{2\pi} \int_0^R \int_0^{2\pi} \int_0^L \int_{-z}^{L-z} (i_{bnw} - i_{bnp})(CS_v)(\frac{e^{-kS}}{S^2})(\frac{S^2 + R^2 - r^2 - y^2}{2RS})(r) \, dy \, dz \, d\Psi \, dr \, d\theta \quad (2.17)$$

which is the final expression to be evaluated for a black tube wall and black particles.

Solution for Integrals of Heat Transfer Equation

The indicated integrations remain to be performed after all the quantities of equation (2.17) are evaluated. The integral expression may be simplified by considering the particles not to radiate back to the wall either by radiation scattering or by significant thermal radiation. The development is then valid for the radiant heating of aerosols by direct transmission, which is of prime interest in this investigation. Secondary emissions and reverse thermal radiation is more appropriately considered in a separate analysis since i_{bnp} cannot be taken as constant and be removed from the integration process. It must be further assumed that the radiation intensity of the emitting tube wall is constant over the entire surface. These modifications yield for the total heat absorbed

$$Q_b = (R)(i_{bnw}) \int_0^{2\pi} \int_0^R \int_0^{2\pi} \int_0^L \int_z^{L-z} (CS_v)(\frac{e^{-kS}}{S^2})(\frac{S^2 + R^2 - r^2 - y^2}{2RS})(r) \, dy \, dz \, d\Psi \, dr \, d\theta \quad (2.18)$$

A second change may now be made to treat the integration with respect to the first two variables, y and z, as one operation which is a lengthy development itself and then to integrate the remaining ones separately. The following notation will be employed

$$Q_b = (R)(i_{bnw})(CS_v)\int_0^{2\pi}\int_0^R\int_0^{2\pi} Ird\Psi drd\theta = (2\pi R)(i_{bnw})(CS_v)\int_0^R\int_0^{2\pi} Ird\Psi dr \quad (2.19)$$

where

$$I = \int_0^L\int_{-z}^{L-z}(\frac{e^{-k}}{S^2})(\frac{S^2+R^2-r^2-y^2}{2RS})dydz . \quad (2.20)$$

The θ integration is performed directly.

The evaluation of I is initiated with an expansion of the exponential term. Thus,

$$e^{-kS} = 1 - kS + \frac{k^2S^2}{2!} - \frac{k^3S^3}{3!} + \frac{k^4S^4}{4!} - \ldots \quad (2.21)$$

The $\cos\beta_w$ factor can also be expressed as

$$\frac{S^2+R^2-r^2-y^2}{2RS} = \frac{S^2}{2RS} + \frac{R^2-r^2}{2RS} - \frac{y^2}{2RS} \quad (2.22)$$

With these changes equation (2.20) becomes

$$I = (\frac{1}{2R})\int_0^L\int_{-z}^{L-z}[\frac{1}{S} - k + \frac{k^2S}{2!} - \frac{k^3S^2}{3!} + \frac{k^4S^3}{4!} - \ldots]dydz$$

$$+ (\frac{1}{2R})\int_0^L\int_{-z}^{L-z}(R^2-r^2)(\frac{1}{S^3}) - \frac{k}{S^2} + \frac{k^2}{2!S} - \frac{k^3}{3!} + \frac{k^4S}{4!} - \ldots)dydz$$

$$- (\frac{1}{2R})\int_0^L\int_{-z}^{L-z}(\frac{y^2}{S^3} - \frac{ky^2}{S^2} + \frac{k^2y^2}{2!S} - \frac{k^3y^2}{3!} + \frac{k^4y^2S}{4!} - \ldots)dydz \quad (2.23a)$$

In summation notation and with $(m^2+y^2)^{1/2}$ substituted for S the terms are

$$I = (\frac{1}{2R}) \int_o^L \int_{-z}^{L-z} \sum_{n=3}^n \left[\frac{(-k)^{n-3}}{(n-3)!}\right]\left[m^2+y^2\right]^{(\frac{n-4}{2})} dydz$$

$$+ (\frac{1}{2R}) \int_o^L \int_{-z}^{L-z} \sum_{n=1}^n \left[\frac{(-k)^{n-1}}{(n-1)!}\right]\left[R^2-r^2\right]\left[m^2+y^2\right]^{(\frac{n-4}{2})} dydz$$

$$- (\frac{1}{2R}) \int_o^L \int_{-z}^{L-z} \sum_{n=1}^n \left[\frac{(-k)^{n-1}}{(n-1)!}\right]\left[y^2\right]\left[m^2+y^2\right]^{(\frac{n-4}{2})} dydz \qquad (2.23b)$$

The first two sums can be combined; therefore,

$$I = (\frac{1}{2R}) \int_o^L \int_{-z}^{L-z} \left\{\frac{R^2-r^2}{(m^2+y^2)^{3/2}} + \frac{(R^2-r^2)(-k)}{(m^2+y^2)} + \sum_{n=3}^n \left\{ \left[\frac{(-k)^{n-3}}{(n-3)!}\right.\right.\right.$$

$$\left.\left.+ \left[\frac{(-k)^{n-1}}{(n-1)!}\right]\left[R^2-r^2\right] \right\} \left[m^2+y^2\right]^{(\frac{n-4}{2})} dydz$$

$$- (\frac{1}{2R}) \int_o^L \int_{-z}^{L-z} \sum_{n=1}^n \left[\frac{(-k)^{n-1}}{(n-1)!}\right]\left[y^2\right]\left[m^2+y^2\right]^{(\frac{n-4}{2})} dydz \qquad (2.23c)$$

The latter summation contains an extra y^2 factor and, consequently, has to be treated separately. At this point it is advantageous to consider equation (2.23c) in two parts, namely

$$I = I_\alpha + I_\beta \qquad (2.24)$$

where I_α and I_β are integrals of the two summations.

Integrations for I_α

Because of the mathematics involved, it is necessary to perform the integration in four separate divisions classified according to the position of the term in the series being integrated. Two classifications

are simply for the first and second terms of the I_α series, a third for all successive odd terms and a fourth for all subsequent even terms. The terms are even or odd according to the value of n. The total integral, therefore, is

$$I_\alpha = I_{\alpha 1} + I_{\alpha 2} + I_{\alpha 3} + I_{\alpha 4} \tag{2.25}$$

where $I_{\alpha 3} \equiv I_{\alpha(odd)}$ and $I_{\alpha 4} \equiv I_{\alpha(even)}$.

Evaluation of I_1 and I_2. The initial term of the series is

$$I_{\alpha 1} = (\frac{1}{2R}) \int_0^L \int_{-z}^{L-z} (R^2-r^2) \left[\frac{1}{(m^2+y^2)^{3/2}} \right] dy\, dz \tag{2.26a}$$

which becomes

$$I_{\alpha 1} = (\frac{1}{2R}) \int_0^L (R^2-r^2) \left\{ (\frac{L-z}{m^2}) \left[\frac{1}{[m^2+(L-z)^2]^{1/2}} \right] + (\frac{z}{m^2}) \right.$$

$$\left. \left[\frac{1}{[m^2+z^2]^{1/2}} \right] \right\} dz \tag{2.26b}$$

and

$$I_{\alpha 1} = (\frac{1}{R}) (\frac{R^2-r^2}{m^2}) \left[(m^2+L^2)^{1/2} - m \right] \tag{2.26c}$$

The second term of the exponential expansion is

$$I_{\alpha 2} = (\frac{1}{2R}) \int_0^L \int_{-z}^{L-z} (-k)(R^2-r^2) \left[\frac{1}{(m^2+y^2)} \right] dy\, dz \tag{2.27a}$$

which by successive integration and simplification becomes

28

$$I_{\alpha 2} = \frac{(-k)(R^2-r^2)}{2mR} \int_0^L [\tan^{-1} (\frac{L-z}{m}) + \tan^{-1} (\frac{z}{m})] \, dz \quad (2.27b)$$

and

$$I_{\alpha 2} = \frac{(-k)(R^2-r^2)}{2mR} \left[(2L)\tan^{-1} (\frac{L}{m}) - (m) \ln (1 + \frac{L^2}{m^2}) \right] \quad (2.27c)$$

In the integration of equation 2.27b use is made of the trigonometric identity,

$$\tan^{-1} (\frac{z}{m}) = - \tan^{-1} (\frac{-z}{m}) \quad (2.28)$$

Also, since z and m are both positive and their ratio, z/m, varies from zero to infinity, the inverse tangent of (L/m) involved only the principle values of the function.

Evaluation of $I_{\alpha 3}$. Since n is odd and larger than 1, the exponent $(\frac{n-4}{2})$ in equation (2.23c) is a member of the set of fractions, $-1/2$, $1/2$, $3/2$, $5/2$, $7/2$, $9/2$, etc.; and the complete integration for the first n terms is

$$I_{\alpha 3} = (\frac{1}{2R}) \sum_{\substack{n=3 \\ odd}}^{n} \left\{ \left[\frac{k^{n-3}}{(n-3)!} \right] + \left[\frac{k^{n-1}}{(n-1)!} \right] \left[R^2-r^2 \right] \right\} \int_0^L \int_{-z}^{L-z} (m^2+y^2)^{\frac{n-4}{2}} \, dy dz \quad (2.29a)$$

For a particular value of n. the relationship reduces to

$$I_{\alpha 3n} = (\frac{1}{2R}) \left\{ \left[\frac{k^{n-3}}{(n-3)!} \right] + \left[\frac{k^{n-1}}{(n-1)!} \right] \left[R^2-r^2 \right] \right\} \int_0^L \int_{-z}^{L-z} (m^2+y^2)^{\frac{n-4}{2}} \, dy \, dz \quad (2.30a)$$

This equation then can be integrated by the following expressions from a table of integrals:[32]

$$\int X^n \sqrt{X} \, dx = \frac{2cx+b}{4(n+1)c} X^n \sqrt{X} + \frac{2n+1}{2(n+1)f} \int \frac{X^n}{\sqrt{X}} \, dx \quad (2.31)$$

$$\int \frac{\chi^h dx}{\sqrt{\chi}} = \int \chi^{h-1} \sqrt{\chi} \ dx \qquad (2.32)$$

and

$$\int \frac{1}{\sqrt{\chi}} \ dx = \frac{1}{\sqrt{c}} \ \sinh^{-1} \left(\frac{2cx+b}{\sqrt{4ac+b^2}}\right) \text{ if } c > o \qquad (2.33)$$

where $\chi = cx^2 + bx + a$,

and $f = \dfrac{4c}{4ac-b^2}$.

Equation (2.31) is more conveniently employed when transformed to yield

$$\int \chi^p \ dx = \frac{2cx+b}{4(p+\frac{1}{2})c} \chi^p + \frac{2(p-\frac{1}{2})+1}{2(p+\frac{1}{2})f} \int \frac{\chi^{p-\frac{1}{2}}}{\sqrt{\chi}} \ dx \qquad (2.34)$$

The integral formulas can be applied to equation (3.30a) by making $\chi = m^2+y^2$. Then it follows that $x = y$, $a = m^2$, $b = 0$, $c = 1$, and $f = 1/m^2$.

The first two members of series are integratable directly. The results are

$$I_{\alpha33} = \left(\frac{1}{2R}\right) \left\{ \left[\frac{k^{n-3}}{(n-3)!}\right] + \left[\frac{k^{n-1}}{(n-1)!}\right]\left[R^2-r^2\right] \right\} \int_o^L \left[\sinh^{-1}\left(\frac{L-z}{m}\right) + \sinh^{-1}\left(\frac{z}{m}\right)\right] dz$$

$$= \left(\frac{1}{2R}\right) \left[1 + \left(\frac{k^2}{2}\right)(R^2-r^2)\right] \int_o^L \left[\sinh^{-1}\left(\frac{L-z}{m}\right) + \sinh^{-1}\left(\frac{z}{m}\right)\right] dz \qquad (2.30b)$$

and

$$I_{\alpha35} = \left(\frac{1}{2R}\right) \left\{ \left[\frac{k^{n-3}}{(n-3)!}\right] + \left[\frac{k^{n-1}}{(n-1)!}\right]\left[R^2-r^2\right] \right\} \int_o^L \left\{ \left[\frac{L-z}{2}\right]\left[m^2+(L-z)^2\right]^{\frac{1}{2}} + \right.$$

$$\left. \left[\frac{z}{2}\right]\left[m^2+z^2\right]^{\frac{1}{2}} + \left[\frac{m^2}{2}\right]\left[\sinh^{-1}\left(\frac{L-z}{m}\right) + \sinh^{-1}\left(\frac{z}{m}\right)\right] \right\} dz \qquad (2.30c)$$

$$I_{\alpha 35} = (\frac{1}{2R}) \left[\frac{k^2}{2} + (\frac{k^4}{24})(R^2-r^2) \right] \int_0^L \left\{ \left[\frac{L-z}{2} \right]\left[m^2+(L-z)^2 \right]^{\frac{1}{2}} + \left[\frac{z}{2} \right]\left[m^2+z^2 \right]^{\frac{1}{2}} \right\} dz$$

$$+ (\frac{1}{2R}) \left[\frac{m^2 k^2}{4} + (\frac{m^2 k^4}{48})(R^2-r^2) \right] \int_0^L \left[\sinh^{-1} (\frac{L-z}{m}) + \sinh^{-1} (\frac{z}{m}) \right] dz \quad (2.30c)$$

where the final subscripts 3 and 5 refer to the particular value of n.

By use of equations (2.30a) and 2.34) the integral becomes for higher values of n

$$I_{\alpha 3n} = (\frac{1}{2R}) \left\{ \left[\frac{k^{n-3}}{(n-3)!} \right] + \left[\frac{k^{n-1}}{(n-1)!} \right]\left[R^2-r^2 \right] \right\} \left\{ \int_0^L \left[(\frac{y}{2p+1})(M,Y)^p \right]_{-z}^{L-z} dz \right.$$

$$\left. + (\frac{2pm^2}{2p+1}) \int_0^L \int_{-z}^{L-z} \frac{(M,Y)^{p-\frac{1}{2}}}{\sqrt{M,Y}} dy dz \right\} \quad (2.30d)$$

where p is a member of the set of exponents and the notation $(M,Y)^p$ symbolizes the integrand, $(m^2+y^2)^{\frac{n-4}{2}}$. A second application of equation (2.34) gives

$$I_{\alpha 3n} = (\frac{1}{2R}) \left\{ \left[\frac{k^{n-3}}{(n-3)!} \right] + \left[\frac{k^{n-1}}{(n-1)!} \right]\left[R^2-r^2 \right] \right\} \left\{ \int_0^L \left[(\frac{y}{2p+1})(M,Y)^p \right. \right.$$

$$\left. + \frac{2pm^2}{2p+1} \left[\frac{y}{2(p-1)+1} (M,Y)^{p-1} \right] \right]_{-z}^{L-z} dz$$

$$\left. + \left[\frac{2pm^2}{2p+1} \right]\left[\frac{2(p-1)m^2}{2(p-1)+1} \right] \int_0^L \int_{-z}^{L-z} \frac{(M,Y)^{p-3/2}}{\sqrt{M,Y}} dy dz \right\} \quad (2.30e)$$

and repeated use of the integration formulas produces the series

$$I_{\alpha 3n} = \left(\frac{1}{2R}\right) \left\{ \left[\frac{k^{n-3}}{(n-3)!}\right] + \left[\frac{k^{n-1}}{(n-1)!}\right]\left[R^2 - r^2\right] \right\} \left\{ \int_0^L \left[\left(\frac{y}{2p+1}\right)(M,Y)^p \right.\right.$$

$$+ \frac{2pm^2}{2p+1}\left[\frac{y}{2(p-1)+1}\right.(M,Y)^{p-1} + \frac{2(p-1)m^2}{2(p-1)+1}\left[\frac{y}{2(p-2)+1}\right.(M,Y)^{p-2}$$

$$+ \frac{2(p-2)m^2}{2(p-2)+1}\left[\frac{y}{2(p-3)+1}\right.(M,Y)^{p-3} + \dots \left.\left.\left.\right]\right]\right]\Big]_{-z}^{L-z} dz$$

$$+ \left[\left[\frac{2pm^2}{2p+1}\right]\left[\frac{2(p-1)m^2}{2(p-1)+1}\right]\left[\frac{2(p-2)m^2}{2(p-2)+1}\right] \dots \right] \int_0^L \int_{-z}^{L-z} (M,Y)^{-\frac{1}{2}} dy dz \qquad (2.30f)$$

The series continues until the exponent (M,Y) in the last integral is (-1/2), and for this case equation (2.33) is employed to integrate the final term. With the substitution of $\left(\frac{n-4}{2}\right)$ for p, the complete result for any n value greater than 5 can be written

$$I_{\alpha 3n} = \left(\frac{1}{2R}\right) \left\{ \left[\frac{k^{n-3}}{(n-3)!}\right] + \left[\frac{k^{n-1}}{(n-1)!}\right]\left[R^2 - r^2\right] \right\} \int_0^L \left\{ \left(\frac{y}{n-3}\right)(m^2 + y^2)^{\frac{n-4}{2}} \right.$$

$$+ \sum_{i=1}^{i=\frac{(n-5)}{2}} \left[\frac{y}{n-3-2i}\right]\left[2m^2\right]^i \left[\prod_{j=1}^{j=i} \left(\frac{n-2-2j}{2n-2-4j}\right)\right]\left[m^2+y^2\right]^{\left(\frac{n-4}{2}\right)-i}$$

$$+ \left[\prod_{i=0}^{i=\left(\frac{n-5}{2}\right)} \left(\frac{n-4-2i}{2n-6-4i}\right)\right]\left[2m^2\right]^{\frac{n-3}{2}} \sinh^{-1}\left(\frac{y}{m}\right) \Big\}_{-z}^{L=z} dz \qquad (2.30g)$$

and with the limits evaluated, it becomes

$$I_{\alpha 3n} = \left(\frac{1}{2R}\right) \left\{ \left[\frac{k^{n-3}}{(n-3)!}\right] + \left[\frac{k^{n-1}}{(n-1)!}\right]\left[R^2 - r^2\right] \right\} \int_0^L \left\{ \frac{(L-z)}{(n-3)}\left[m^2+(L-z)^2\right]^{\frac{n-4}{2}} \right.$$

$$+ \left(\frac{z}{n-3}\right)\left[m^2+z^2\right]^{\frac{n-4}{2}} + \sum_{i=1}^{i=\frac{n-5}{2}} \left[\frac{1}{n-3-2i}\right]\left[\prod_{j=1}^{j=i}\left(\frac{n-2-2j}{2n-2-4j}\right)\right]\left[2m^2\right]^i\left[(L-z)\right.$$

$$\left[m^2 + (L-z)^2\right]^{\left(\frac{n-4}{2}-i\right)} + [z]\left[m^2+z^2\right]^{\left(\frac{n-4}{2}-i\right)}\right] + \left[\prod_{i=0}^{i=\left(\frac{n-5}{2}\right)}\left(\frac{n-4-2i}{2n-6-4i}\right)\right]$$

$$\left[2m^2\right]^{\frac{n-3}{2}} \left[\sinh^{-1}\left(\frac{L-z}{m}\right) + \sinh^{-1}\left(\frac{z}{m}\right)\right] \Big\} dz \qquad (2.30h)$$

Next to be performed is the integration with respect to z, which involves power functions of $[m^2 + (L-z)^2]$ and $[m^2 + z^2]$ and the inverse hyperbolic relations, $\sinh^{-1}(\frac{L-z}{m})$ and $\sinh^{-1}(\frac{z}{m})$. The former are treated directly by making the substitutions,

$$u = m^2 + (L-z)^2$$

$$du = -2(L-z)dz$$

$$v = m^2 + z^2$$

$$dv = 2zdz,$$

and integrating. The result is still a set of similar power functions. The inverse hyperbolic sines are collected and, when integrated by parts, become

$$\int_o^L \left[\sinh^{-1}(\frac{L-z}{m}) + \sinh^{-1}(\frac{z}{m})\right]dz = 2m + (2L)\ \sinh^{-1}(\frac{L}{m}) - 2(m^2+L^2)^{\frac{1}{2}} \quad (2.34)$$

Equations (2.30b),(2.30c) and (2.30h), after integration with respect to z are then summed for all values of n according to equation (2.29a) to yield the final result

$$I_{\alpha 3} = (\tfrac{1}{2R}) \left[1 + \frac{m^2 k^2}{4} + (\frac{k^2}{2} + \frac{m^2 k^4}{48})(R^2 - r^2) \right]\left[(2m) + (2L)\ \sinh^{-1}(\frac{L}{m}) \right.$$

$$\left. - 2(L^2 + m^2)^{\frac{1}{2}} \right] + (\tfrac{1}{2R})\left[\frac{k^2}{2} + (\frac{k^4}{24})(R^2 - r^2) \right]\left[\frac{1}{3} \right]\left[(m^2 + L^2)^{3/2} - m^3 \right]$$

$$+ (\tfrac{1}{2R}) \sum_{n=7}^{n=n} \left[\frac{k^{n-3}}{(n-3)!} \right] + \left[\frac{k^{n-1}}{(n-3)!} \right]\left[R^2 - r^2 \right] \left\{ \left[\frac{1}{n-3} \right]\left[\frac{2}{n-2} \right]\left[(m^2 + L^2)^{\frac{n-2}{2}} \right.\right.$$

$$\left. + (m^2)^{\frac{n-2}{2}} \right] + \sum_{i=1}^{i=(n-5)/2} \left[\frac{1}{n-3-2i} \right]\left[\prod_{j=1}^{j=i} (\frac{n-2-2j}{2n-2-4j}) \right]\left[2m^2 \right]^i \left[\frac{2}{n-2-2i} \right]$$

$$\left[(m^2 + L^2)^{\frac{(n-2-2i)}{2}} - (m^2)^{\frac{(n-2-2i)}{2}} \right] + \left[\prod_{i=0}^{i=(\frac{n-5}{2})} (\frac{n-4-2i}{2n-6-4i}) \right]\left[2n^2 \right]^{(\frac{n-3}{2})}$$

$$\left[(2m) + (2L)\ \sinh^{-1}(\frac{L}{m}) - 2(L^2 + m^2)^{\frac{1}{2}} \right] \right\} \tag{2.29b}$$

Evaluation of $I_{\alpha 4}$. The expression for $I_{\alpha 4}$ is

$$I_{\alpha 4} = (\tfrac{1}{2R}) \int_o^L \int_{-z}^{L-z} \sum_{\substack{n=4 \\ \text{even}}}^{n=n} \left\{ \left[\frac{-k^{n-3}}{(n-3)!} \right] + \left[\frac{-k^{n-1}}{(n-1)!} \right]\left[R^2 - r^2 \right] \right\}(m^2 + y^2)^{(\frac{n-4}{2})} \, dy \, dz \tag{2.35a}$$

Since n is even and larger than 2, the exponent $(n-4)/2$ is an integer. The quantity to be integrated then could be expressed with the binomial theorem as

$$(m^2 + y^2)^{(\frac{n-4}{2})} = \sum_{i=0}^{i=(\frac{n-4}{2})} \left[\frac{(\frac{n-4}{2})!}{(i)!(\frac{n-4}{2} - i)!} \right] y^{2i}(m^2)^{(\frac{n-4}{2} - i)} \tag{2.36}$$

This sum, substituted into $I_{\alpha 4}$, can be integrated directly to give

$$I_{\alpha 4} = \left(\frac{1}{2R}\right) \sum_{\substack{n=4 \\ even}}^{n=n} \left\{ \left[\frac{-k^{n-3}}{(n-3)!}\right] + \left[\frac{-k^{n-1}}{(n-1)!}\right]\left[R^2-r^2\right] \right\} \int_o^L \left\{ \sum_{i=0}^{i=\left(\frac{n-4}{2}\right)} \right.$$

$$\left. \left[\frac{\left(\frac{n-4}{2}\right)!}{(i)!\left(\frac{n-4}{2}-i\right)!(2i+1)}\right]\left[m^2\right]^{\left(\frac{n-4}{2}-i\right)}\left[(L-z)^{2i+1} + (z)^{2i+1}\right] \right\} dz \quad (2.35b)$$

Likewise the integration with respect to z can be readily accomplished, the final result being

$$I_{\alpha 4} = \left(\frac{1}{2R}\right) \sum_{\substack{n=4 \\ even}}^{n=n} \left\{ \left[\frac{-k^{n-3}}{(n-3)!}\right] + \left[\frac{-k^{n-1}}{(n-1)!}\right]\left[R^2-r^2\right] \right\}$$

$$\left\{ \sum_{i=0}^{i=\left(\frac{n-4}{2}\right)} [2]\left[\frac{\left(\frac{n-4}{2}\right)!}{(i)!\left(\frac{n-4}{2}-i\right)!}\right]\left[\frac{1}{2i+1}\right]\left[\frac{1}{2i+2}\right]\left[m^2\right]^{\left(\frac{n-4}{2}-i\right)} \right.$$

$$\left. \left[L\right]^{2i+2} \right\} \quad (2.35c)$$

Integrations for I_β (See equation 2.24)

The evaluation of the function I_β is very similar to that for I_α. The result is somewhat different, however, because of the y^2 term in the integral which is

$$I_\beta = -\left(\frac{1}{2R}\right) \int_o^L \int_{-z}^{L-z} \sum_{n=1}^{n=n} \left[\frac{(-k)^{n-1}}{(n-1)!}\right]\left[y^2\right]\left[m^2+y^2\right]^{\left(\frac{n-4}{2}\right)} dy\, dz \quad (2.37a)$$

As before, it is necessary to treat the first two terms individually. The remaining ones can then be integrated by parts. This operation produces a set of integrals exactly like those for $I_{\alpha 3}$ and $I_{\alpha 4}$ except for the coefficients. The integrations for these situations are therefore combined.

Evaluation of $I_{\beta 1}$ and $I_{\beta 2}$. The expression for $I_{\beta 1}$ is

$$I_{\beta 1} = -(\frac{1}{2R}) \int_{o}^{L} \int_{-z}^{L-z} \frac{y^2}{(m^2+y^2)^{3/2}} \, dy \, dz \qquad (2.38a)$$

which by use of a formula from a standard set of integral tables becomes

$$I_{\beta 1} = -(\frac{1}{2R}) \int_{o}^{L} \left[\frac{-y}{(m^2+y^2)^{1/2}} + \ln\left[y+(m^2+y^2)^{1/2} \right] \right] \Bigg|_{-z}^{L-z} \, dz$$

$$= -(\frac{1}{2R}) \int_{o}^{L} \left\{ \frac{-(L-z)}{[m^2+(L-z)^2]^{1/2}} + \sinh^{-1}(\frac{L-z}{m}) \right.$$

$$\left. - \frac{z}{(m^2+z^2)^{1/2}} + \sinh^{-1}(\frac{z}{m}) \right\} \, dz \qquad (2.38b)$$

The terms containing square roots integrate directly, while the parts formula was required for the inverse hyperbolic sines. After intermediate operations and simplifications, the final result is

$$I_{\beta 1} = -(\frac{1}{R})\left[2m-2(m^2+L^2)^{1/2} + (L)\sinh^{-1}(\frac{L}{m}) \right] \qquad (2.38c)$$

The second term of the series, $I_{\beta 2}$, is

$$I_{\beta 2} = -(\frac{1}{2R}) \int_{o}^{L} \int_{-z}^{L-z} \frac{-ky^2}{(m^2+y^2)} \, dy \, dz \qquad (2.39a)$$

The evaluation of this term is straightforward and almost like the one above. The results for the two integrals are

$$I_{\beta 2} = +(\frac{k}{2R}) \int_{o}^{L} \left[(L-z) - (m)\tan^{-1}(\frac{L-z}{m}) + z - (m)\tan^{-1}(\frac{z}{m}) \right] \, dz \qquad (2.39b)$$

and

36

$$I_{\beta 2} = + \left(\frac{k}{2R}\right) \left[L^2 - (2mL)\tan^{-1}\left(\frac{L}{m}\right) + (m^2) \ln\left(1 + \frac{L^2}{m^2}\right) \right] \qquad (2.39c)$$

I_β Terms for $n > 2$. The general expression for I_β is given by equation (3.37a). With n larger than 2 the relationship can be integrated by parts, the parts formula being

$$\int u\,dv = uv - \int v\,du \qquad (2.40)$$

With $u = y$ and $dv = (m^2 + y^2)^{(n-4)/2} y\,dy$, the required integration is

$$I_{\beta,n>2} = -\left(\frac{1}{2R}\right) \sum_{n=3}^{n=n} \left[\frac{(-k)^{n-1}}{(n-1)!}\right] \left\{ \int_0^L \left(\frac{y}{2}\right) \left[\frac{(m^2+y^2)^{\frac{n-4}{2}+1}}{\frac{n-4}{2}+1}\right] \Bigg|_{-z}^{L-z} dz \right.$$

$$\left. - \left(\frac{1}{2}\right) \int_0^L \int_{-z}^{L-z} \frac{(m^2+y^2)^{\frac{n-4}{2}+1}}{\frac{n-4}{2}+1} \, dy\,dz \right\} \qquad (2.37b)$$

Evaluation of the limits gives

$$I_{\beta,n>2} = -\left(\frac{1}{2R}\right) \sum_{n=3}^{n=n} \left[\frac{(-k)^{n-1}}{(n-1)!}\right] \int_0^L \left\{ \left(\frac{L-z}{2}\right) \left[\frac{[m^2+(L-z)^2]^{\frac{n-4}{2}+1}}{\frac{n-4}{2}+1}\right] \right.$$

$$\left. + \left(\frac{z}{2}\right) \left[\frac{[m^2+z^2]^{\frac{n-4}{2}+1}}{\frac{n-4}{2}+1}\right] \right\} dz + \left(\frac{1}{2R}\right) \sum_{n=3}^{n=n} \left[\frac{(-k)^{n-1}}{(n-1)!}\right] \int_0^L \int_{-z}^{L-z}$$

$$\left(\frac{1}{2}\right) \left[\frac{(m^2+y^2)^{\frac{n-4}{2}+1}}{\frac{n-4}{2}+1}\right] dy\,dz \qquad (2.37c)$$

The single integral of this result can be further integrated to give

$$I_{\beta, n > 2} = - \left(\frac{1}{4R}\right) \sum_{n=3}^{n=n} \left[\frac{(-k)^{n-1}}{(n-1)!}\right]\left[\frac{1}{(\frac{n-4}{2}+1)(\frac{n-4}{2}+2)}\right]\left[(m^2+L^2)^{\frac{n-4}{2}+2}\right.$$

$$\left. - (m^2)^{\frac{n-4}{2}+2}\right] + \left(\frac{1}{4R}\right) \sum_{n=3}^{n=n} \left[\frac{(-k)^{n-1}}{(n-1)!}\right] \int_0^L \int_{-z}^{L-z}$$

$$\left[\frac{(m^2+y^2)^{\frac{n-4}{2}+1}}{\frac{n-4}{2}+1}\right] dy\,dz \qquad (2.37d)$$

At this point, there remain the integrals that arise from use of the parts formula. Fortunately, however, their solutions can be obtained from the I_α integrals. The similarity between equation (2.37d) and the previous integrals is demonstrated by redesignating the summations variable as $j = n+2$. The relationship becomes

$$I_{\beta, n > 2} = - \left(\frac{1}{4R}\right) \sum_{j=5}^{j=j} \left[\frac{(-k)^{j-3}}{(j-3)!}\right]\left[\frac{1}{(\frac{j-4}{2})(\frac{j-6}{2})}\right]\left[(m^2+L^2)^{(\frac{j-4}{2})} - (m^2)^{\frac{j-4}{2}}\right]$$

$$+ \left(\frac{1}{2R}\right) \sum_{j=3}^{j=j} \left[\frac{(-k)^{j-3}}{(j-3)!}\right] \int_0^L \int_{-z}^{L-z} \left(\frac{1}{2}\right) \left[\frac{(m^2+y^2)^{(\frac{j-4}{2})}}{(\frac{j-4}{2})}\right] dy\,dz \qquad (2.37e)$$

The integrals then in terms of j are, except for the coefficients, identical to those in equations (2.29a) and (2.35a) for $I_{\alpha3}$ and $I_{\alpha4}$, respectively. This condition means that the series of terms to be integrated in equation (3.37) is the same as the I_α series beginning with its third term. Since equation (2.37e) is to be integrated for $n = 3$ to $n = n$, the result can be obtained by using the I_α series from its 5th term to its n+2nd term. This series, then, with the

38

coefficients of the terms modified as by equation (3.36e) gives the required integral. The results are given in the following summary of the y and z integrations.

Summary of First Two Integrations

After the first two integrations, the relationship describing the function I can be expressed as

$$I = (I_{\alpha 1} + I_{\alpha 2} + I_{\alpha 3} + I_{\alpha 4}) + (I_{\beta 1} + I_{\beta 2} + I_{\beta, n > 2}) \qquad (2.41)$$

where the subscripted I-functions are:

$$I_{\alpha 1} = (\frac{1}{R})(\frac{R^2 - r^2}{m^2})\left[(m^2 + L^2)^{\frac{1}{2}} - m\right]$$

$$I_{\alpha 2} = \frac{(-k)(R^2 - r^2)}{2mR}\left[(2L)\tan^{-1}(\frac{L}{m}) - (m)\ln(1 + \frac{L^2}{m^2})\right]$$

$$I_{\alpha 3} = (\frac{1}{2R})\left[1 + \frac{m^2 k^2}{4} + (\frac{k^2}{2} + \frac{m^2 k^4}{48})(R^2 - r^2)\right]\left[(2m) + (2L)\sinh^{-1}(\frac{L}{m}) - 2(L^2 + m^2)^{\frac{1}{2}}\right]$$

$$+ (\frac{1}{2R})\left[\frac{k^2}{2} + \frac{k^4}{24}(R^2 - r^2)\right]\left[\frac{1}{3}\right]\left[(m^2 + L^2)^{3/2} - m^3\right] + (\frac{1}{2R})\sum_{\substack{n=7 \\ \text{odd}}}^{n=n} \left\{ \left[\frac{k^{n-3}}{(n-3)!}\right]\right.$$

$$+ \left[\frac{k^{n-1}}{(n-1)!}\right]\left[R^2 - r^2\right] \right\} \left\{ \left[\frac{1}{n-3}\right]\left[\frac{2}{n-2}\right]\left[(m^2 + L^2)^{(\frac{n-2}{2})} - (m^2)^{(\frac{n-2}{2})}\right]\right.$$

$$+ \sum_{i=1}^{i=(\frac{n-5}{2})} \left[\frac{1}{n-3-2i}\right]\prod_{j=1}^{j=i}(\frac{n-2-2j}{2n-2-4j})\left[2m^2\right]^i\left[\frac{2}{n-2-2i}\right]\left[(m^2 + L^2)^{(\frac{n-2-2i}{2})}\right.$$

$$\left. - (m^2)^{(\frac{n-2-2i}{2})}\right] + \left[\prod_{i=0}^{i=(\frac{n-5}{2})}(\frac{n-4-2i}{2n-6-4i})\right]\left[2m^2\right]^{(\frac{n-3}{2})}\left[(2m) + (2L)\sin^{-1}(\frac{L}{m})\right.$$

$$\left. - 2(L^2 + m^2)^{\frac{1}{2}}\right] \right\}$$

39

$$I_{\alpha 4} = (\tfrac{1}{2R}) \sum_{\substack{n=4 \\ \text{even}}}^{n=n} \left\{ \left[\frac{-k^{n-3}}{(n-3)!}\right] + \left[\frac{-k^{n-1}}{(n-1)!}\right]\left[R^2-r^2\right] \right\} \left\{ \sum_{i=0}^{i=(\frac{n-4}{2})} [2] \left[\frac{(\frac{n-4}{2})!}{(i)!(\frac{n-4}{2}-i)!}\right] \right.$$

$$\left. \left[\frac{1}{2i+1}\right]\left[\frac{1}{2i+2}\right]\left[m^2\right]^{(\frac{n-4}{2}-i)}[L]^{2i+2} \right\}$$

$$I_{\beta 1} = -(\tfrac{1}{R})[2m-2(m^2+L^2)^{\frac{1}{2}} + (L)\sinh^{-1}(\tfrac{L}{m})]$$

$$I_{\beta 2} = + (\tfrac{k}{2R})[L^2-(2mL)\tan^{-1}(\tfrac{L}{m}) + (m^2)\ln(1+\tfrac{L^2}{m^2})]$$

$$I_{\beta,(n>2)} = (-\tfrac{1}{4R}) \sum_{n=3}^{n=n} \left[\frac{-k^{n-1}}{(n-1)!}\right]\left[\frac{4}{n(n-2)}\right]\left[(m^2+L^2)^{\frac{n-4}{2}+2} - (m^2)^{\frac{n-4}{2}+2}\right]$$

$$+ (\tfrac{1}{4R})(\tfrac{k^2}{2})(2) \left\{ (\tfrac{1}{3})\left[(m^2+L^2)^{3/2}-m^3\right] + \left[\frac{m^2}{2}\right]\left[2m+(2L)\sinh^{-1}(\tfrac{L}{m})\right.\right.$$

$$\left.\left. - 2(L^2+m^2)^{\frac{1}{2}}\right]\right\} + (\tfrac{1}{4R}) \sum_{\substack{n=5 \\ \text{odd}}}^{n=n} \left[\frac{k^{n-1}}{(n-1)!}\right]\left[\frac{2}{n-2}\right] \left\{ \left[\frac{2}{(n)(n-1)}\right] \right.$$

$$\left[(m^2+L^2)^{\frac{1}{2}} - (m^2)^{\frac{1}{2}}\right] + \sum_{i=1}^{i=\frac{n-3}{2}} \left[\frac{1}{n-1-2i}\right]\left[\prod_{g=1}^{g=i}(\frac{n-2g}{2n+2-4g})\right]$$

$$(2m^2)^i \left[\frac{2}{n-2i}\right]\left[(m^2+L^2)^{\frac{n-2i}{2}} - (m^2)^{\frac{n-2i}{2}}\right] + \left[\prod_{i=0}^{i=\frac{n-3}{2}}(\frac{n-2-2i}{2n-2-4i})\right]$$

$$\left[2m^2\right]^{\frac{n-1}{2}}\left[2m+(2L)\sinh^{-1}(\tfrac{L}{m}) - 2(L^2+m^2)^{\frac{1}{2}}\right]\right\} + (\tfrac{1}{4R}) \sum_{\substack{n=4 \\ \text{even}}}^{n=n}$$

$$\left[\frac{-k^{n-1}}{(n-1)!}\right]\left[\frac{2}{n-2}\right] \sum_{i=0}^{i=\frac{n-2}{2}} [2]\left[\frac{(\frac{n-2}{2})!}{(i)!(\frac{n-2}{2}-i)!}\right]\left[\frac{1}{2i+1}\right]\left[\frac{1}{2i+2}\right]$$

$$\left[m^2\right]^{\frac{n-2}{2}+i}[L]^{2i+2}$$

Integration With Respect to Ψ

At this point in the development, a numerical solution must be sought since the integrand of equation (2.19) does not readily lend itself to further analytical operations. Also, it becomes desirable to solve the problem on a digital computer and to make numerical evaluations for the final integration variables.

The numerical integrations were accomplished by applying an appropriately selected member of the closed type Newton-Cotes quadrature formulae. These formulae,[33] under the proper conditions, represent quite accurately the integral of a function with respect to one of its variables provided the value of the function is known for several equally spaced values of the integration variable. The specific formula employed for the numerical computations was

$$\int_{x_1}^{x_2} y \, dx = \frac{6h}{840} (41y_0 + 216y_1 + 27y_2 + 272y_3 + 27y_4$$
$$+ 216y_5 + 41y_6) - \frac{9y^{(8)}h^9}{1400} \tag{2.42}$$

which was found to give accurate results with an acceptable amount of numerical work. In this equation, y, symbolizes a function to be integrated and the subscripted y variables represent the ordinates of the function at seven uniformly spaced values of the independent variable, indicated by x. The interval between ordinates is h. The symbols, x and h, in this particular problem represent Ψ and $\Delta\Psi$ respectively. The quantity, $9y^{(8)}h^9/1400$, is the error incurred by use of the formula, where $y^{(8)}$ is the eighth derivative of the function with respect to the variable of integration. If the interval is small (h^9, small) and the

function is not exceedingly irregular ($y^{(8)}$ known everywhere to be small) the integral for most practical purposes may be considered exact.[34] These conditions were met except for r and Ψ simultaneously approaching R and zero, respectively. This case is treated separately.

To execute the numerical calculations, a set of values for the radiation system must be chosen. Since the theoretical work was intended to be complemented by an experimental investigation, initial calculations were made for variables applying to the experimental system. Specifically, these were a tube diameter of 0.043 ft., a length of 1.04 ft., and appropriately selected k (attenuation coefficient) values of 0.5, 1.0, 4.0, and 5.0 ft.$^{-1}$, these being of primary interest to the experimental study. Later, these constants were varied to study their effect on the final solution.

With the above constants assigned, the development may be continued by treating the terms of equation (2.41), according to the following arrangement:

$$J = 2 \int_{0}^{\pi} \left\{ \left[\frac{R^2 - r^2}{Rm^2} \right] \left[m^2 + L^2 \right]^{\frac{1}{2}} - \left[\frac{R^2 - r^2}{Rm} \right] - \left[\frac{m}{R} \right] + \left[\frac{(m^2 + L^2)^{\frac{1}{2}}}{R} \right] \right\} d\Psi$$

$$+ 2 \int_{0}^{\pi} \left[\sum (\text{Remaining Terms}) \right] d\Psi \qquad (2.43a)$$

or with abbreviated notation,

$$J = 2 \int_{0}^{\pi} (I_1) d\Psi + 2 \int_{0}^{\pi} (I_\Sigma) d\Psi \qquad (2.43b)$$

and

$$J = J_1 + J_\Sigma \qquad (2.43c)$$

42

where the integration for Ψ is defined by equation (2.19). Inspection of the equation shows that these separate integrals have special significance. I_1 is the collection of terms not having a k-coefficient and, hence, represents a pseudo view-factor between the radiating wall and the absorbing particles. Physically, the result from the treatment of I_1 may be envisioned as an evaluation of the total direct transfer of heat with no particle shading. This function also has the characteristic of being undefined for m = 0; it requires special treatment. The second integral, I_Σ, represents the effect of radiant energy attenuation by particle shading. Since attenuation reduces the exposure of the particle cloud, J_Σ is always negative and subtracts from J_1. Finally, I_Σ is defined for all values of m and its numerical evaluation is much different for computer programming than it was for I_1.

Numerical calculations were initiated with the evaluation of the attenuation function, J_Σ, which, as previously denoted, was accomplished by use of equation (2.42). The procedure using the integral formula to establish the final result was to calculate ordinates (I_Σ) at seven uniformly spaced values of Ψ within the range of Ψ across which the integration was being performed and to incorporate these ordinates in the integral formula. The range of values of Ψ across which the formula was applied was variable, and the procedure could be repeated as many times as required to yield the accuracy desired, i.e., the increment h (or $\Delta\Psi$) of the error function was arbitrary. For this investigation, the integral formula was applied twice, once in each interval $0 \leq \Psi \leq \pi/2$ and $\pi/2 \leq \Psi \leq \pi$, and the total integral was the sum of the results for each interval.

Calculated results for I_Σ applying to the experimental system are presented in Figures 7 through 10. The data are given for radii of 0.0, 0.25R, 0.50R, 0.75R, and 1.00R since results for these points were required for the final integration with respect to radius. The functional behavior of the I_Σ curves shown on the figures was employed in studying the correctness of the first two integrations (y and z) which resulted in a lengthy, complex function. Physically, the I_Σ curves represent the attenuation within an elemental volume receiving radiation from a wall element where the linear dimension of each element along the axis of the cylinder has been integrated; the magnitude of the ordinates are measures of the associated reductions in radiation intensity of rays passing through the absorbing element. The numerical values, although being for the experimental system, are generalized results, since they are functions of L/R, the attenuation coefficient k, and the cylinder radius R. The magnitude of the parameter kR (attenuation coefficient times the radius) relative to unity affects the appearance of the curves, however. The influence of the parameter is subsequently discussed. The results presently considered are for small kR values of 0.1 and less. As shown by the figures, there is no angular dependence for r = 0, as would be expected. At r = R, on the other hand, the attenuation is greatest when the two differential elements are diametrically opposed ($\Psi = \pi$) and monotonically decreases with Ψ until the element occupies the same position ($\Psi = 0$). At that point, there is no attenuation within the differential volume. At intermediate radii, the attenuation, conversely, is largest at $\Psi = 0$, and is a minimum at some angle, Ψ_m. The angle at which the minima occur is a function of radius and attenuation coefficient. The
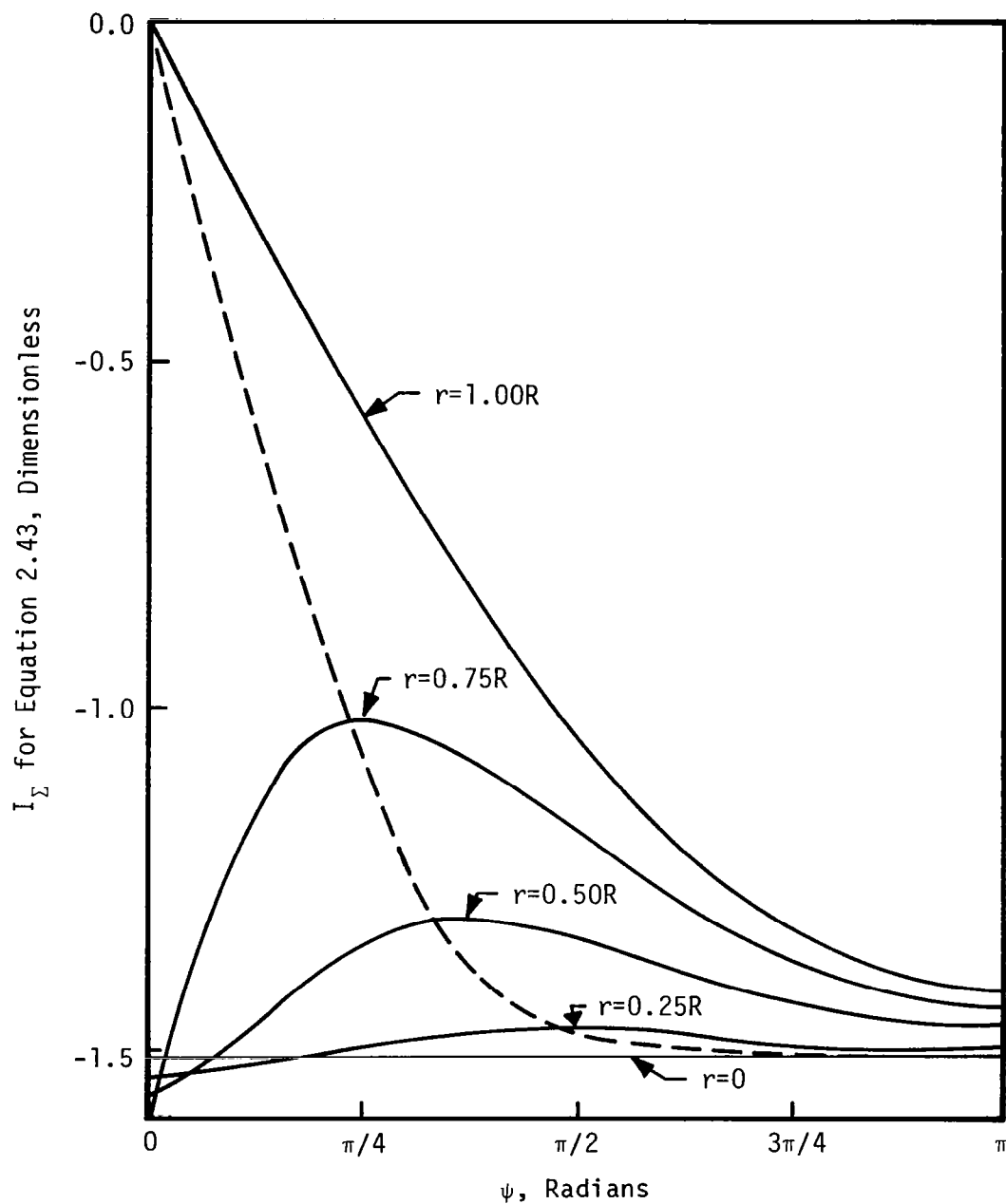
Figure 7. I_Σ as Function of ψ and Radial Position for $k = 0.5$.
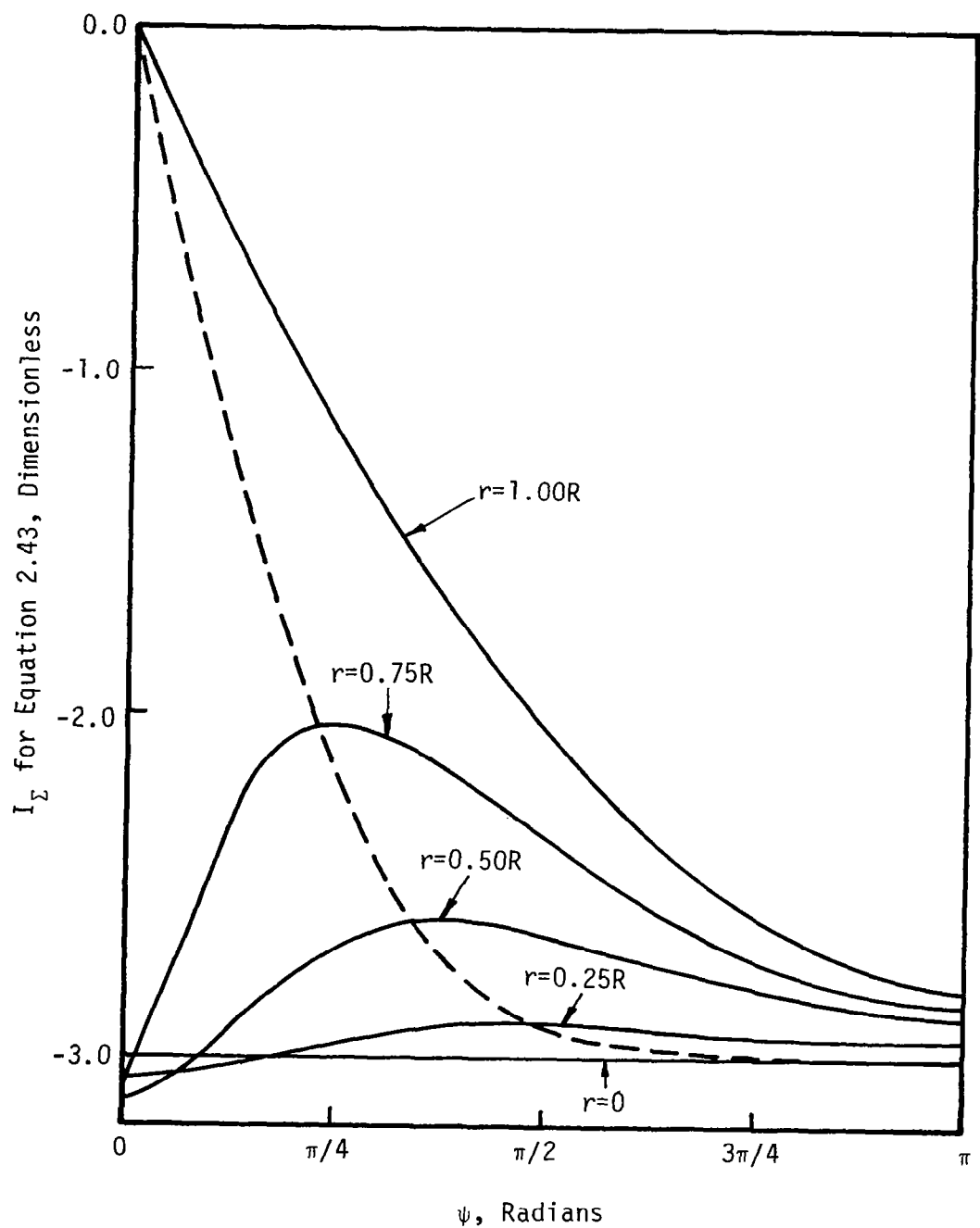
Figure 8. I_Σ as Function of ψ and Radial Position for k= 1.0.
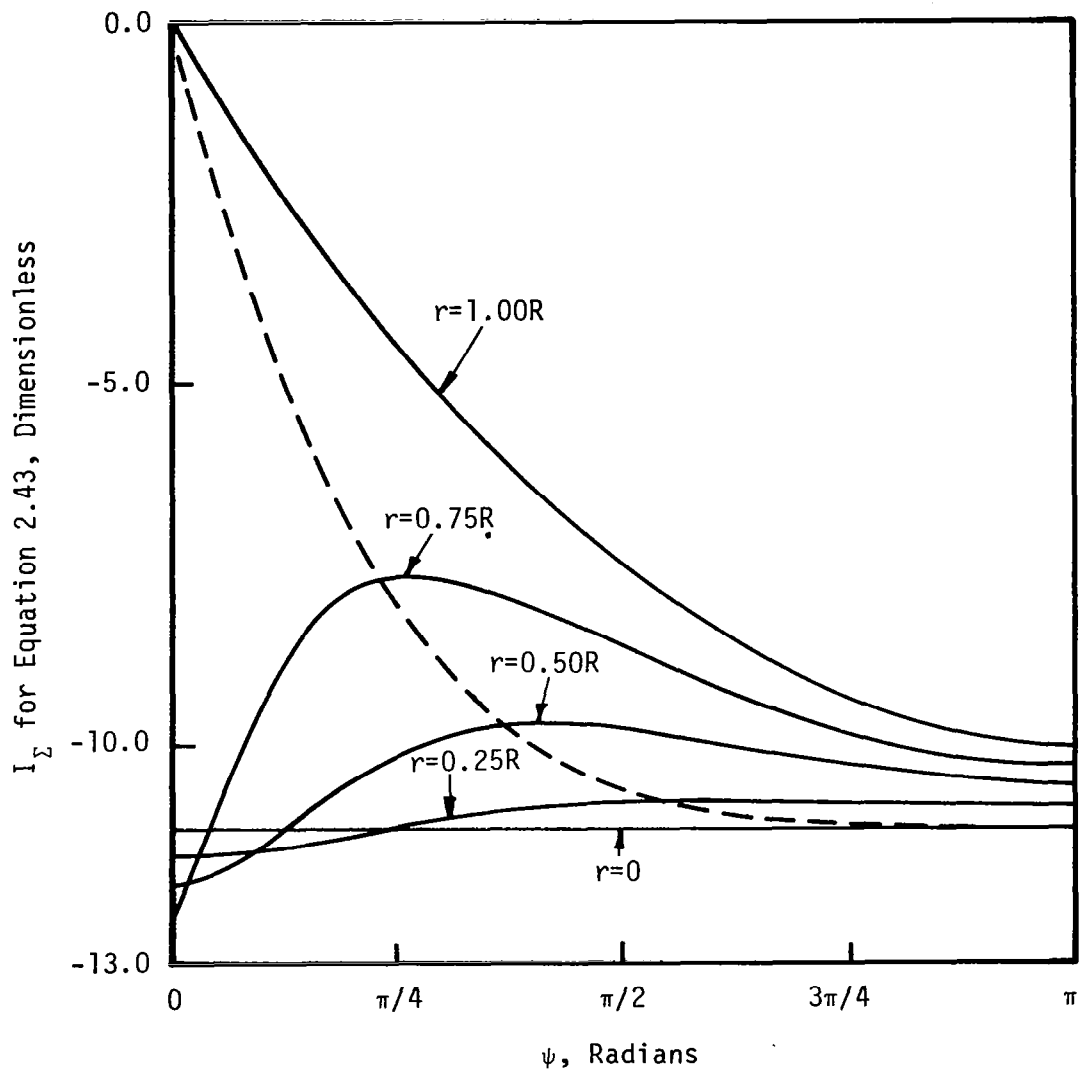
Figure 9. I_Σ as Function of ψ and Radial Position for k= 4.0.

47
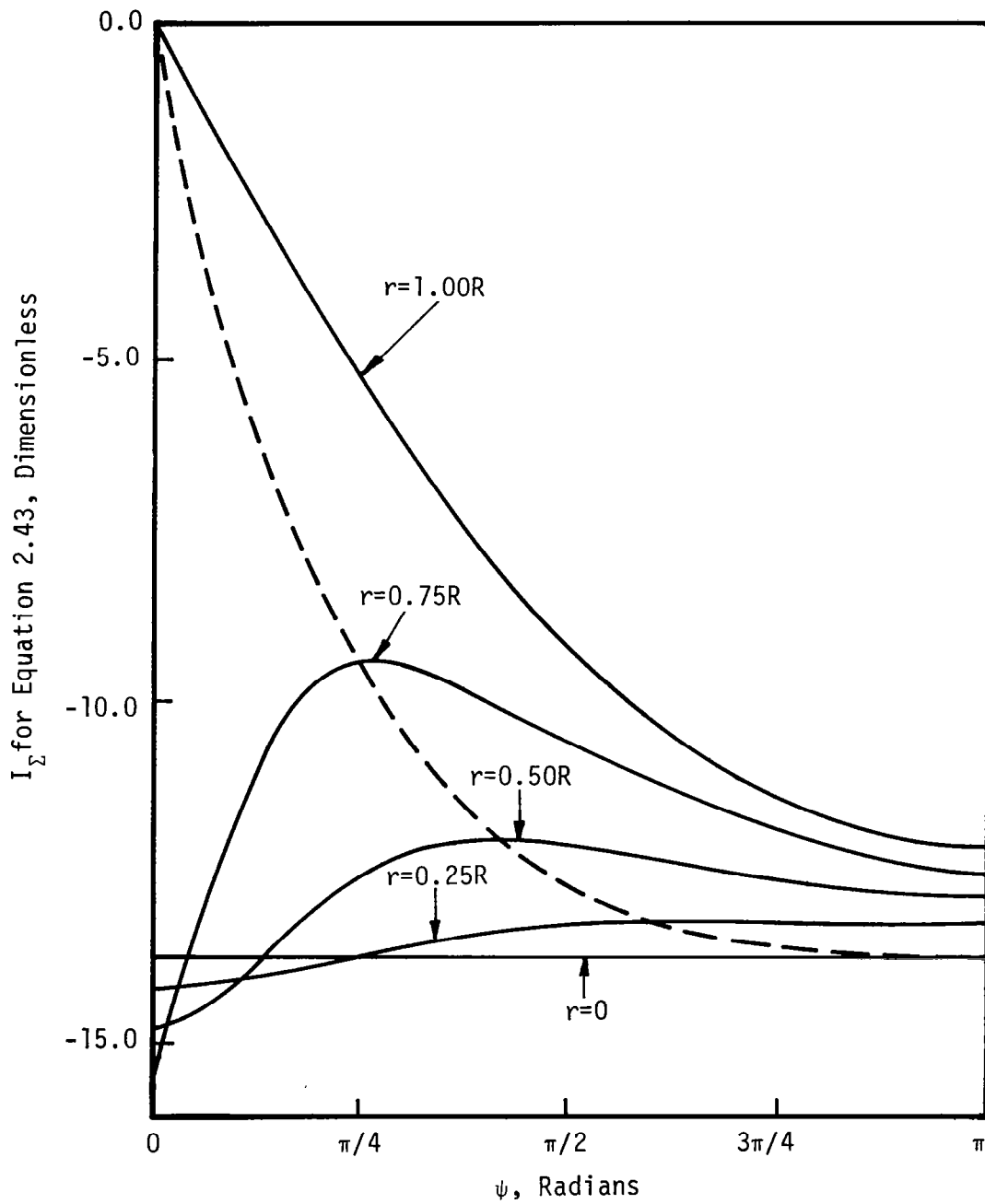
Figure 10. I_Σ as Function of ψ and Radial Position for k= 5.0.

loci of these points are indicated on the figures by dotted lines.

That the attenuation should be largest at the point of nearest approach might, at first, seem illogical. This is correct, however, for attenuation is a first order process, as evidenced by the applicability of Beer's law, i.e., $i_x = i_o e^{-kx}$. Hence the decrement of radiation within a differential volume is proportional to the intensity ($di_x = -ki_x dx$). Since the intensity of a beam is largest at $\Psi = 0$, the attenuation there is a maximum for all radii. This maximum for the $r = R$ curve is $-\pi kL$, but, because of reasons given below, this particular curve must pass through zero first and the $-\pi kL$ limit has no significance.

The skewed, sinusoidal behavior of the I_Σ curves for constant radius is due to Lambert's cosine law. Hence, when $\cos\beta_w$ decreases the radiant intensity of a beam must be reduced and, because of first-order behavior, the attenuation is decreased. The minimum attenuation then occurs where $\cos\beta_w$ is the smallest. This position is located where the radiant beam is tangent to the radial circle being considered. On either side of this value the angle β_w must decrease thus giving a larger intensity ($i_{b\beta w} = i_{bnw} \cos\beta_w$). The loci of these minima are given by

$$\Psi_m' = \cos^{-1}\left(\frac{r}{R}\right) \tag{2.44}$$

The angular function described by equation (2.44), however, is not the only factor in determining the position of minimum attenuation. It may be seen from the figures that the actual minimum attenuation occurs at a larger angle than the Ψ_m' predicted by equation (2.44). For example, when k is -5.0, and $r = 0.50R$, the minimum should be at $\pi/3$,

but is actually at $5\pi/12$. Further inspection of the curves show that the discrepancy is a function of k and r. At large r and small k values, equation (2.44) approximates the correct result very closely; as r approaches zero, however, the equation does not hold at all as the minimum attenuation point approaches π. The shift in the angle giving smallest attenuation to values larger than predicted by equation (2.44) is due to the first order dependence of attenuation on the distance between the emitting wall element and the differential volume of absorbing aerosol. Equation (2.44), then, is exact for constant intensity but it must be amended for decreasing intensity with distance. The exact effects of changing intensity are not readily calculable; it is apparent, however, that the angular dependence is dominant for large radii $(r \to R)$ while for small radii $(r \to 0)$ the distance of separation is more important. Each of the factors are completely controlling for r = R and r = 0, respectively. Special attention should be given to the fact that at r = R the angle with minimum attenuation is exactly zero and that the curve steadily decreases with Ψ and approaches zero as a limit. At $\Psi = 0$ and r = R, there is also a discontinuous limit of $-\pi kL$, but this point is of no consequence in evaluating the area between the r = R curve and the axis. The $-\pi kL$ point is the limit that all other radial curves approach with increasing r and decreasing Ψ.

The distance between the two elemental areas exchanging radiation influences the above particular results for Figures 7 through 10 slightly, since the parameter kR is small. The curves are characteristically determined by the angular function given by equation (2.44). When kR

is large, however, attenuation, as it is affected by the distance of separation, dominates the result and its dependence on Ψ is almost completely obscured. Some residual dependence on the angle remains near the radiating wall element. Supplementary calculations are presented in Figures 11 and 12 to emphasize these characteristics. There it may be observed that for small values of Ψ the curves behave similar to those already described for small kR. As Ψ or r changes so as to separate further the radiating wall element and the absorbing volume element, the energy attenuated by the latter is drastically reduced because of the rapidly decreasing intensity therein received. Hence, the curves for any radius approach zero with increasing ψ . It will also be noted that the position of the r = 0 curve is relatively much closer to the axis for very large kR values. The minimum ordinate for all curves (except r→R) is at $\Psi = \pi$.

When the I_Σ functions are integrated with respect to Ψ the result again has physical significance and may be thought of as being the energy attenuated from radiation passing through a cylindrical shell with length L, radius r, and thickness dr. The calculated results designated as J_Σ are given in Figure 13. There it may be observed from the magnitude of the ordinates that shells near the center of the tube screen more energy per unit circumferential length than shells near the wall. This result must be interpreted on a per unit length basis since the variation of r (or circumference) is yet to be considered (next integration). Again the numerical data for the J_Σ calculations really pertain to the experimental system but were employed as generalized functions of L/R and k values, and radial position.
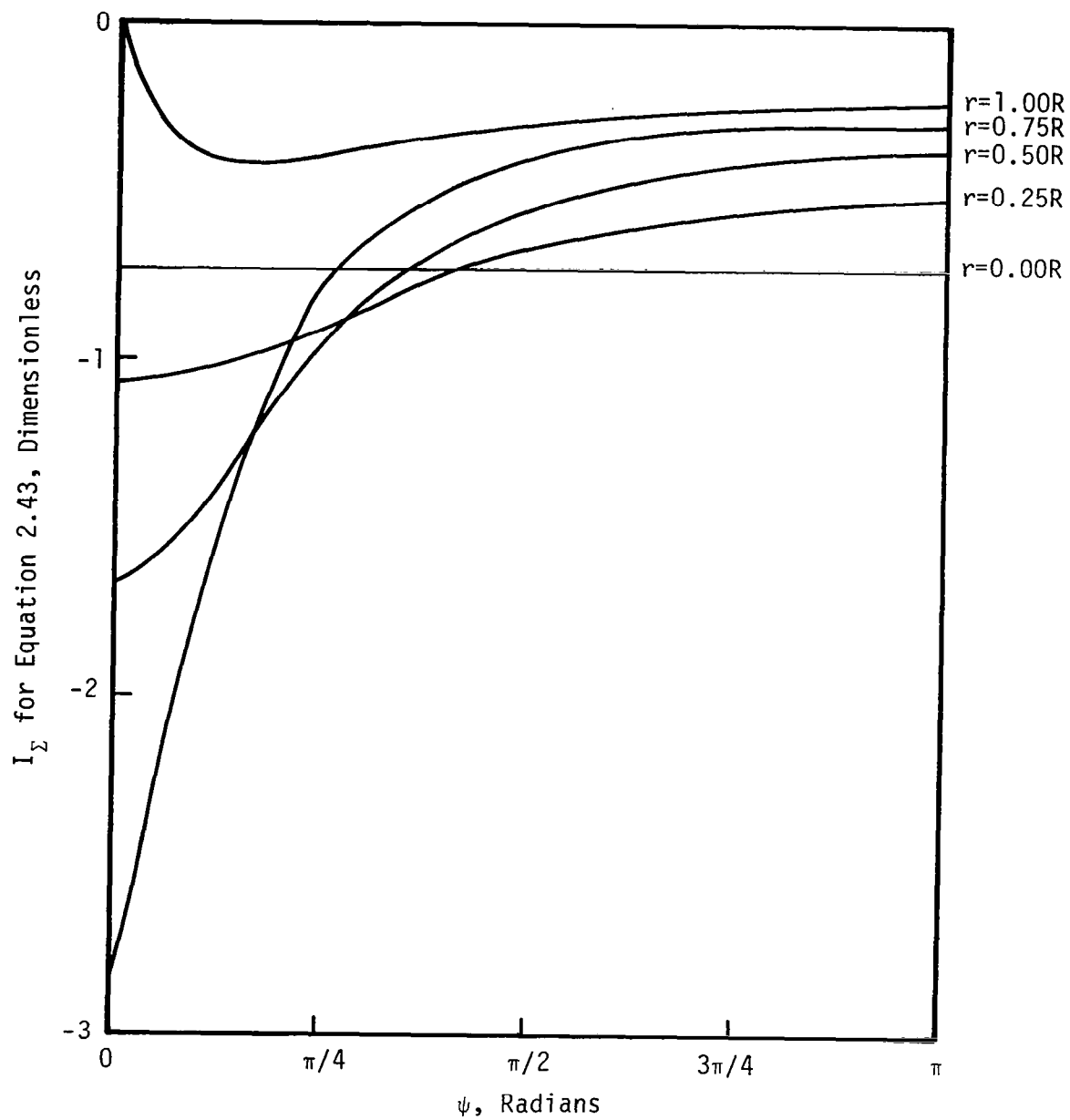
Figure 11. I_Σ as Function of ψ and Radial Position for kR= 2.0.
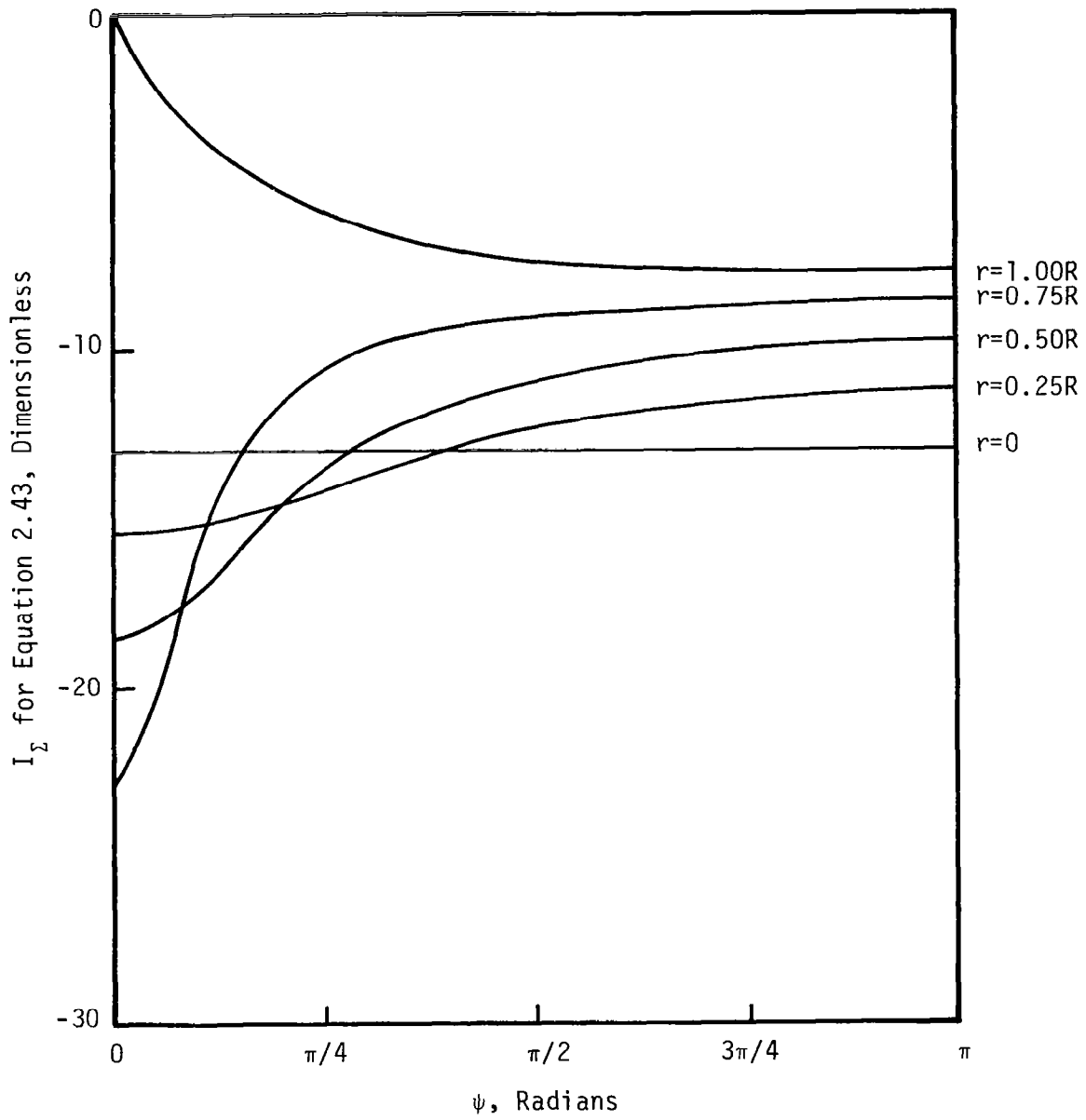
Figure 12. I_Σ as Function of ψ and Radial Position for kR= 1.0
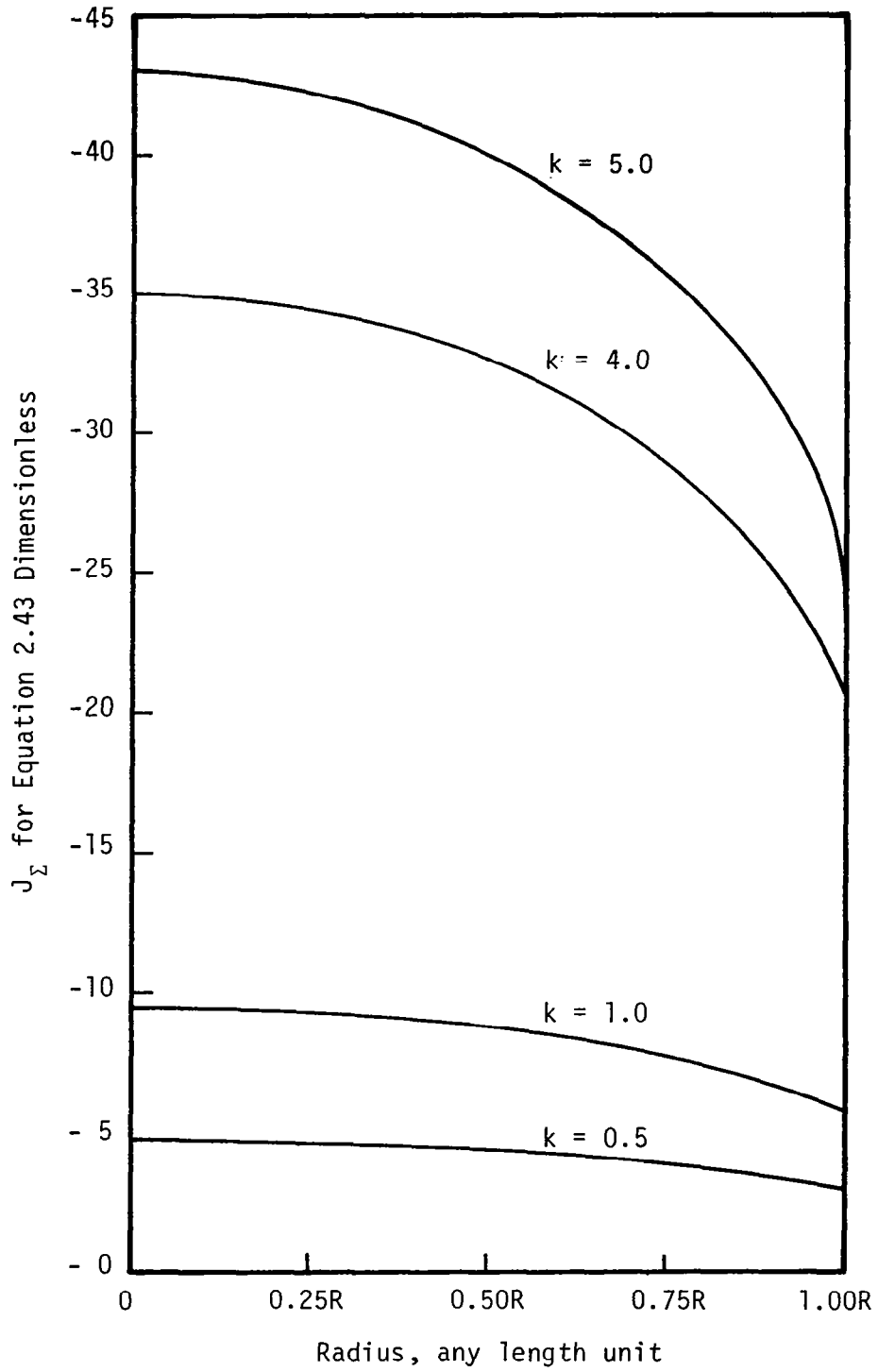
Figure 13. J_Σ as Function of ψ and Radial Position and Attenuation Coefficients.

The evaluation of the J_1 integral is more involved than J_Σ because the function becomes undefined for Ψ approaching zero and the numerical procedure using equation (2.42) becomes invalid. The situation can be overcome, to some extent, by reducing the $\Delta\Psi$ interval and using more applications of the integration formula. Ultimately, however, the limiting case, where m vanishes, requires a complementary analytical analysis. The characteristics of the integrand (I_I) curves are demonstrated in Figure 14. They are functions of L/R and R only. On the figure the curves may be noted as being elliptic with the centerline; the r = R curve is a special, limiting case. While the data shown are for a particular (L/R) of 50, it may be demonstrated from equation (2.42) that the curves are functions of Ψ and (L/R) and the configurations given are general. For smaller (L/R) ratios, however, the ordinates for small Ψ are not quite as large and the nearly horizontal portions of the curves ($r \neq 0$) are less pronounced. The function I_1 for r = R is undefined at $\Psi=0$; and at $\Psi = \pi$, it has the value $\left[\sqrt{\left(\frac{L}{R}\right)^2 + 4} - 2 \right]$.

The procedure for evaluating the integral of I_I with respect to Ψ was to begin operations with r = 0 and to modify the calculations for handling the erratic behavior with increasing radius. At r = 0 the integral, equation (2.43a), readily reduces to

$$J_{1,r=0} = \frac{4}{R} \int_0^\pi \left[(R^2+L^2)^{\frac{1}{2}} - R \right] d\Psi \tag{2.45}$$

and

$$J_{1,r=0} = \frac{4\pi}{R} \left[(R^2+L^2)^{\frac{1}{2}} - R \right] \tag{2.46}$$
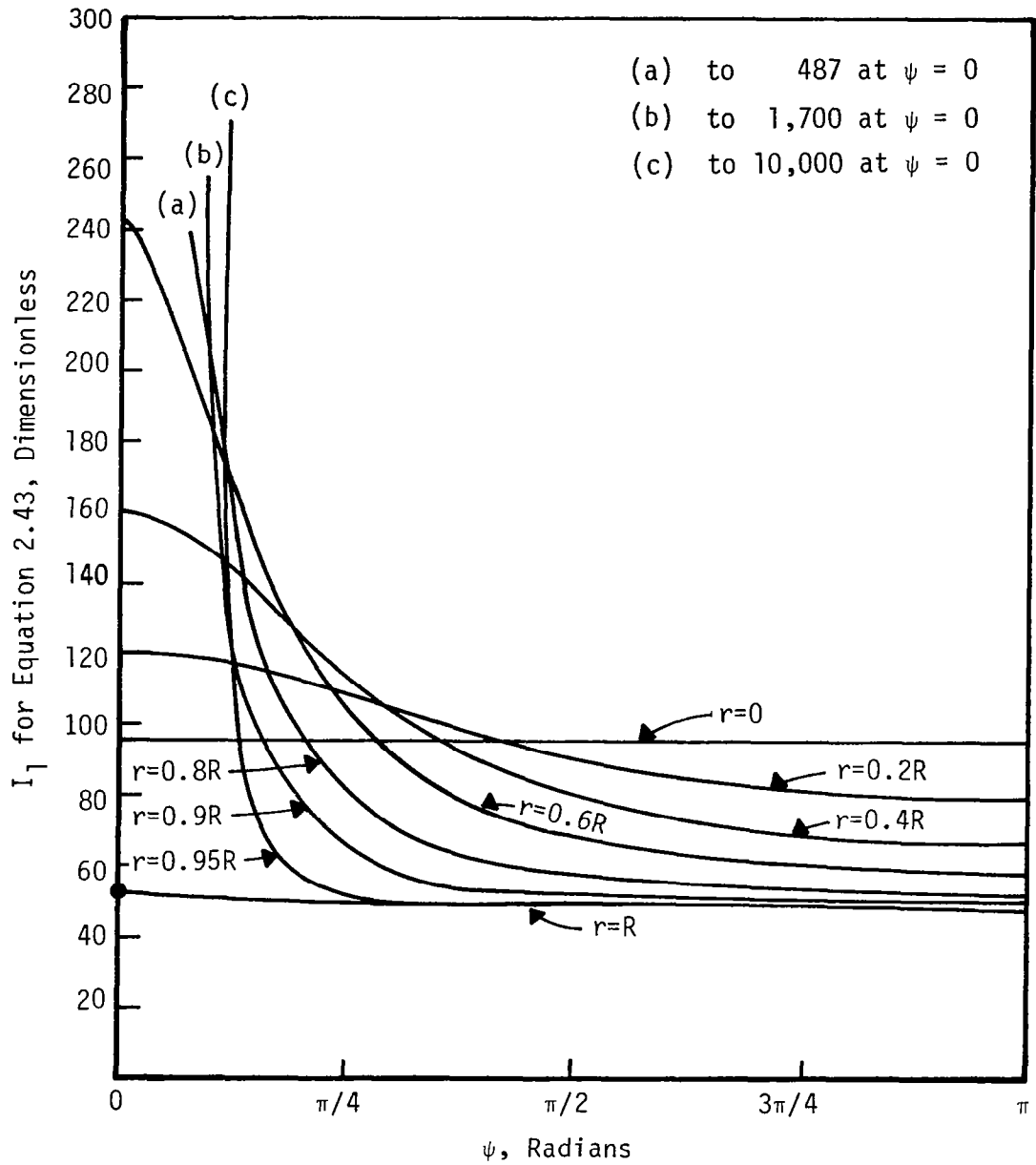
Figure 14. I_1 as Function of ψ and Radial Position.

All other radial positions require numerical treatment and, as before, for the calculation of J_Σ, the Newton-Cotes numerical integration formula, equation (2.42), was employed. For the range of radii $0 \leq r \leq 0.6R$, the integral formula was applied eight times to cover the angular range of Ψ from zero to π, and calculations of J_1 were made for radii of 0.1R, 0.2R, 0.3R, 0.4R, 0.5R, and 0.6R. At still larger radii, calculations of J_1 were made for equally spaced radial values of 0.66R, 0.73R, 0.86R, and 0.93R. The integral formula was used here eight times in each of the angular intervals $0 \leq \Psi \leq 0.05$, $0.05 \leq \Psi \leq 0.1$, and $0.1 \leq \Psi \leq \pi$.

Finally, because the integrand increases without limit as r approaches R, the numerical calculations have to be supplemented with an analytical development. The argument is begun by considering the integral in equation (2.43) to be composed of three parts,

$$J_1 = 2 \int_0^{\Psi i} \left\{ \left[\frac{R^2-r^2}{Rm^2} \right] \left[m^2+L^2 \right]^{\frac{1}{2}} - \left[\frac{R^2-r^2}{Rm} \right] \right\} d\Psi + 2 \int_{\Psi i}^{\pi} \left\{ \left[\frac{R^2-r^2}{Rm^2} \right] \left[m^2+L^2 \right]^{\frac{1}{2}} \right.$$

$$\left. - \left[\frac{R^2-r^2}{Rm} \right] \right\} d\Psi + \int_0^{\pi} \left[- \frac{m}{R} + \frac{(m^2+L^2)^{\frac{1}{2}}}{R} \right] d\Psi \qquad (2.47)$$

with r approaching, but not equal to, R and Ψ_i taken to be small. For these conditions, the result can quite accurately be approximated by

$$J_1 = 2 \int_0^{\Psi_i} \left\{ \left[\frac{L}{R}\right]\left[\frac{R^2-r^2}{m^2}\right] - \left[\frac{R^2-r^2}{Rm}\right] + \left[\frac{L}{R}\right] \right\} d\Psi + 2 \int_{\Psi_i}^{\pi} \left\{ \left[\frac{R^2-r^2}{Rm^2}\right]\left[m^2+L^2\right]^{\frac{1}{2}} \right.$$

$$\left. -\left[\frac{R^2-r^2}{Rm}\right] \right\} d\Psi + \int_0^{\pi} \left[-\frac{m}{R} + \frac{(m^2+L^2)^{\frac{1}{2}}}{R}\right] d\Psi \qquad (2.48)$$

In the limit this expression is exact. Also for small angles, the cosine can be taken as

$$\cos \Psi = 1 - 0.5\Psi^2 \qquad (2.49)$$

which is the first two terms of the power series of cos Ψ. It, too, becomes exact in the limit. With these approximations the integral when r is approaching R can be evaluated:

$$J_1 = 2 \int_0^{\Psi_i} \left\{ \left(\frac{L}{R}\right)\left[\frac{R^2-r^2}{(R-r)^2 + Rr\Psi^2}\right] - \left(\frac{1}{R}\right)\left[\frac{R^2-r^2}{\sqrt{(R-r)^2+Rr\Psi^2}}\right] \right\} d\Psi$$

$$+ 2 \int_{\Psi_i}^{\pi} \left\{ \left[\frac{R^2-r^2}{Rm^2}\right]\left[m^2+L^2\right]^{\frac{1}{2}} - \left[\frac{R^2-r^2}{Rm}\right] \right\} d\Psi$$

$$+ 2 \int_0^{\pi} \left[-\frac{m}{R} + \frac{(m^2+L^2)^{\frac{1}{2}}}{R}\right] d\Psi \qquad (2.50)$$

or

$$J_1 = (2)\left(\frac{L}{R}\right)\left(\frac{R+r}{\sqrt{Rr}}\right)\tan^{-1}\left(\frac{\Psi_i\sqrt{Rr}}{R-r}\right) - \left(\frac{2}{R}\right)\left(\frac{R^2-r^2}{\sqrt{Rr}}\right)\sinh^{-1}\left(\frac{\Psi_i\sqrt{Rr}}{R-r}\right) +$$

$$2 \int_{\Psi_i}^{\pi} \left\{ \left[\frac{R^2-r^2}{Rm^2}\right]\left[m^2+L^2\right]^{\frac{1}{2}} - \left[\frac{R^2-r^2}{Rm}\right] \right\} d\Psi + 2 \int_0^{\pi} \left[-\frac{m}{R} + \frac{(m^2+L^2)^{\frac{1}{2}}}{R}\right] d\Psi$$

$$\qquad (2.51)$$

The following limits are then considered:

$$\lim_{r \to R} (2)\left(\frac{L}{R}\right)\left(\frac{R+r}{\sqrt{Rr}}\right)\tan^{-1}\left(\frac{\Psi i \sqrt{Rr}}{R-r}\right) = \frac{2\pi L}{R} \tag{2.52}$$

$$\lim_{r \to R} \left(\frac{2}{R}\right)\left(\frac{R^2-r^2}{\sqrt{Rr}}\right)\sinh^{-1}\left(\frac{\Psi i \sqrt{Rr}}{R-r}\right) = 0 \tag{2.53}$$

$$\lim_{r \to R} 2\int_0^\pi \left\{ \left[\frac{R^2-r^2}{Rm^2}\right]\left[m^2+L^2\right]^{\frac{1}{2}} - \left[\frac{R^2-r^2}{Rm}\right] \right\} d\Psi = 0 \tag{2.54}$$

$$\lim_{r \to R} 2\int_0^\pi \left[-\frac{m}{R} + \frac{(m^2+L^2)^{\frac{1}{2}}}{R} \right] d\Psi = 2\int_0^\pi \left[-\frac{m}{R} + \frac{(m^2+L^2)^{\frac{1}{2}}}{R} \right] d\Psi \tag{2.55}$$

The value of J_1 for $r=R$ is, finally

$$J_1 = \frac{2\pi L}{R} + 2\int_0^\pi \left[-\frac{m}{R} + \frac{(m^2+L^2)^{\frac{1}{2}}}{R} \right] d\Psi \tag{2.56}$$

Since the integral of the later equation does not become undefined for any value of r or Ψ, it can be evaluated numerically. The r=R asymptote of Figure 14 refers to the experimental system to be described subsequently.

The complete results for J_1 and given in Figure 15 for all values of r. The function represented in this case is the total heat absorption per unit circumferential length occurring within a cylindrical shell of radius r, length L, and thickness dr. It may be noted that the absorption of energy for a large L/R-ratio tube is almost independent of radius whereas the attenuation as shown in Figure 13 has very pronounced variation. The characteristics of each function, J_1 and J_Σ, are probably strong functions of the parameter kR and L/R ratio, however.

Integration with respect to r.

The final integral with respect to r, according to equations (2.19) and (2.43) is
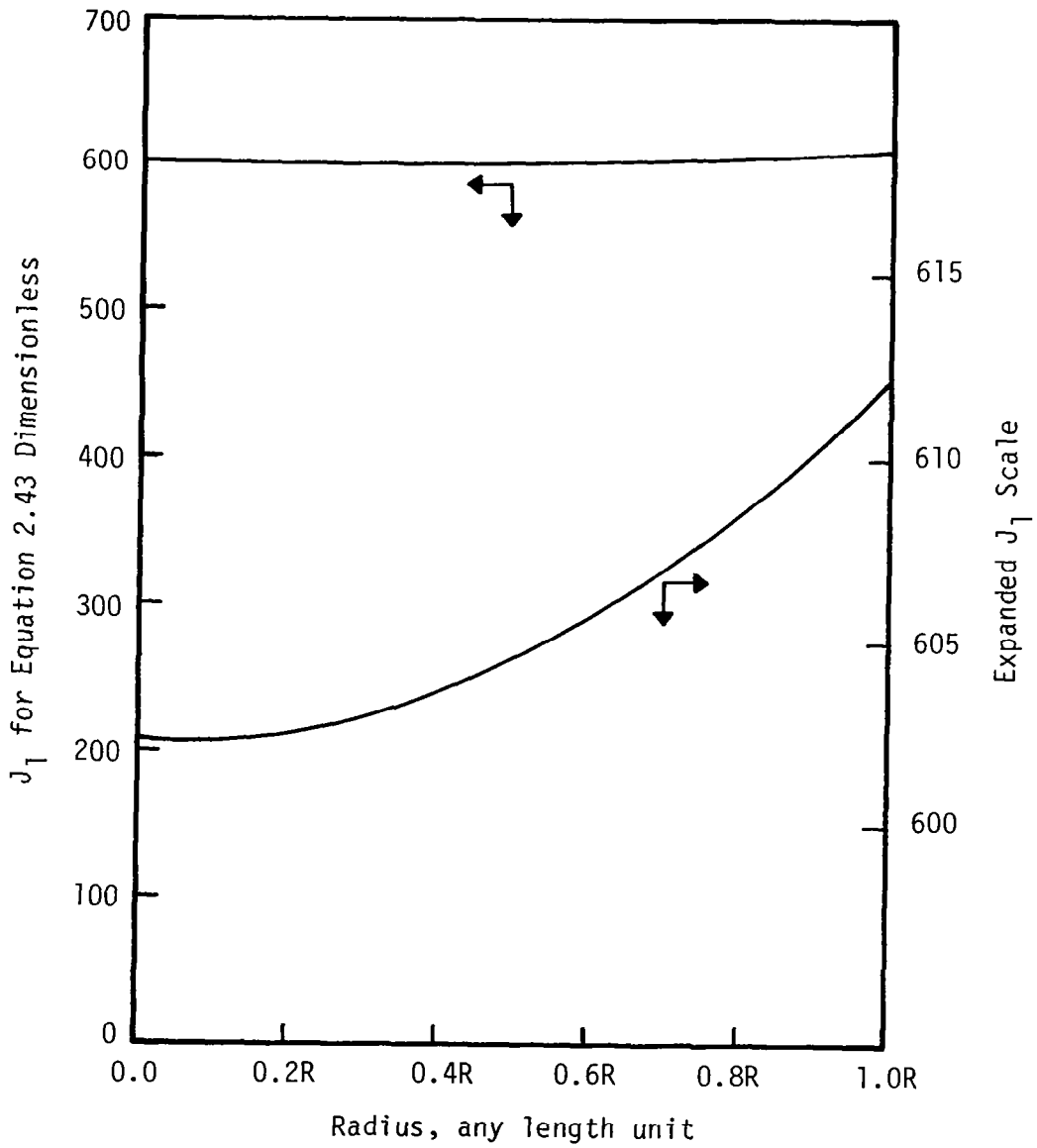
Figure 15. J_1 as Function of Radius.

$$Q_b = 2\pi i_{bnw} C S_v R \int_0^R (J_1 + J_\Sigma) r\, dr \qquad (2.57)$$

and

$$Q_b = 2\pi i_{bnw} C S_v R (F_1' + F_\Sigma') \qquad (2.58)$$

where Q_b is the total direct heat transfer to a cloud of particles.
Like the immediately preceding integration with respect to Ψ, this one
was also performed numerically and the J_1 and J_Σ functions were evalu-
ated at such radial points that a closed Newton-Cotes quadrature for-
mula again could be employed. The J_1 function was integrated by apply-
ing the seven point formula [equation (2.42)], once in the interval
$0 \le r \le 0.6R$ and once in the interval $0.6R \le r \le 1.00R$. Because of the
much longer computer time involved in calculations leading to J_Σ, less
radial points were computed and a five point integration formula was
employed for the evaluation of F_Σ'. The five-point, closed-form,
Newton-Cotes equation is

$$\int_{x_1}^{x_2} y\, dx = \frac{4h}{90} (7y_0 + 32y_1 + 12y_2 + 32y_3 + 7y_4) + \frac{8y^{(6)} h^7}{945} \qquad (2.59)$$

where h is the increment for the integration x, y is the function to
be integrated, the subscripted y's are the ordinate values required,
and $[8y^{(6)} h^7]/945$ is the error with $y^{(6)}$ being the sixth derivative of
the integrand.

The final results for Q_b are presented in the discussion of
results (Chapter IV) where the calculated heat transfer is compared with
experimental data and generalized calculations are evaluated.

CHAPTER III

EXPERIMENTAL INVESTIGATIONS

Description of Apparatus

Procedure and General Operation

Previous studies of heat transfer to particle clouds flowing in cylindrical enclosures have, in general, emphasized the conduction and convection processes, and the contributions of radiation, when significant, have been estimated by theoretical calculations alone.[35,36,37] Experimental studies considering dispersed systems usually treat luminous flames for which the desired radiation properties are derived from optical pyrometer measurements. Hence the direct absorption of radiation by particle-gas systems has not been determined. In this investigation, therefore, measurements were made to provide precise data on the transfer of radiant energy to systems consisting of nonluminous particles well-characterized as to particle size, surface area, and concentration suspended in a gas. The first problem was to develop an experimental system in which a particle cloud could be exposed to a radiant field having conduction and convective heat transfer reduced to a minimum and the energy could be absorbed by the particle cloud in such a way that its magnitude might be determined by enthalpy balances before and after exposure.

The final experimental system exposed a particle cloud to a radiant heat flow by passing it through a quartz tube which transmitted

to its interior a significant portion of the radiation falling on it externally. The quartz tube was protected from extraneous heat transfer effects other than radiation by enclosing it in an evacuated space, the outer surface of which was air-cooled. The surrounding, protective tube was also quartz. The particle cloud was generated at a constant rate and pre-conditioned to a constant known temperature. Then, after passing through the radiation field, the cloud was cooled calorimetrically to determine the heat absorbed. A filter mechanism removed the suspended particles from the air and returned them to an aerosol generator for re-use. The apparatus was thus designed for continuous operation. Repeated experiments could be performed with a limited inventory of powder (one-half pint) which, in some cases, required lengthy preparations meaning that it could not readily be obtained in large quantities. Figure 16 is a photograph of the assembly, and Figure 17 is a diagramatic representation showing the functions of the principal components.

Description of Principal Components

Particle Cloud Preparation. The particle cloud or aerosol was generated with the unit identified as an aerosol generator in Figure 17 and drawn in detail in Figure 18. As shown in section A-A of the latter drawing, a powder charged to the generator collected behind a retaining partition in a slowly rotating container. A thin layer of powder was thus produced along the bottom of the container due to the latter's moving continuously beneath the retaining partition. This layer was carried by the revolving surface under nozzle pickups where the powder was entrained in air passing upward. Particle deagglomera-
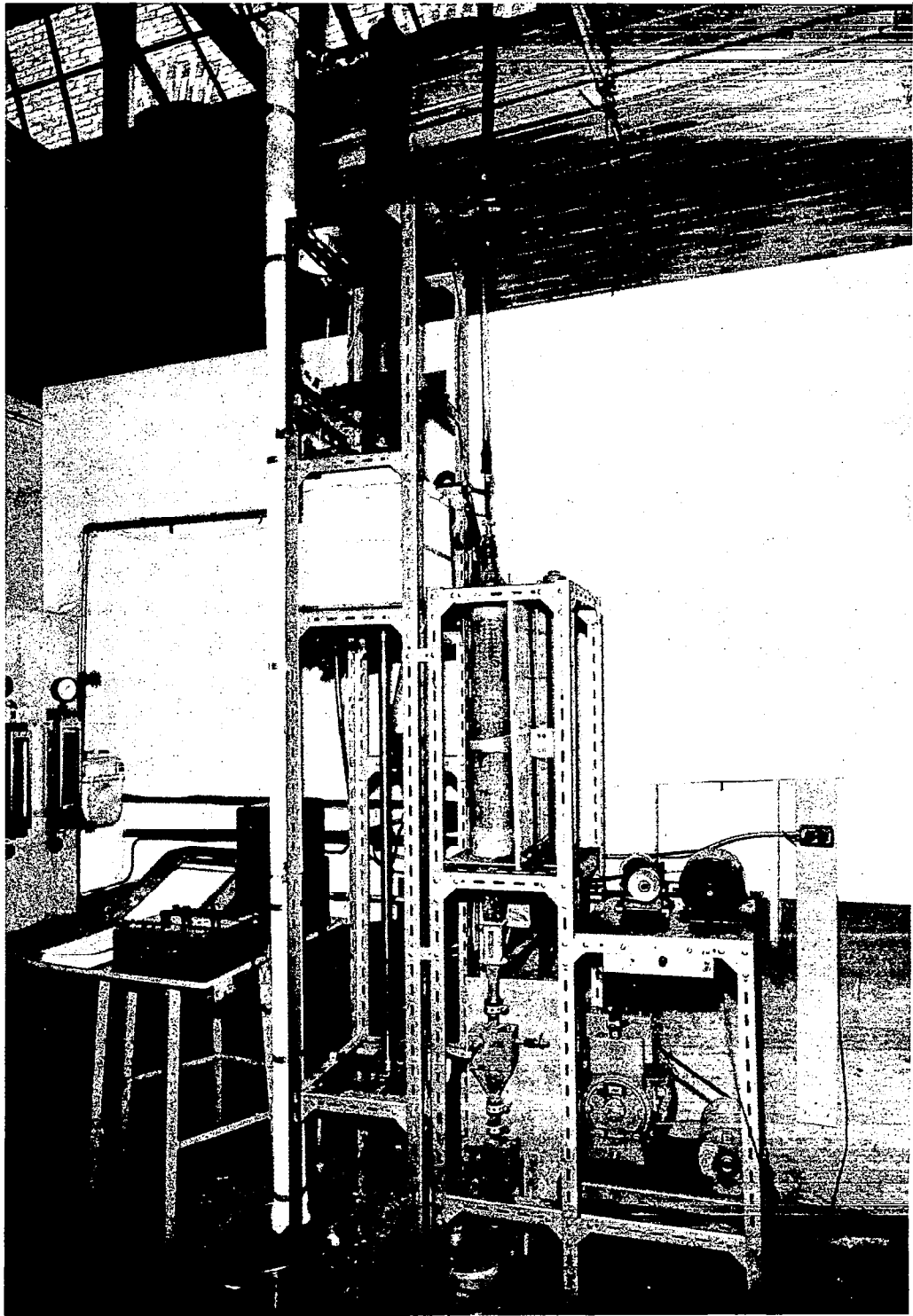
Figure 16.   Heat Transfer Apparatus.
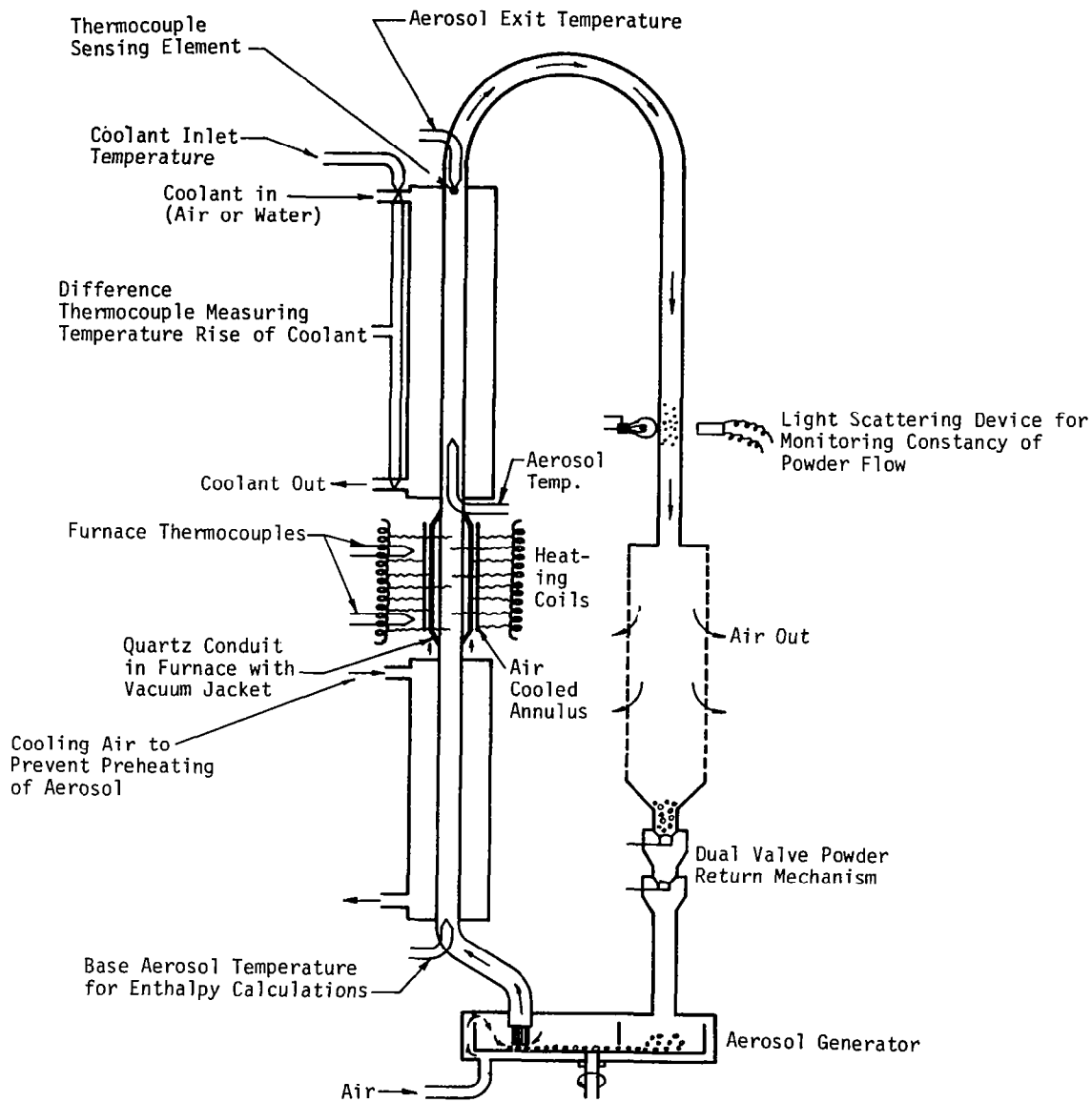
Figure 17. Diagramatic Representation of Heat Transfer Apparatus.

Direction of Rotation of
Powder Container

Powder Input

Retaining Partition

A   A

Plan View

Particle Cloud
Discharge

Felt-lined Surface with Powder Layer

Retaining Partition

Atomizing
Passages

Powder Supply
Behind Partition

Air Flow

Air Inlet

Rotating Container

Shaft

Powder Entrained Here   Section A-A
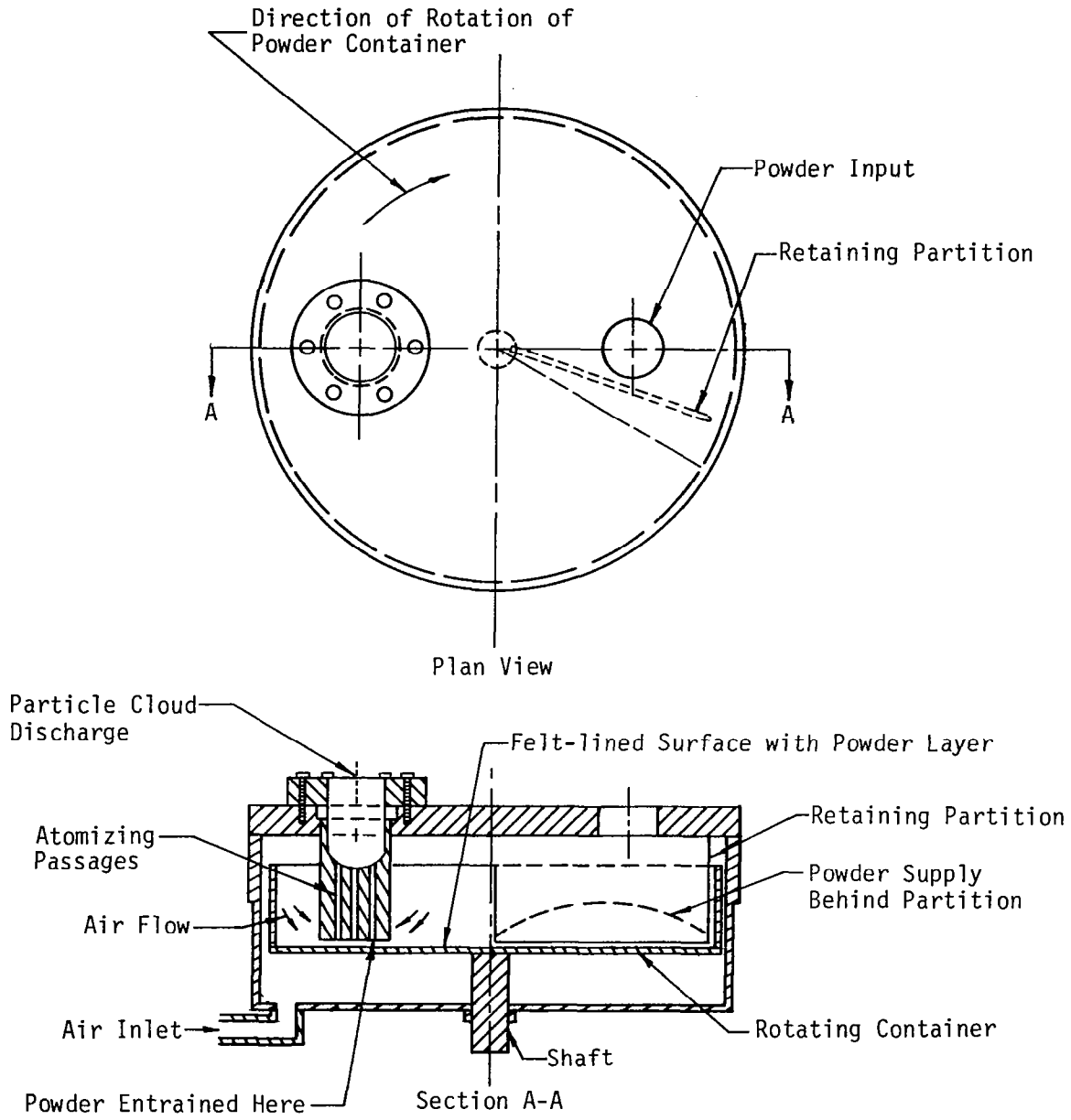
Figure 18.   Particle Cloud Generator.

tion resulted from the shear forces generated by the flow through the small passages; the pressure drop across them was approximately 10 psig. The newly formed particle cloud next passed through a length of pipe (L/D=100) to allow the streams from the nozzle to mix thoroughly and to reach a steady flow condition. The entrance length was enclosed in an air cooled, constant temperature jacket to bring the aerosol to a known temperature for use later in computing an overall heat balance on the suspension system.

Numerous exploratory experiments were required to achieve a suitable deagglomerating nozzle to handle a large flow rate and still produce a uniformly dispersed cloud with steady flow characteristics. Originally, a venturi reducing the channel diameter to about 0.03 inch was employed at the point the powder-air mixture issued from the generator assembly. At that time the powder was made airborne by entrainment with air passing through a perforated plate that covered the inlet to the aerosol conduit. In practically every case heavy agglomerates would form a fluidized bed in the pipe leading to the venturi. The venturi was then placed inside the aerosol generator to avoid the fluidizing effects, but now the powder entrainment was unsteady. The most satisfactory arrangement employed multiple, small-diameter passages inside the generator which served both as pickup tubes and as deagglomeration nozzles. Suspensions up to 0.05 per cent solids by volume -- equivalent to 75 per cent by weight for dense materials -- were produced.

The aerosol conduit was 0.5 inch. in diameter. A larger system could not be operated without overloading the compressed air facility supplying the laboratory.

Radiant Heating Section. After preparation, the particle cloud
was exposed to a radiant field generated by Kanthal wire, (Kanthal
Company, Stanford, Connecticut) electric resistance heaters supported
in grooves spiraling up the inner walls of a refractory enclosure con-
structed with Johns-Mansville 23 refractory brick. Two heaters were
employed, one for the upper and the other for the lower half of the
furnace. Each was composed of 30 feet of 0.333 ohm per foot wire
wound into a 0.375 inch diameter coil. The coil helices were spaced
closer to one another at the ends of the furnace to compensate for the
heat losses there and thus to give a more uniform temperature over the
heated area. Further, the temperatures of the two coils were controlled
independently; this arrangement reduced the temperature differences
resulting from convective currents within the furnace. A maximum of
4 kw could be supplied to the furnace and 2300° F was the maximum
operating temperature for the resistance wire. The directly irradiated
aerosol path was 12.5 inches in length. Figure 19 persents a drawing
of the assembly.

The aerosol conduit passing through the radiant field was a
13 mm ID quartz tube having a 1.0 mm wall thickness. Surrounding this
tube were two others, the inner one 25 mm ID with a 1.0 mm wall thick-
ness and the outer one 54 mm ID with a 1.5 mm wall. The middle tube
was sealed to the aerosol conduit and the annular enclosure thus formed
was evacuated to a pressure of approximately 1.0 micron of mercury to
reduce heat transfer by conduction and convection across the enclosed
space into the suspension. Air was circulated in the outer annulus to
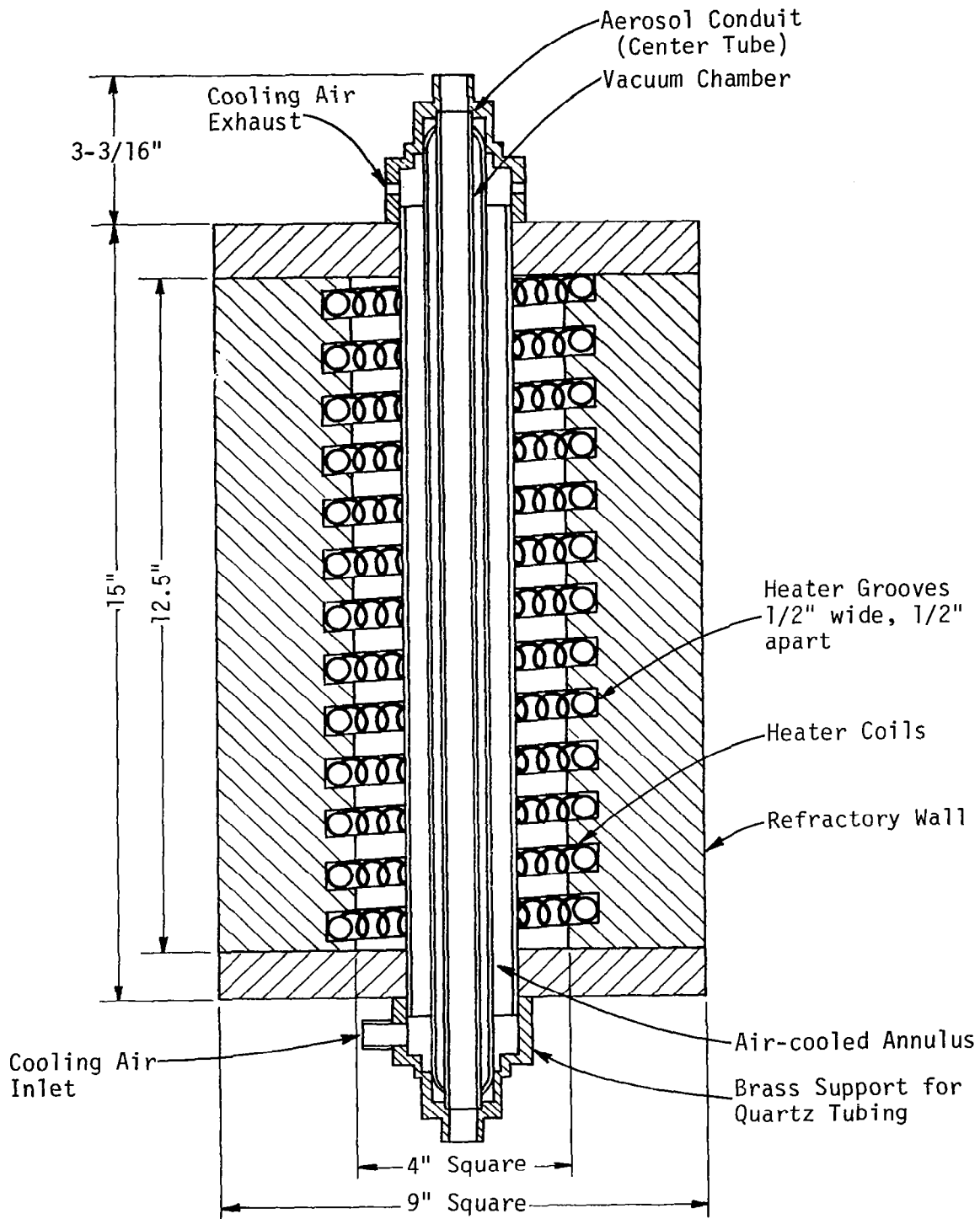
Figure 19. Radiant Heater.

protect the outer quartz tubes from the high furnace temperatures. The
air temperature in the outer tube could be held below 200° F with air
supplied from a suction fan. Because of the vacuum between this enclo-
sure and the aerosol conduit, very little heat could be transferred
other than by radiation to the aerosol system being studied. Some heat
could be transferred, of course, where the vacuum jacket joined the
aerosol conduit, and some energy was absorbed by the quartz tube carry-
ing the aerosol. Nevertheless, these heat losses were small, and
experimental corrections could be applied to evaluate the radiation
transferred to the particles.

Since the radiation had to pass through three quartz walls having
a total thickness of 3.5 millimeters before reaching the aerosol, the
radiation was considerably altered. An estimation of this change was
made from other experiments using the same type quartz as employed in
the furnace section. Figure 20 presents data for a 2 millimeter thick-
ness as supplied by the manufacturer.[38] Reflection losses were not
included, but from other measurements[39] they were found to be small.
As shown, the transmission efficiency was well over 90 per cent in the
0.3 to 3.5 micron wave length interval except for a narrow dip at 2.7
microns, and the transmission was nil over 4.7 microns. Most of the
radiation exposure for the aerosol, then, was in the range between
0.3 and 3.7. Since the temperature of the furnace was near 2500° R,
the shorter wave lengths were further limited to those above about
1 micron. The peak intensity was around 2 microns. The effective
radiation field, then, was almost completely between 1.0 and 3.0
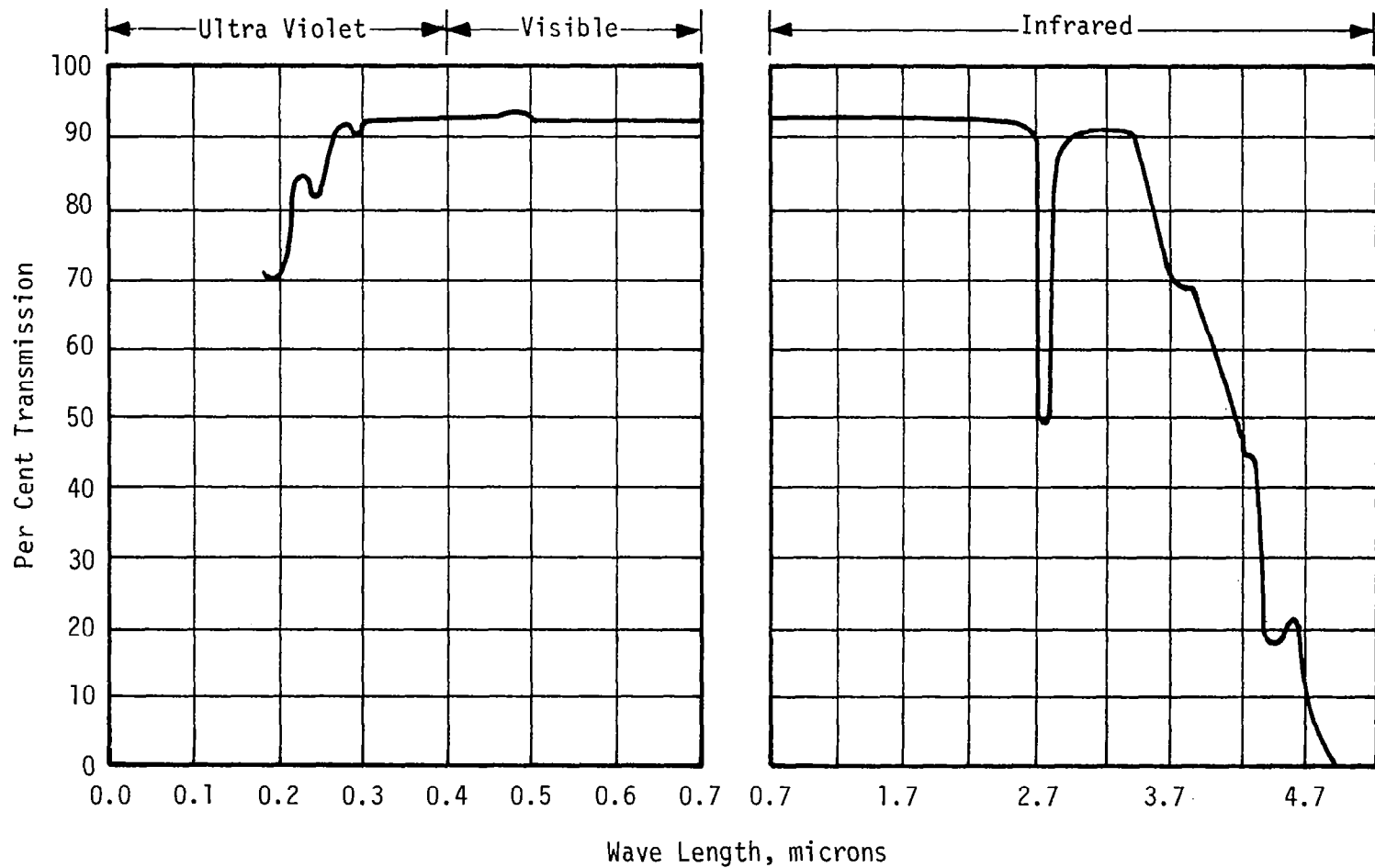
Figure 20.   Transmission Characteristics of Quartz Tubing Used in Radiant Heater.

microns. The average intensity of this field was determined by experiment.

Heat Exchange Section. The purpose of the experimental work was to measure the heat gained by the aerosol system from the radiation within the furnace. It would have been desirable to make the measurements directly as the aerosol passed from the furnace, but experiments of this type did not give satisfactory results. Heat was conducted as well as radiated into the downstream conduit, and this was found to lead to ambient effects that obscured the desired measurements. Equilibrium was both slowly attained and unstable. Changes in temperature could be detected when particles were added to the system, but interruption of the powder flow frequently did not return the system to its original thermal state.

Better results were obtained when the aerosol conduit was incorporated in a concentric, single pass, tube-and-shell heat exchanger. The latter unit, which was well insulated from the surroundings, served as a controlled heat sink between the furnace and a downstream point where the aerosol temperature was measured. The steady removal of heat stabilized the thermal behavior of the apparatus because disturbances were readily absorbed by the heat exchanger coolant and were not permitted to remain as sensible heat in the apparatus to be removed by the aerosol stream. Hence, measurements at a given time were more precise and were not dominated by transient thermal conditions. A sectional drawing of the heat exchanger is shown in Figure 21. The enclosed conduit conveying the particle-gas suspension was 0.5 inch in diameter and
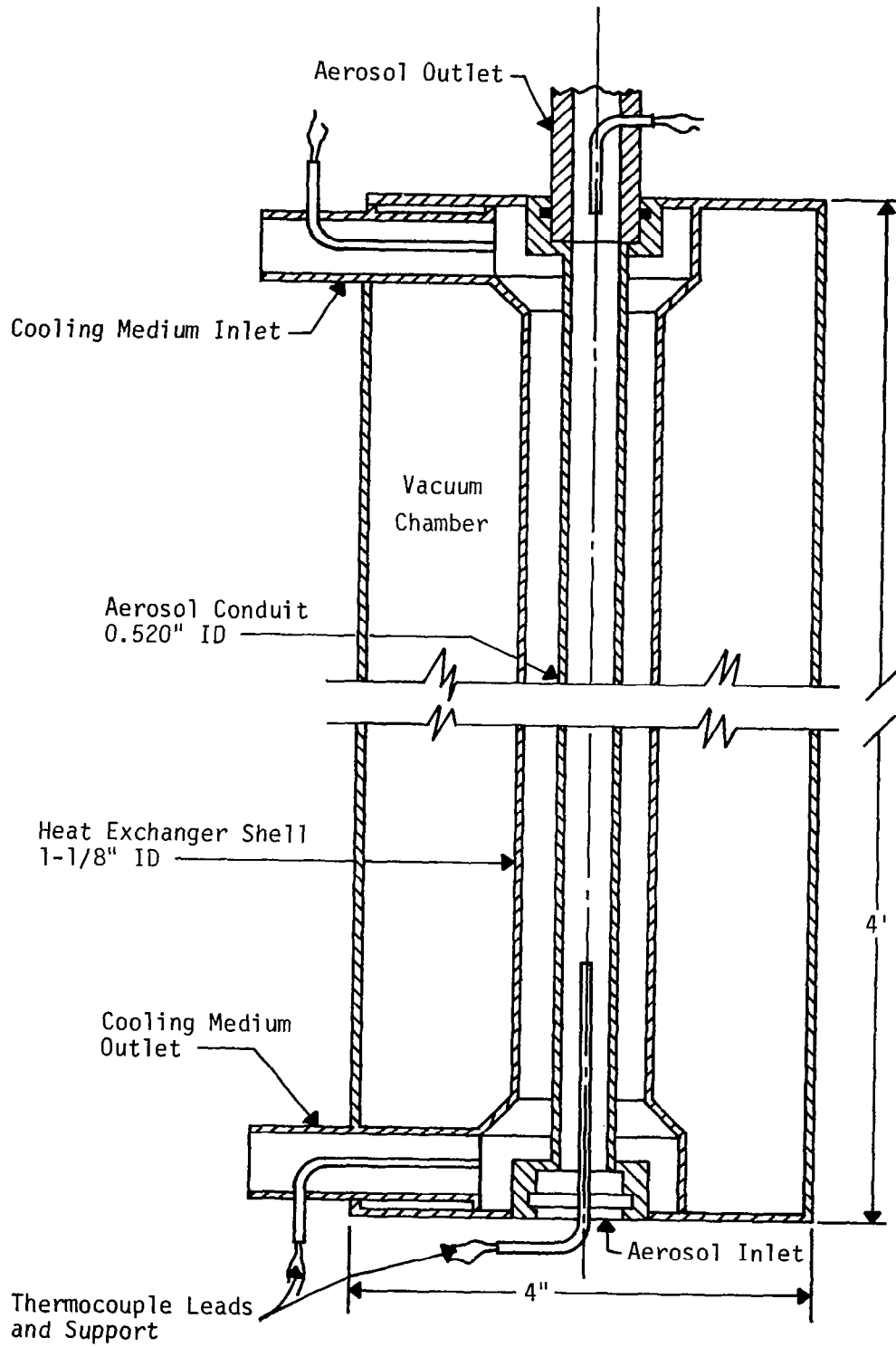
Figure 21. Heat Exchanger with Thermocouple Installations.

four feet long. The conduit was surrounded by a one-inch tube through which a cooling medium flowed countercurrent to the suspension. Either air or water could be the coolant, and a choice could be made on the basis of which had the appropriate heat capacity to give a readily measured temperature rise in passing through the system. For the particular suspensions studied, air gave better results. A vacuum chamber surrounded the heat exchanger to insulate it from the ambient room conditions. The inside wall of this chamber was lined with aluminum foil and the outer surface of the heat exchanger shell was polished to reduce radiation losses. End pieces were made as thin as possible to minimize the losses there, and insulation was provided to stabilize the temperatures to which the highly conducting end pieces were exposed. The assumption was made that the localized heat disturbances at the ends were approximately constant during an experiment and could be eliminated by heat balance calculations.

Measurements of the inlet and exit temperatures of the cooling medium and the aerosol exit temperature were made with copper-constantan thermocouples arranged as shown on the figure. These temperatures together with the mass flow rates of the two streams permitted making a heat balance for each and, from these, evaluating the heat content of the aerosol. The temperature of the aerosol itself was also measured by a thermocouple installed 6.5 inches from the entrance to the heat exchanger. By assuming a linear temperature gradient for the aerosol along the heat exchanger, this measurement could be corrected to give the aerosol temperature at the entrance. A supplementary heat balance made exclusively on the aerosol system was then possible. A radiation

shield in the aerosol stream prior to its entrance to the heat exchanger stopped downstream radiation in the heat exchanger and, because of the turbulence generated, induced a more rapid adjustment of particle and gas temperatures. This enhanced the reliability of the lower temperature measurement. The shield consisted of a round-edge flow nozzle gently reducing the conduit cross-section to about one fourth its original size and a downstream conical section with its apex at the discharge side of the orifice to cut off direct longitudinal transmission of radiation.

Particle Concentration Monitoring and Sampling Methods. Upon leaving the heat exchanger, the particle cloud passed through a return bend at the top of the apparatus. In the downward path it was monitored for consistency of concentration by means of light transmission measurements made as shown in Figure 17 (page 65) The principal component of the device was the special electronic circuit diagrammed in Figure 22; it provided a constant voltage for the lamp which generated a light beam of substantially constant intensity. The lamp was positioned so that it illuminated a photoelectric cell diametrically across the aerosol path. Since the light transmitted across this space was a function of the particle concentration, the photocell current was a measure of the number of particles present.

Light transmission measurements were intended to serve primarily as a means of monitoring the fluctuations in particle concentration during the course of experiments. In theory, the electronic instrument could have been calibrated for each powder and the transmissivities

110
Power Source

Triad Filament
Transformers F-41X,
25.2v, 2a., C. t.

Silicon Diode
750 ma at 600 v

25 Ω

100 μf
at 50 v.

40 Ω
1 watt

Zener Diode
1N1589

Power
Transistor,
1.0 a.

Stabilized
Voltage to
Light Source

Lamp

Silicon Diode
750 ma at 600 v

100 μf
at 50 v

25 Ω

1N1524
Zener Diode

100 Ω

1N1508
Zener Diode

200 Ω

1000 Ω

Stabilized
Voltage to
Wheatstone
Bridge

Clairex
Photocell
CL-404

30KΩ

10KΩ

50KΩ

10KΩ

Output
to
Recorder

Zero adjust
Resistance

Figure 22.   Schematic Diagram of Electronic Particle Concentration
Monitor.

could have been then converted directly into concentration. In practice however, considerable uncertainty is introduced by this approach. For instance, the illumination varies with the cleanness of the conduit windows. The device, therefore, was not reliable for absolute measurements, but it was useful for detecting concentration changes during an experiment and for assuring steady operation of the aerosol generator.

An absolute measure of the particle cloud concentration was obtained by direct sampling. The total powder output of the aerosol generator was measured for the four different speeds available in its operation. These results, together with measurements of the air flow through the system, then permitted the particle concentration to be calculated. The experimental procedure was to close off the aerosol from its normal path around the heat transfer circuit and to open simultaneously a sample tube leading to an extraction thimble which collected the entrained particles. After a short interval of time, usually about 30 seconds, the aerosol flow was diverted back to its normal path and the sample was removed and weighed. The results were corrected to account for the powder retained in the sampling connector. Between 6 and 10 determinations were made for each concentration level, and, to be considered acceptable tests, agreement between results had to be within ± 10 per cent; they frequently were within ± 5 per cent. A Staplex industrial air sampler (The Staplex Company, 777 Fifth Avenue, Brooklyn 32, New York) maintained constant pressure across the thimble filter to minimize the interference of the sampling procedure with the normal operation of the system.

<u>Powder Collection and Return Mechanism</u>. Finally the aerosol entered the sleeve filter (shown in Figure 17) where the powder was separated from the air stream. The filter medium was 4 inches in diameter and had 22 inches of useful length. The filter was traversed outside by a circumferential air jet which dislodged the filtered material and provided continuous operation of the filter. The traversing action was obtained with a guide that followed a right-hand helical groove along a cylinder in one direction and, at the end, reversed to follow a left-hand helix to the opposite end. The shifting of the guide from one helix to the other was accomplished by a connecting groove at each end of the cylinder. The guide had sufficient length to avoid changing helixes where they cross. The mechanism was driven by a motor and gear speed-reducing unit.

Two discharge valves below the filter transferred the collected powder back to the aerosol generator for reuse. These valves, shown in Figure 23, were arranged in series and were operated so that one valve was always closed to prevent escape of particles from the system. The valves were operated manually.

<u>Controls and Instrumentation</u>. Several control and measurement devices were required for the operation of the apparatus. Figure 24 is a photograph of them. The right side of the panel contained the necessary rotameters for measuring the various air and water flow rates. The rotameter at the extreme right measured the air flow rate supplied to the heat exchanger for cooling the particle cloud, while the intermediate rotameters metered air to the particle cloud generator for producing the aerosol. The remaining rotameter was to meter water to
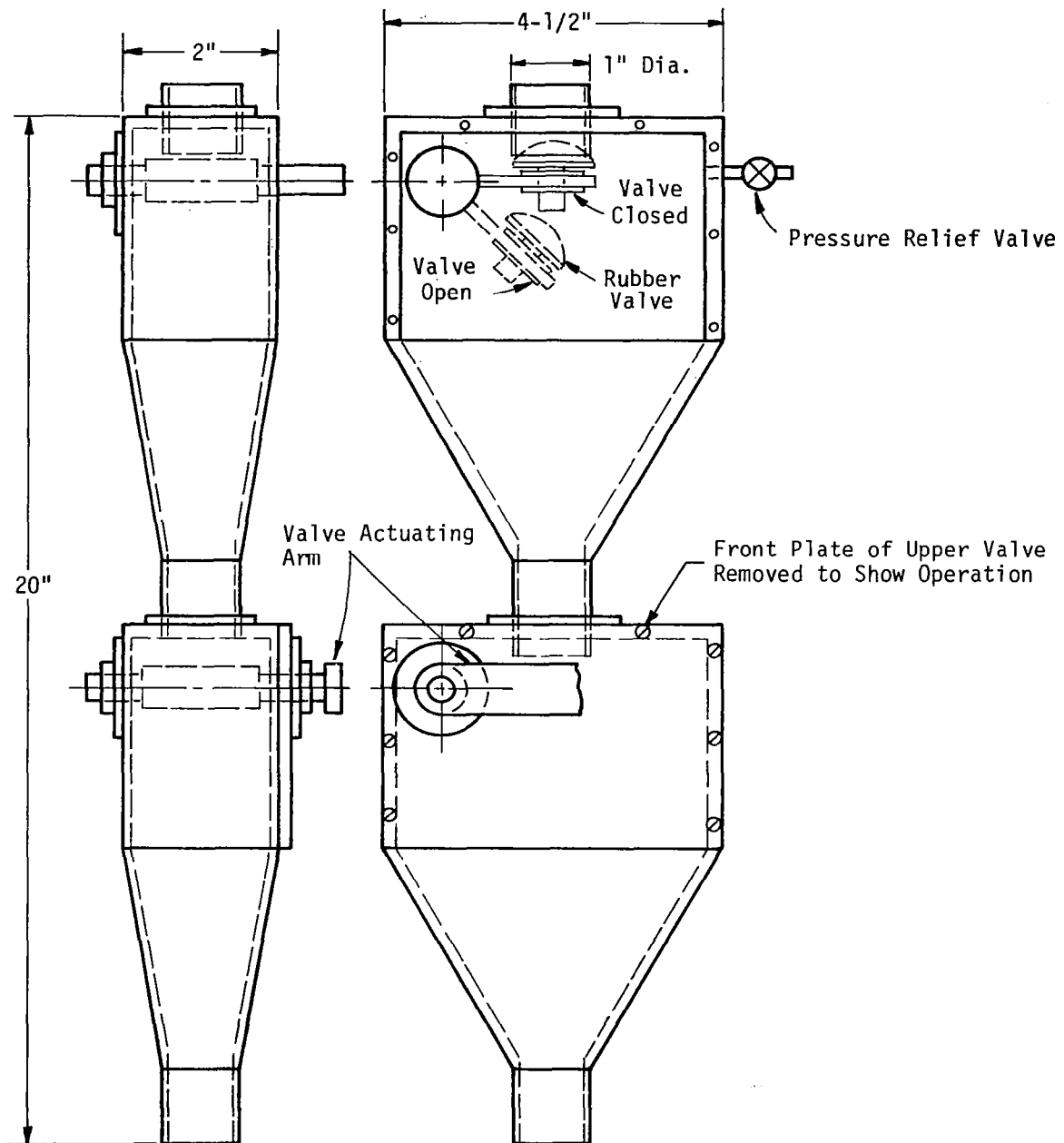
Figure 23. Powder Discharge Mechanism.
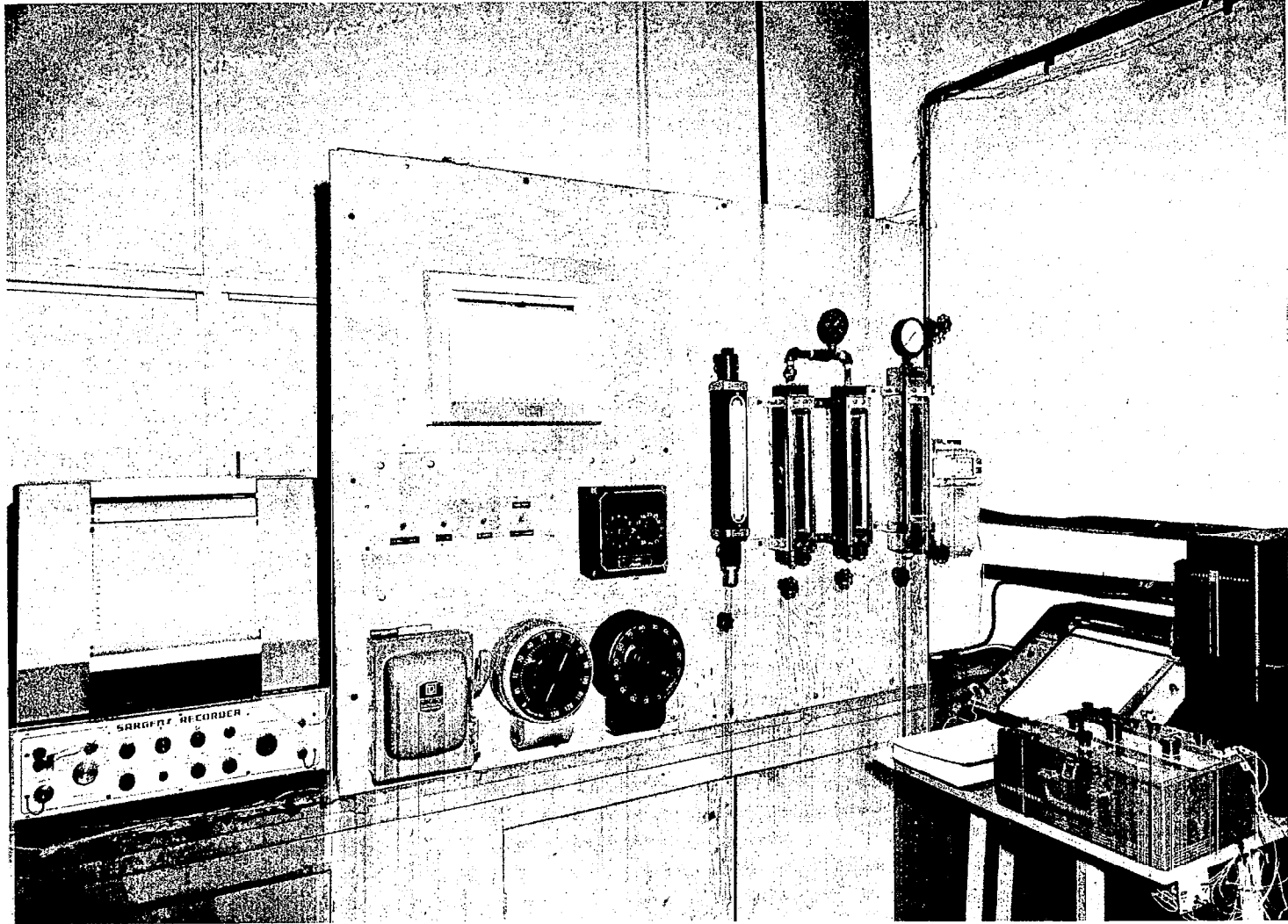
Figure 24. Instrument and Control Panel.

the heat exchanger when water served as the cooling medium. The valves

beneath each rotameter controlled the flow through the meter above.

The left part of the panel contained the power and electronic

equipment. Across its lower portion was a master switch for the

apparatus and the two variable auto-transformers that supplied power

to the furnace coils. Above was the switch panel for the various

power sources throughout the apparatus. And at the right-center was

the thermocouple selection switch for the temperature indicating system.

The recorder (Speedomax W, Leeds and Northrup, Philadelphia, Pa.) indi-

cated the furnace temperature.

Unmounted equipment included a model MR multi-range and a model

SR Sargent recorder (E. H. Sargent & Co., Chicago 30, Ill.), a Leeds

and Northrup No. 8686 potentiometer, and a Leeds and Northrup No. 2430-A

galvanometer. These units measured the required stream temperatures and

temperature changes, and monitored the particle cloud concentration.

The potentiometer also served as a calibration standard for the other

recorders.

Energy Balance Procedures

Energy Balance at the Entrance of the Heat Exchanger

The energy absorbed by the aerosols was determined from one of

two energy balance calculations. One balance was made between the

reference state and the thermal conditions at the entrance of the heat

exchanger and the other between the reference state and the exit condi-

tions. They were made by taking the reference temperature as that of

the stream at the exit of the aerosol generator which was, effectively,

the same as the temperature of the aerosol at the entrance of the furnace. This base temperature was assumed constant. Actually, variations in it never exceeded one or two degrees over a period of several hours and were not more than a few tenths of a degree over the duration of a test.

With the reference temperature, the temperature at the entrance of the heat exchanger, and a knowledge of the properties of the aerosol particles, energy balances over this part of the heat transfer system could be established. The difference of the enthalpy gain per unit time of the air in the stream with particles and the gain without particles is described by

$$\Delta H_{1A} = (H_1^1 - H_0^1)_A - (H_1^0 - H_0^0)_A \tag{3.1}$$

where the subscripts $(A,0,1)$ and the superscripts $(0,1)$ indicate the following:

A = a property of the air,

0 = the property evaluated at the furnace inlet,

1 = the property evaluated at the heat exchanger inlet,

0 = evaluation when no particles flowing,

1 = evaluation when particles are flowing.

With the assumption of a constant base temperature, equation (3.1) simplifies to:

$$\Delta H_{1A} = H_{1A}^1 - H_{1A}^0 \tag{3.2}$$

which in terms of temperature is

$$\Delta H_{1A} = (W\overline{C})_A (t_{1A}^1 - t_{1A}^0)$$

where $\overline{C}_A$ is the average heat capacity of the air stream between the temperatures under consideration, and W_A is the mass flow rate of air.

The enthalpy gain per unit time of the particles in the stream is given by the relation

$$\Delta H_{1p} = H_{1p}^1 - H_{0p}^1 \qquad (3.4)$$

which may also be written

$$\Delta H_{1p} = (W\overline{C})_p (t_{1p}^1 - t_{0p}^1) \qquad (3.5)$$

where the subscript p indicates a property of the particles, $\overline{C}$ is the average heat capacity of the particle material between the temperatures under consideration, and W_p is the powder flow rate.

The total enthalpy gain per unit time due to the presence of particles in the system is, finally, the sum

$$\Delta H_{total} = \Delta H_{1A} + \Delta H_{1p} \qquad (3.6)$$

Energy Balance at the Exit of the Heat Exchanger

A thermocouple at the upper end of the heat exchanger sensed the temperature of the aerosol stream there, and a difference thermocouple indicated the temperature rise of the cooling air as it passed through the heat exchanger. From these temperatures and the flow rates of the streams, a second energy balance was established that included the heat exchanger. The total balance involved the sum of the heat effects in the air portion of the aerosol, the particles, and the heat exchanger coolant.

For air, the difference of the enthalpy gain per unit time with the particles and the gain without particles is given by

$$\Delta H_{3A} = (H_3^1 - H_0^1)_A - (H_3^0 - H_0^0)_A \tag{3.7}$$

where the subscript 3 indicates the property at the conditions of the heat exchanger exit.

Since the base temperature was constant, equation (3.7) reduces to

$$\Delta H_{3A} = H_{3A}^1 - H_{3A}^0 \tag{3.8}$$

or,

$$\Delta H_{3A} = (W\overline{c})_A (t_{3A}^1 - t_{3A}^0) \tag{3.9}$$

The enthalpy gain of the particles per unit time is then

$$\Delta H_{3p} = H_{3p}^1 - H_{0p}^1 \tag{3.10}$$

which can be expressed

$$\Delta H_{3p} = (W\overline{c})_p (t_{3p}^1 - t_{0p}^1) \tag{3.11}$$

Finally, the difference in enthalpy gain per unit time for the cooling air is

$$\Delta H_c = (W\overline{c})_c [(\Delta t_c^1 - \Delta t_c^0)] \tag{3.12}$$

or,

$$\Delta H_c = (W\overline{c})_c \cdot \Delta(\Delta t_c) \tag{3.13}$$

84

where,

$$\Delta(\Delta t_c) = [\Delta t_c^1 - \Delta t_c^0] \qquad (3.14)$$

The notation, $\Delta(\Delta t_c)$, indicates the difference in temperature rise of the heat exchanger coolant with and without particles in the aerosol stream. The total enthalpy gain per unit time due to the flow of particles is thus the sum

$$\Delta H_{total} = \Delta H_{3A} + \Delta H_{3p} + \Delta H_c \qquad (3.15)$$

Materials for Study

Selection

Initial measurements were made with zinc powder aerosols since this material was used in developing the apparatus and in establishing experimental procedures. Being a metal, it has a low absorptivity and afforded an operational test of the apparatus with that type of powders. Also, the zinc was well chosen for testing the bag filter since it had an average particle diameter of about 6 microns.

Most of the later experimental work was conducted, however, with ferrous sulfide and copper oxide aerosols. These materials were selected primarily because of their noncorrosive nature and their availability in lump or granular form which permitted them to be subdivided into various size fractions.

Preparation

The zinc powder was a paint pigment obtained from the Decatur Chemical Company, Decatur, Georgia. It was used as received. Prolonged circulation of it through the experimental apparatus during the period

of development eroded the individual particles until they became almost

spherical. The particle diameters then ranged from one micron to a

maximum of 10 microns with an average of very nearly 6.5 microns. The

actual particle distribution curve is given in Figure 43 of Appendix A.

The ferrous sulfide was the technical grade product of the Baker

Chemical Company, Phillipsburg, New Jersey. Preparation of it consisted

of first reducing the lumps to minus 144 U.S. Standard Sieve Size with a

mortar and pestle. The product was then ball-milled for one hour inter-

vals and screened until all of it passed an 88 micron screen. There-

after, standard sieving was continued to yield 88 to 53, 53 to 44, and

less than 44 micron diameter fractions. Special screens (Buckbee

Mears Co., St. Paul, Minn.) were then employed to separate the less

than 44 micron material into 44 to 30, 30 to 20, and less than 20 micron

diameter fractions.

The cupric oxide was also reagent grade material and obtained

from the Baker Chemical Company. This high purity product was employed

since only it could be located with particles larger than 20 microns.

Particle size fractions ranging from the 88 micron screen size to 20

microns were prepared by the same procedure as was the ferrous sulfide.

Particle Properties and Size Measurements

After preparation of the different fractions, precise measure-

ments of particle diameters, distribution of diameters, and surface

area were made, since these parameters were thought to be significant

in establishing the absorptive properties of particle clouds formed

from them. Attempts were also made to establish the size of cracks

and fissures within the particles. These tests involved microscopic determinations of thousands of particle diameters, statistical treatment of the data, and low temperature nitrogen absorption measurements in accordance with standard procedures.[40] Effective particle surface areas were calculated from the size distributions, for it was this quantity that determined the specific absorptive capability of the powder (radiation properties excepted). It was anticipated that the nitrogen absorption surface areas, when allowance was made for the porous structure of the surface,[41,42] might be employed to yield an effective specific surface area (ft^2/lb). The attempts might have been successful with some powders, particularly with very small, hard-to-disperse particles where the nitrogen absorption measurements are more reliably made than are microscopic determinations. Unfortunately, adsorption determinations could not be obtained with adequate precision. There still remains the possibility that krypton adsorption might make the method reliable.[43] More research is required, however, before pore structure can be determined with krypton.[*]

Physical measurements were made both before and after several of the powder fractions were used in the heat transfer experiments to determine if any changes in properties had resulted. As expected, significant size and shape differences were found, particularly in the first experiments that required long-time operations to produce useful results. Prolonged particle attrition produced broadened size

---

[*] This is being pursued in another thesis investigation now being conducted by Korstiaan Van Wijngaarden of this laboratory.

distributions and resulted in particles, in some cases, well below the intended size. The powders, appeared to change most rapidly during the first few minutes of use. Thereafter changes were much slower, and size distributions determined immediately after use were employed for the correlations. These distributions are given in Appendix A.

One of the most unexpected observations is presented in Table 1. There it may be seen that the powders' specific surface areas were reduced by use. The fact at first seemed paradoxical since the particles undoubtedly underwent size reduction. The effect, however, resulted from the capture in the bag filter of submicron particles which initially were present but were attached to the large particles. These were not included in the original particle size distribution measurements. Figure 25 is a series of photographs of a powder before use, the portion retained in the bag, and a fraction after use.

Calculated Particle Cross Sectional Areas

The particle area actually participating in the radiation interchange was evaluated from an experimentally determined quantity, S_v, the cross sectional area per unit volume of solids (ft^2/ft^3). S_v was constant for each powder studied and was a function of particle geometry and particle size distribution. Its value was calculated as follows:

For a spherical particle of diameter, d_p, the volume is

$$V = \frac{\pi d_p^3}{6} \qquad (3.16)$$

and the cross sectional area is

Table 1. Surface Areas of Powdered Materials as
Determined by Nitrogen Absorption

Ferrous Sulfide Diameter Range (μ)	Specific Surface Area	
	Before Use (m^2/gm)	After Use (m^2/gm)
53-88	0.37	0.13
44-53	0.35	0.14
30-44	0.45	0.23
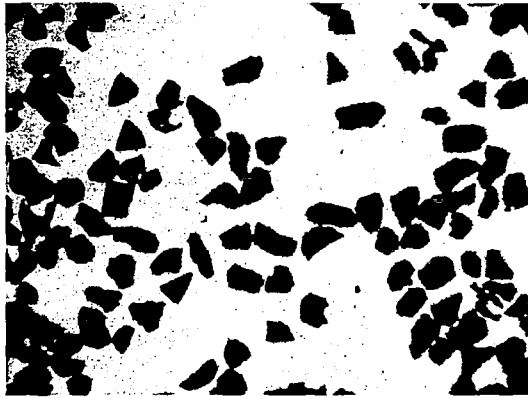
(a) Original Material
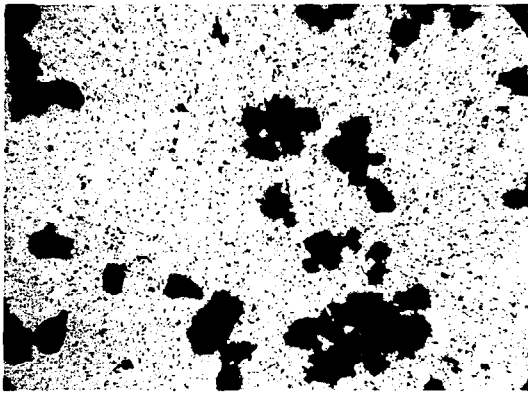
(b) Material Retained in Bag Filter
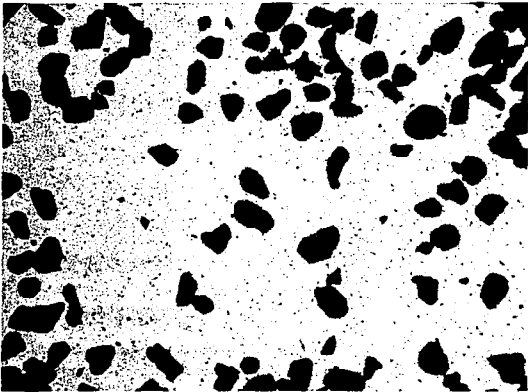
(c) Circulated Material

Figure 25. Photomicrographs of Ferrous Sulfide Powder ($44-53\mu$) Showing the Preferential Capture of the Very Small Particles in the Bag Filter.

90

$$A_c = \pi d_p^2 \tag{3.17}$$

The ratio of A_c to V gives S_v, which in this case is $6/d_p$. For a powder having a range of particle sizes, the contributions from particles within a differential diameter increment may be written

$$d\, A_c = (\frac{1}{N})(\frac{dn}{d(d_p)})(A_c)_{nd}\, d(d_p) \tag{3.18}$$

and

$$d\, V = (\frac{1}{N})(\frac{dn}{d(d_p)})(V_d)_{nd}\, d(d_p) \tag{3.19}$$

which, when integrated give the total area and total particle volume of N particles, respectively

$$A_c = \int_{d_1}^{d_2} (\frac{1}{N})(\frac{dn}{d(d_p)})(\pi d^2)\, d(d_p) \tag{3.20}$$

and

$$V = \int_{d_1}^{d_2} (\frac{1}{N})(\frac{dn}{d(d_p)})(\frac{\pi d^3}{6})\, d(d_p) \tag{3.21}$$

Again S_v is the ratio A_c/V.

Under certain conditions the indicated integrations have classical solutions. If, for instance, the particle size distributions were log-normally distributed the two results would be[44]

$$A_c = \frac{1}{4} A_s = \frac{1}{4} \exp\, (2\ln x_g + 2\ln^2 \sigma_g) \tag{3.22}$$

$$V = \exp\, (3\ln x_g + 4.5\ln^2 \sigma_g) \tag{3.23}$$

Where x_g is the geometric mean diameter and σ_g is the geometric standard deviation. Many powders in nature can be described accurately by this distribution and for such cases the final result for S_v is immediately available.

The powders employed in this investigation, unfortunately, did not follow the log normal distribution law, since this type of distribution was destroyed by the sizing processes. Log normal particle size distributions are, in general, produced by natural comminution. The actual particle size distributions, in some cases, were bimodal. Attrition in the heat transfer apparatus, if continued, would undoubtedly eventually have produced a log normal distribution but much less than this length of time was allowed.

A numerical procedure was employed to evaluate the surface-to-particle volume ratio since no mathematical representation for describing the distribution was available. Equations (3.20) and (3.21), were integrated numerically by taking diameter increments of about one to two microns and computing the required areas and volumes for the average diameter of the increment. The results were summed, and area-to-volume ratio were formed to give the final answer. These calculations were performed with the Burroughs 220 digital computer.

Experimental Data

With Water-Cooled Heat Exchanger

The heat transferred to a given dispersion was determined by energy balances as already described. For the initial experiments, water was the coolant for the heat exchanger and the energy balance

given by equation (3.15) was employed to calculate the heat absorbed by the aerosol. Data were collected in this manner for the zinc powder and the 53-88 micron diameter fraction of ferrous sulfide. These experimental and calculated results are given in Tables 3 and 4 of Appendix B.

The tabulated results for these experiments include the thermal data for the streams involved; the air and powder flow rates; the indicated furnace temperature; and, finally, the calculated enthalpy changes produced by the addition of particles to the system. The temperatures for the aerosol and the heat exchanger coolant are presented directly as indicated by thermocouples located as shown on Figure 17 (page 65). The difference quantity, $\Delta(\Delta t)$, however, is a combination of two measurements, one the temperature rise of the heat exchanger coolant when only air was flowing in the system, and the other when both air and powder were flowing. The temperature rise of the heat exchanger coolant was a temperature difference, hence the notation (Δt). The difference between these two (Δt) quantities represents the change in temperature rise of the heat exchanger coolant when particles were added to the system. The second difference was represented by $\Delta(\Delta t)$. This quantity in some cases was positive and in others negative, depending on whether more or less heat was absorbed by the heat exchanger when particles were added to the system.

Making an energy balance for these experiments required, as shown by equation (3.15), the enthalpy changes incurred by the aerosol components as well as the heat exchanger coolant when particles were

flowing. The latter could not be calculated directly but was estimated to be comparatively small. Tables 3 and 4, therefore, present only the calculations for the aerosol particles and the carrier air.

As shown by the tabulated data, the $\Delta(\Delta t)$ for the heat exchanger coolant was approximately $\pm 0.5^\circ$ F. With a water flow rate of 0.095 CFM this means a (ΔHc) of 3 Btu/min. The result, however, was unreliable since the possible error in determining $\Delta(\Delta t)$ was on the order of 100 per cent. Other measurements, therefore, were required to assess this quantity accurately. A thermocouple was installed in the aerosol stream near the entrance of the heat exchanger, as previously described, and was employed as a supplementary measurement in analyzing the operations of the heat exchanger. Since, with the new measurement, the entrance and exit conditions of both streams were known, log-mean temperature differences between the coolant and the aerosol system could be calculated. These differences, when powder was flowing, were found to range from 5 to 15 per cent less than these differences when only air was flowing. It was noted further that the overall heat transfer coefficient was correspondingly increased for the powder concentrations studied.[45] These conditions, then, meant that the heat transferred $(UA\ \Delta t)$ to the coolant in each case was essentially the same, and it followed further that the $\Delta(\Delta t)$ must have been very nearly zero. Thus, it was assumed that the heat exchanger absorbed approximately the same amount of heat with and without powder and the enthalpy change ΔHc for the coolant was disregarded. These results are shown in Figure 26 for the zinc and in Figure 27 for the 53 to 88 micron ferrous sulfide particle aerosols.
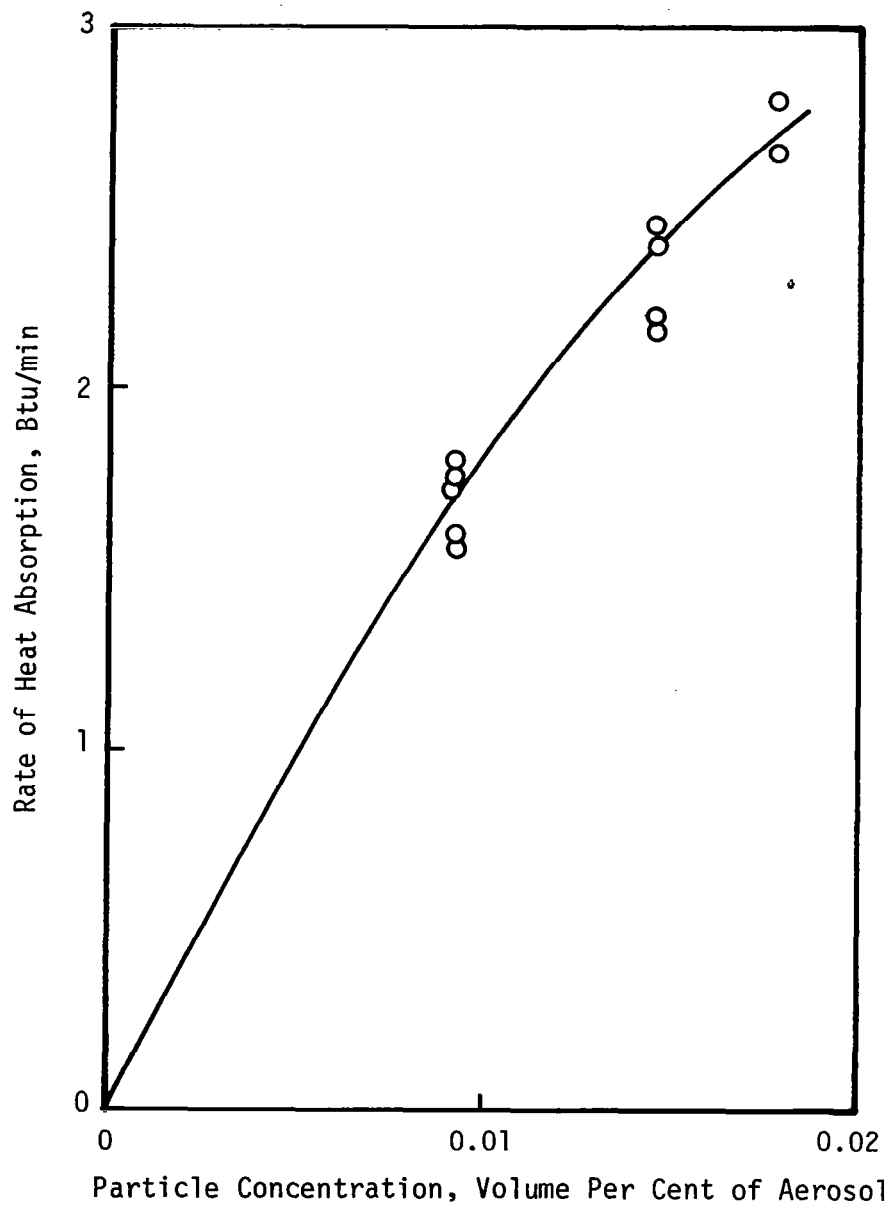
Figure 26. Rate of Heat Absorption by Zinc Particle Clouds.
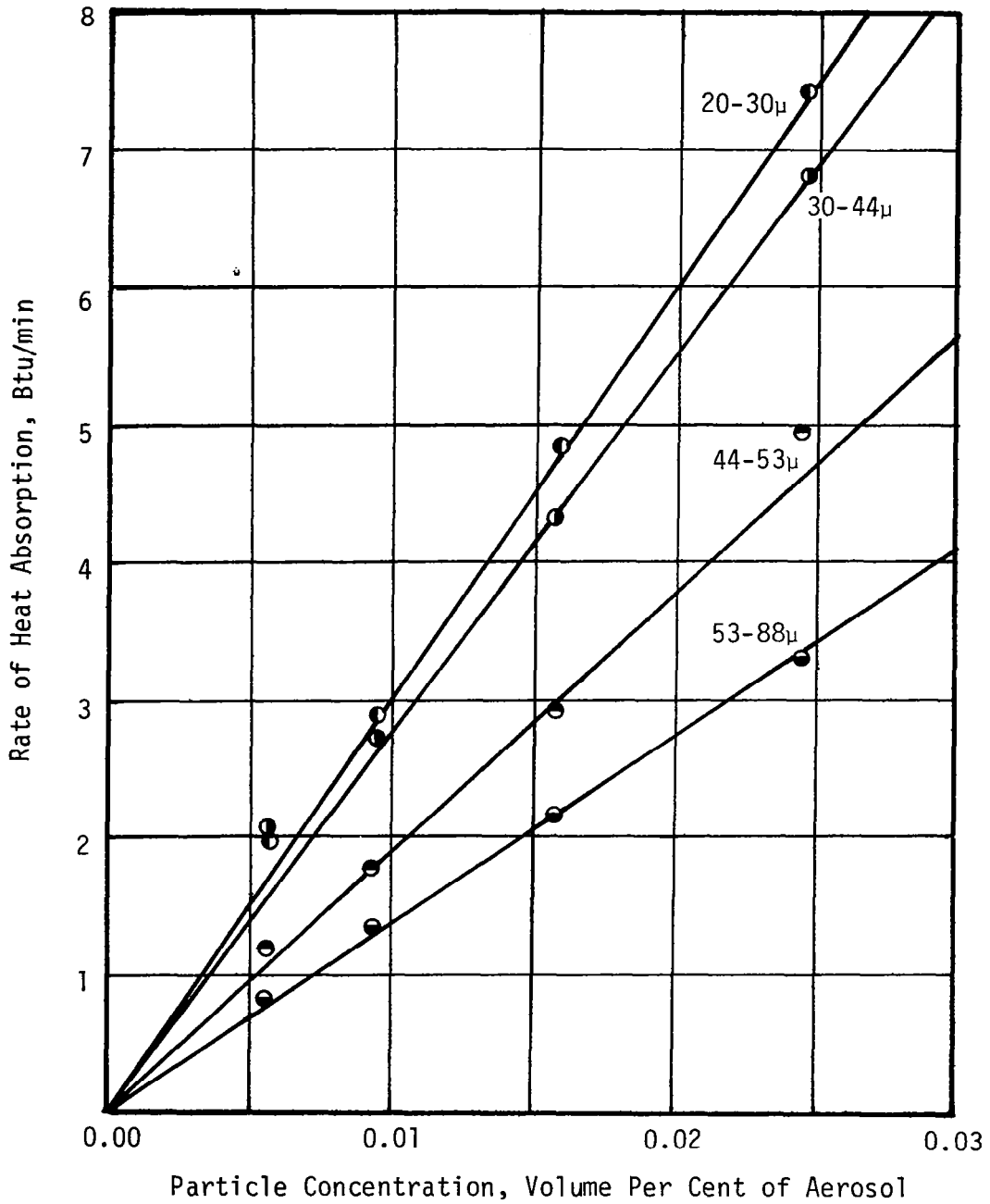
Figure 27. Rate of Heat Absorption by Ferrous Sulfide Particle Clouds.

Subsequent data with other ferrous sulfide powders, also presented in the latter figure, gave support to this conclusion.

With Air-Cooled Heat Exchanger

For optimum operation the heat exchanger should be near room temperature to reduce to a minimum extraneous heat effects associated with the surroundings. For this purpose water is a better coolant due to its greater heat capacity. Its use, however, was actually a disadvantage in evaluating the amount of energy absorbed by the water with acceptable precision. When the water rate was sufficiently high to provide stable operation, the temperature differences involved were too small to measure accurately, and when the water rate was reduced to give measurable temperature differences, the heat exchanger was not thermally stable and too much time was required for equilibration. Air, therefore, was employed as the heat exchanger coolant in an effort to achieve better measurements and more stable operation. Air, having a much smaller heat capacity than water, could have its flow rate regulated to give measurable temperature differences as well as rapid response to transient heat transfer effects. Data were collected with this modification for the 44 to 53, 30 to 44 and the 20 to 30 micron ferrous sulfide powders. The results of these experiments are presented in Tables 5 through 8 and on the preceding figure. The absorption determinations were reproducible within ± 0.5 Btu/min. and showed a considerable reduction in the uncertainty of the heat removed by the heat exchanger coolant as compared with the results using water. Air was used in all subsequent experiments. Also, starting with the 20 to 30 micron ferrous sulfide powder (Table 8), data were recorded so that heat balances could be

made over the complete heat exchanger [equation (3.15)] as well as on the aerosol system alone [equation (3.6)], except for one experiment with cupric oxide (Table 12).

Final measurements were made on aerosols of cupric oxide powders. Four size distributions were prepared as previously described. Again samples designated by screen sizes of 53 to 88, 44 to 53, 30 to 44 and 20 to 30 microns were selected. Tables 9 through 12 present the data obtained while Figure 28 gives the results graphically.

Radiant Heat Flux Determinations

The radiant heat flux penetrating the quartz enclosures and traversing the particle cloud was basic to the theoretical heat transfer calculations of this study. To determine this quantity, the aerosol conduit was coated with a highly absorbing material -- carbon black -- and experiments were conducted in which water was forced to flow upward through the inner quartz conduit to remove the heat absorbed thereon. The contribution of the radiation had to be separated from the total result, however, because the aerosol conduit received heat by conduction and convection as well as radiation. This separation was accomplished by performing additional experiments with the inner wall of the aerosol conduit being made as reflective as possible so that radiation effects would be minimized. A gold coating was employed for this purpose. The difference, then, between the results, when adjusted for the actual absorptivities of the two coatings, was the heat transferred to the aerosol conduit by radiation.

The radiant heat flux determinations were made with water as the
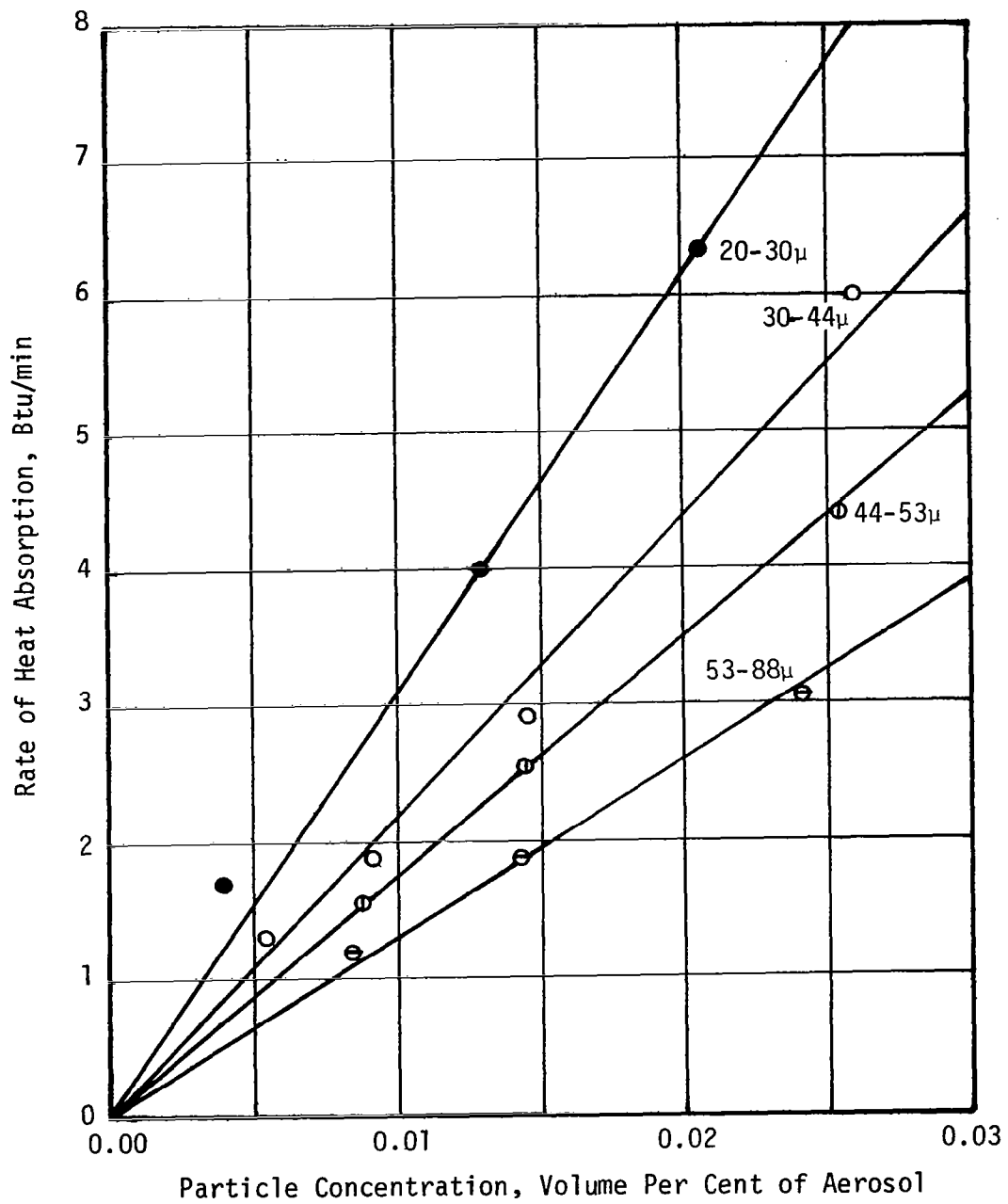
Figure 28.   Rate of Heat Absorption by Cupric Oxide Particle Clouds.

coolant, rather than air, to permit better control of the temperature of the system. When air was the coolant and the conduit wall was made highly absorptive, a sufficiently high flow rate of air could not be accommodated by the rotameter metering the air to avoid thermal damage to the coating. Further, it was desired that the conductive and the convective heat transfer to the system be as nearly identical as possible with both the reflective and the absorptive coatings. The entrance and exit temperatures of the coolant had to be maintained sufficiently close to avoid large discrepancies, since both these processes were a function of the temperature distributions throughout the complete system. With water as the coolant, flow rates could be selected to keep the temperature rises within about 5° F of each other. For a pair of experiments, one with each type of coating, the flow rates had to be identical since the extent of the convective and conductive heat transfer was a function of the coolant flow rate.

The conduit wall was made highly absorbing by coating it with lamp black in a small amount of epoxy resin (Resinweld Plastic Alloy, H. B. Fuller Co., St. Paul, Minn.). The absorptivity of the surface was taken as 0.95°.[46] The reflective surface was a thin gold film baked onto the inner conduit wall. A fluid suspension of gold particles supplied by B. F. Drakenfeld and Co. Inc., Washington, Penn. was used. Baking a deposit of this suspension to a temperature (1060° F) near the melting point of gold volatilized the suspending fluids and formed a smooth reflective metallic surface. The absorptivity was assumed to be 0.03.[47]

Experimental and calculated heat transfer data are presented
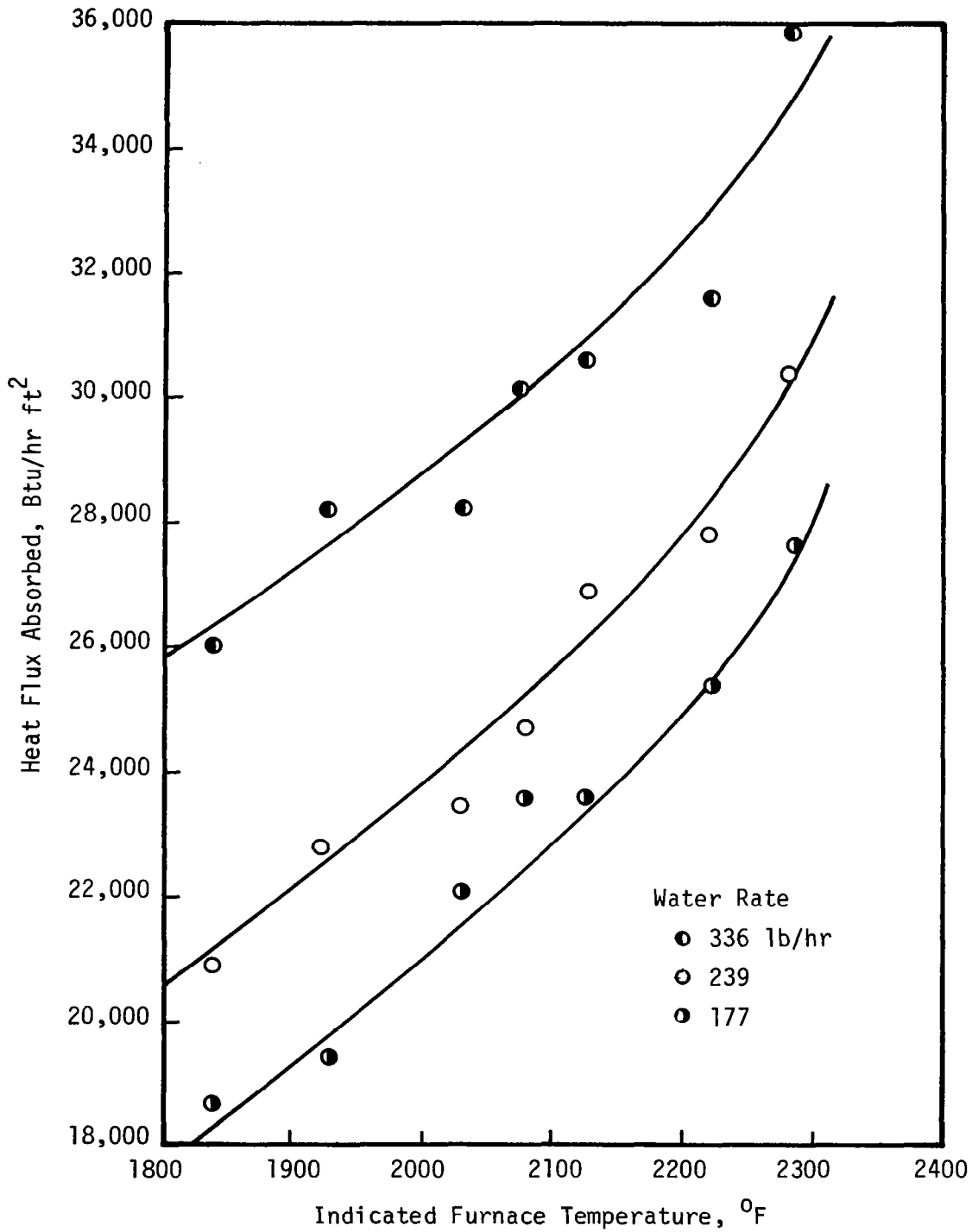
Figure 29. Heat Flux Absorbed by Aerosol Quartz Conduit with Inner Wall Coated with Lampblack.
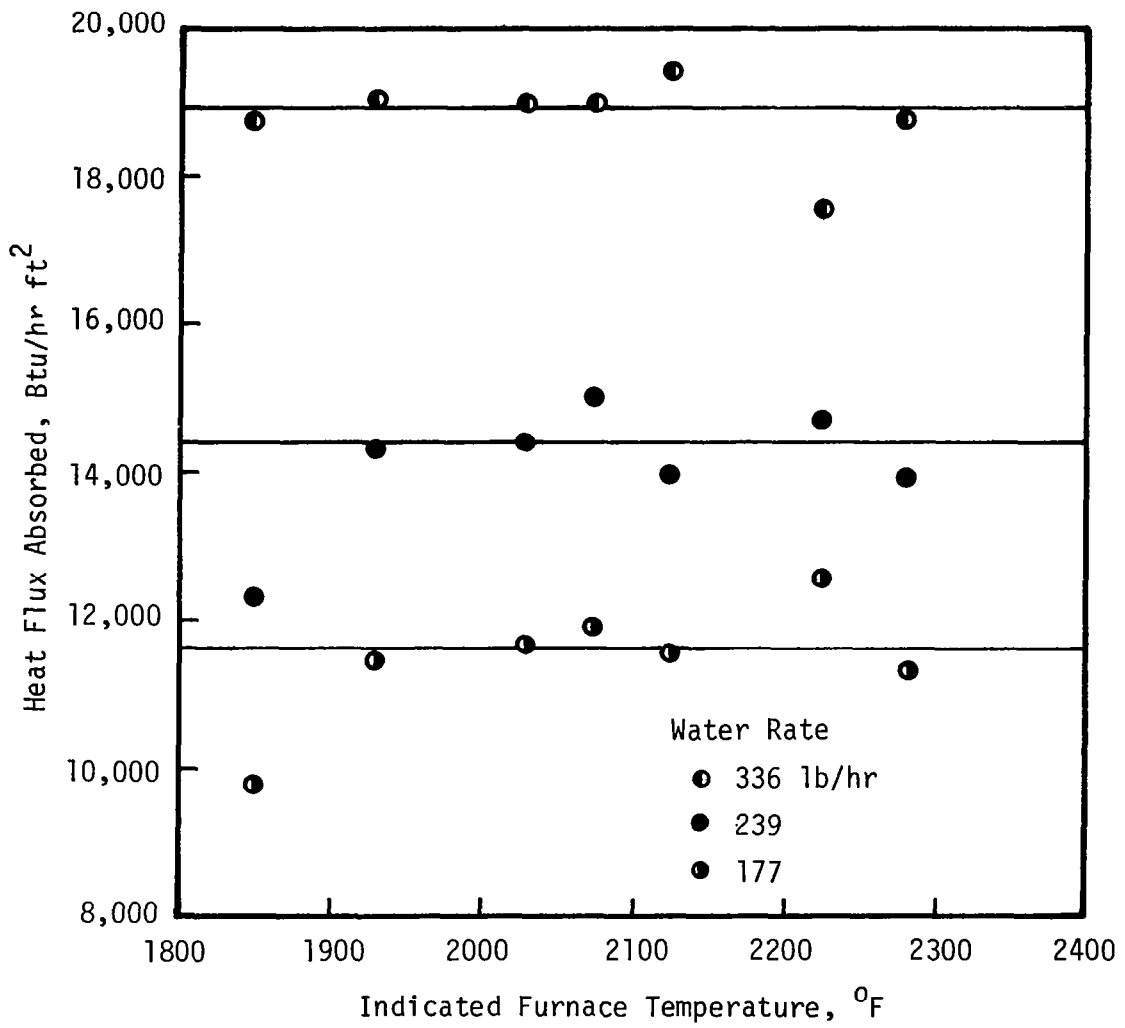
Figure 30. Heat Flux Absorbed by Aerosol Quartz Conduit with Inner
Wall Coated with Gold Film.
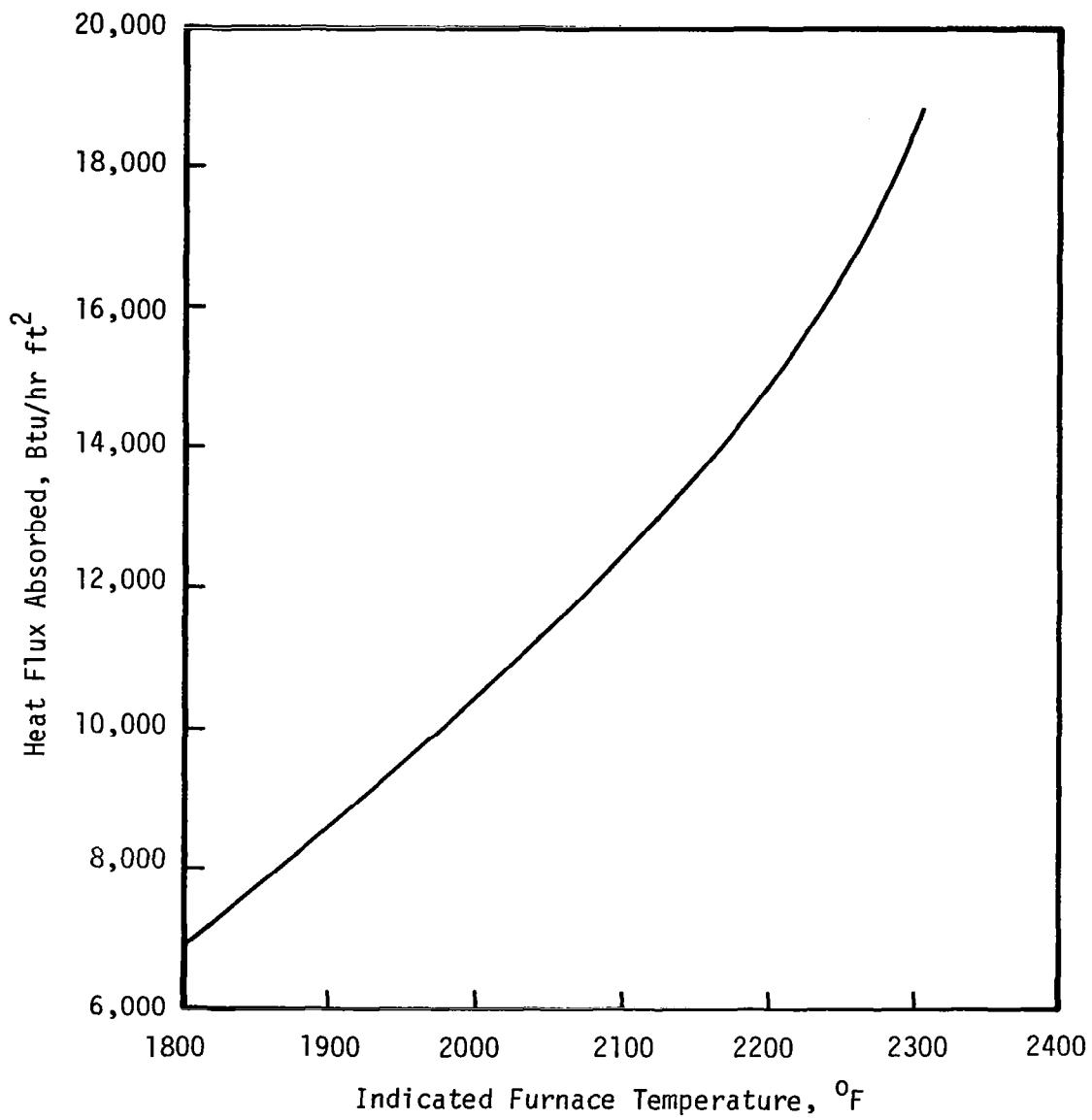
Figure 31. Average Heat Flux Impinging on Aerosol Quartz Conduit as a Function of Indicated Furnace Temperature.

graphically in Figures 29, 30, and 31. The first two figures give the total heat absorbed by the blackened and the reflective walls, respectively, as a function of the indicated furnace temperature and three water flow rates. The latter figure presents the furnace heat flux as a function of temperature after corrections were made for the small absorptivity deviation in the emissive properties of the wall coatings, i.e., 0.95 instead of 1.00 for the blackened wall and 0.03 instead of 0.00 for the reflective coating. At the indicated operating temperature of the furnace (2280° F), the heat flux was 17,600 Btu/hr ft^2.

CHAPTER IV

RESULTS AND DISCUSSION

Theoretical Developments

Generalized Calculations

The theoretical considerations of this study led to the development of an equation for evaluating the direct radiant heat transfer from a black cylindrical enclosure to a suspension of black particles contained within. The final result, as given previously by equations (2.57) and (2.58), is

$$Q_b = 2\pi i_{bnw} CS_v R \int_0^R (J_1 + J_\Sigma)\, r\,dr \qquad (4.1)$$

and with the integral evaluated

$$Q_b = 2\pi i_{bnw} CS_v R(F_1' + F_\Sigma') \qquad (4.2)$$

These relationships, however, are dimensional; they may be transformed into a more useful form by rendering them dimensionless. Thus,

$$\frac{Q_b}{(i_{bnw})(\pi R^2)} = 2kR \int_0^R (J_1 + J_\Sigma)\left(\frac{r}{R}\right)d\left(\frac{r}{R}\right) \qquad (4.3)$$

and

$$\frac{Q_b}{(i_{bnw})(\pi R^2)} = 2kR(F_1 + F_\Sigma) \qquad (4.4)$$

where F_1, F_Σ, and k are F_1'/R^2, F_Σ'/R^2, and CS_v respectively. The rate

of heat absorption (Q_b) and the product $(i_{bnw})(\pi R^2)$ have the units of Btu per unit time; their ratio is therefore non-dimensional. The quantity, kR, is the absorption coefficient (units = reciprocal length) times the radius of the system enclosure and is therefore a characteristic quantity independent of the length unit. From equations (2.19), (2.43), (2.57) and (2.58) it may be seen that F_1 is a function of L/R only and F_Σ is a function of L/R and kR.

A computer program for the Burroughs 5000 digital computer of the institution's Rich Electronic Computer Center was developed for evaluating the terms of the heat transfer equation and a general study of it was made. Sufficient results were calculated to construct a generalized plot describing the radiation process. The results are given in Figure 32 where the quantity $Q_b/(i_{bnw})(\pi R^2)$ is plotted versus L/R with kR as a parameter. The ordinate represents the rate of heat absorbed per unit radiation intensity per unit cross sectional area and is solely determined by the geometrical term L/R and the absorption parameter kR. For a constant L/R, the absorption ordinate increases with the absolute value of kR and finally when kR is infinite the absorption is a maximum given by the uppermost line. This limiting curve represents the total emissive power of the system enclosure, and the equation for it is

$$\frac{Q_{emit}}{(i_{bnw})(\pi R^2)} = \frac{(\pi)(i_{bnw})(2\pi RL)}{(i_{bnw})(\pi R^2)} = 2\pi(\frac{L}{R}) \qquad (4.5)$$

Being that the total emitted energy is represented, the plot has the desirable feature that the absorption efficiency is immediately

106
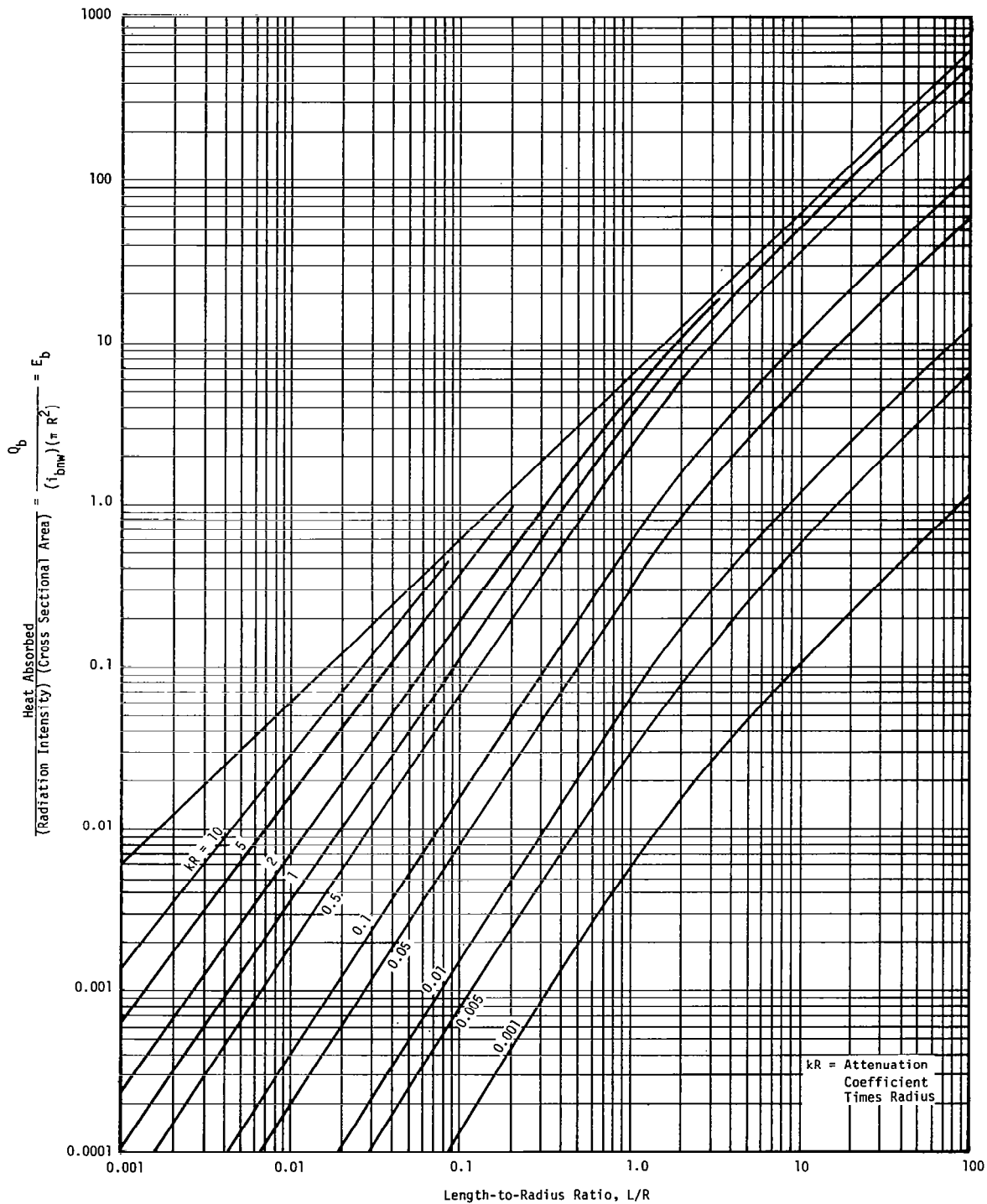
Figure 32. Generalized Correlation for the Absorption of Radiant Energy by an Evenly Dispersed Particle Cloud within a Uniformly Radiating Cylindrical Enclosure.

available by inspection; it is only necessary to divide the ordinate for a given system by the total emission represented by the uppermost curve. The efficiency, then is

$$\gamma = \frac{\dfrac{Q_b}{(i_{bnw})(\pi R^2)}}{\dfrac{Q_{emit}}{(i_{bnw})(\pi R^2)}} = \frac{Q_b}{Q_{emit}} \tag{4.6}$$

Each parametric curve has three distinct regions classifiable by the L/R ratio. For very small or very large values of the abiscissa, each curve is very nearly a straight line. Between these regions each curve has a variable slope such that the functions are smoothly continuous between the two characteristically linear regions. The linear extensions of the curves make them suitable for indefinite extrapolation.

Construction of Additional Parametric Curves

While the generalized graph gives accurately the effect of the geometric variables, the particle cloud absorption properties were limited to selected parametric curves for kR, and interpolation between them is uncertain. The data, however, may be replotted to yield results for any value of kR, if L/R is made the parameter. The graph, for the most part, is very nearly linear, except near total absorption, and results for a particular kR can be read very accurately. If only one system is being studied, the plot is made for the required L/R. If, however, a completely new parametric curve is needed the process is repeated for several L/R values and as many points as desired can be plotted on the generalized graph, and the new curve constructed. Five

charts of this nature are given in Figures 33 through 37 for several widely spaced L/R values. The construction of additional curves by this method is very accurate and results from the procedure were checked with the computer and almost exact agreement was found. For points near total absorption, however, calculated data were not obtained because of arithmetic or exponential overflows in the computer operations, unsuitable accuracy in partial results, and unsatisfactory convergence. Extrapolation of these data to kR values larger than those given may be attempted but the results will be outside the range of computations.

Use of the Generalized Chart

The generalized graph was developed specifically for the evaluation of the absorption of radiant energy by clouds of uniformly dispersed black particles while within a black, uniformly radiating cylinder. The result for a particular problem is obtained by forming the length-to-radius ratio and the absorption parameter, kR; determining the corresponding ordinate for these values and multiplying this number by the radiation intensity and the cross sectional area of the enclosure. The result is the heat absorbed by direct emission from the radiating wall; the value divided by the total emission from the enclosure gives the particle cloud absorption efficiency. This is the primary use of the generalized graph.

If the total length of an enclosure is not heated and unheated sections extend beyond the heated region, there is additional absorption of radiation by particles contained in the unheated extensions.
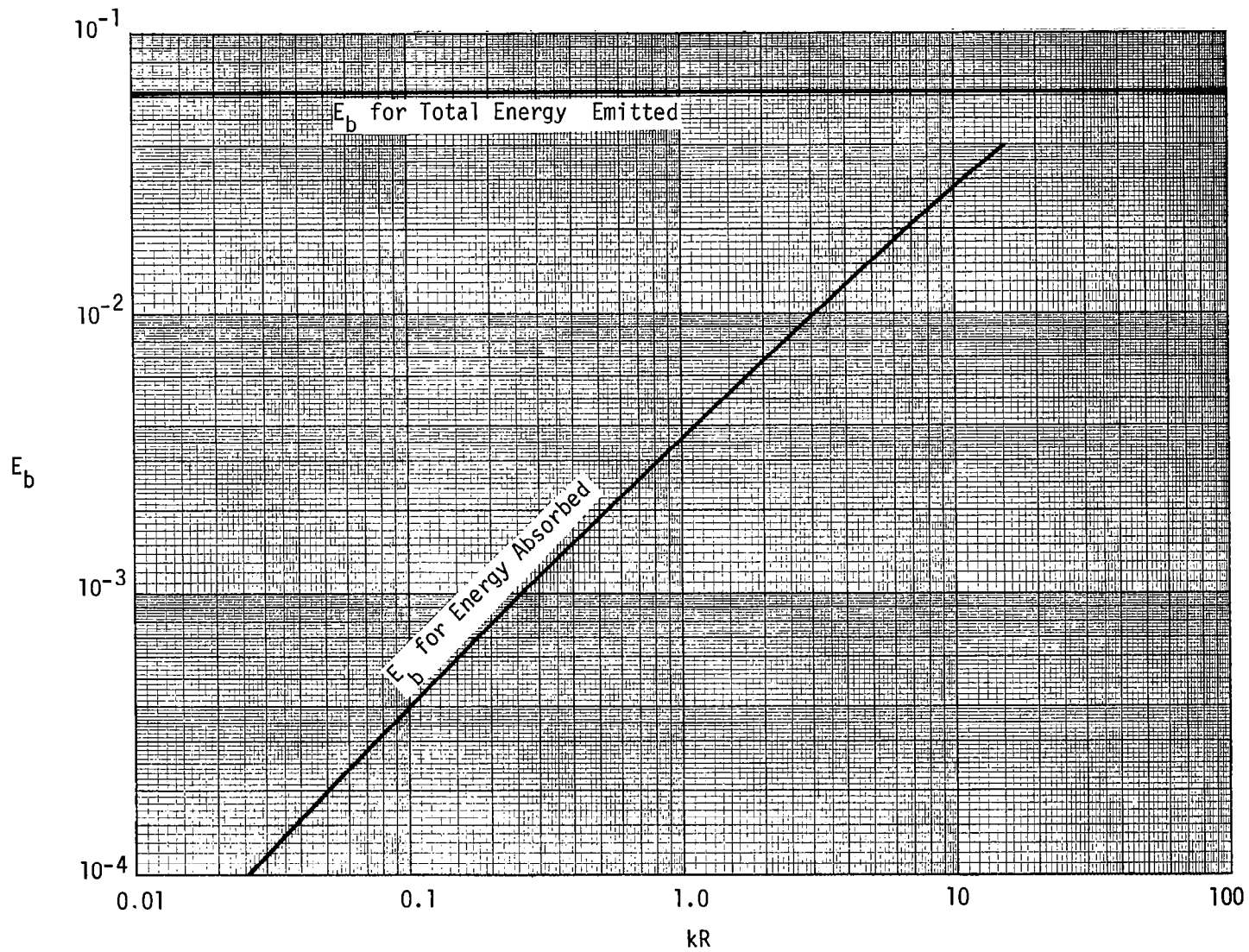
Figure 33. Generalized Results for a Length-to-Radius Ratio of 0.01.
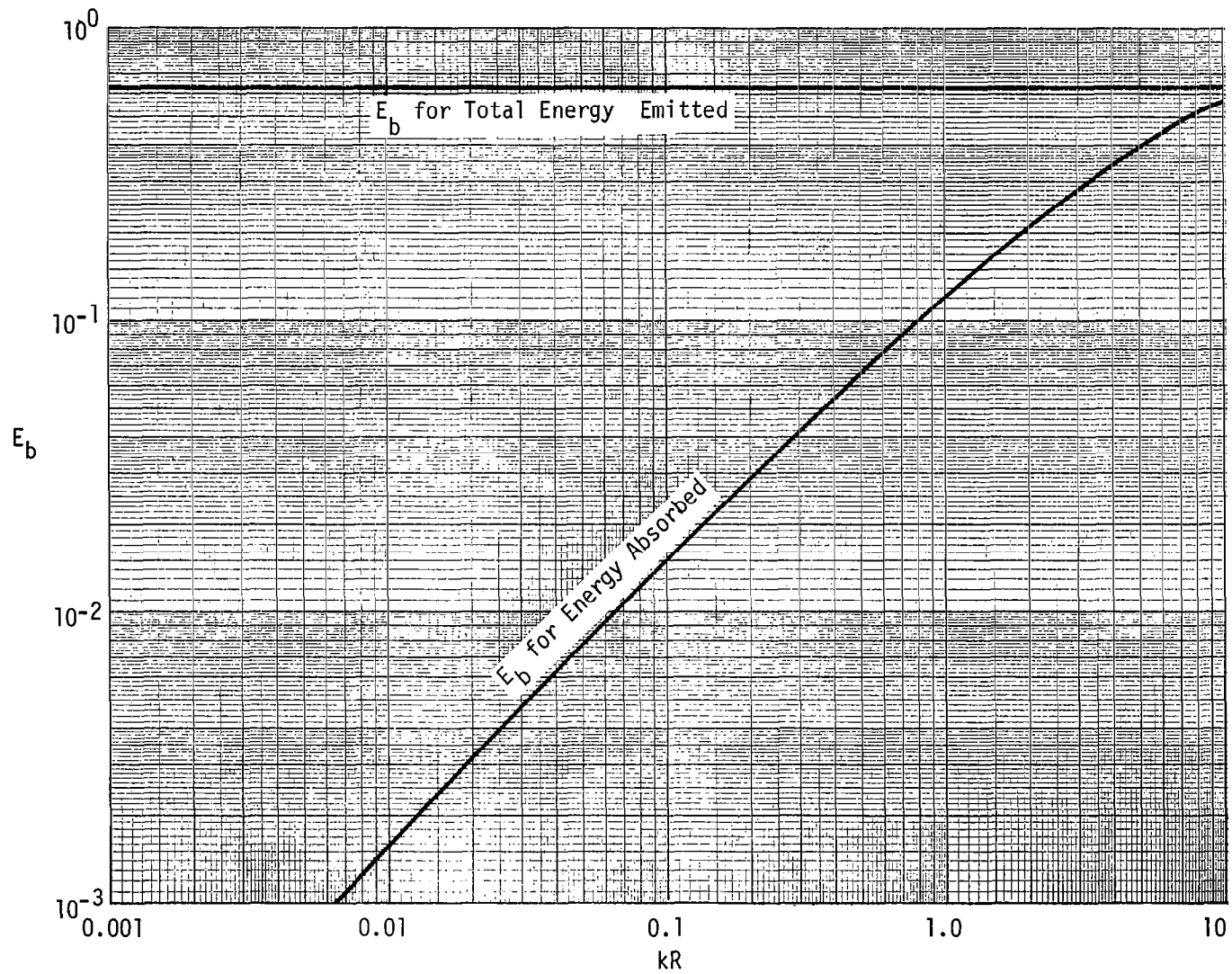
Figure 34.   Generalized Results for a Length-to-Radius Ratio of 0.1.
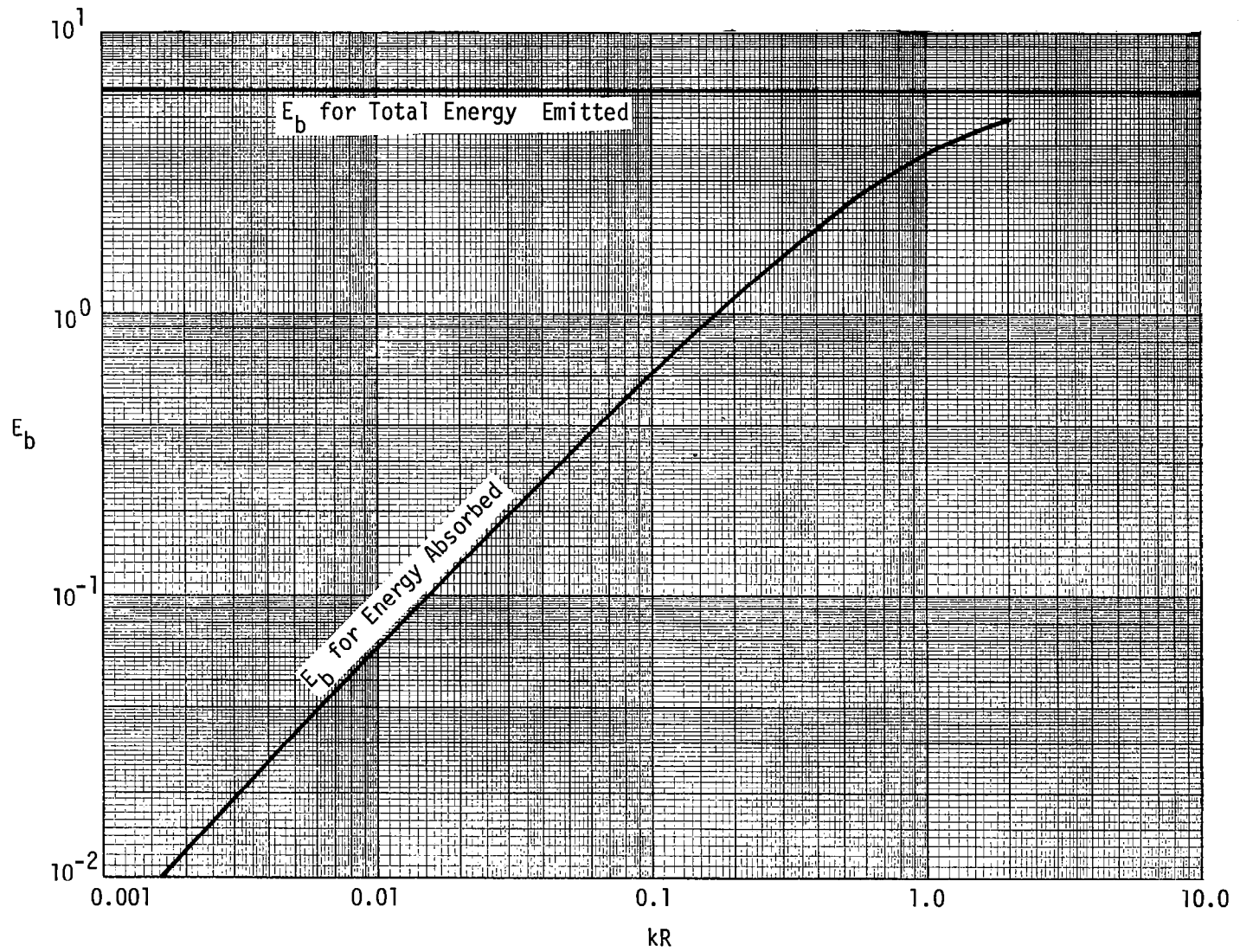
Figure 35.   Generalized Results for a Length-to-Radius Ratio of 1.0.
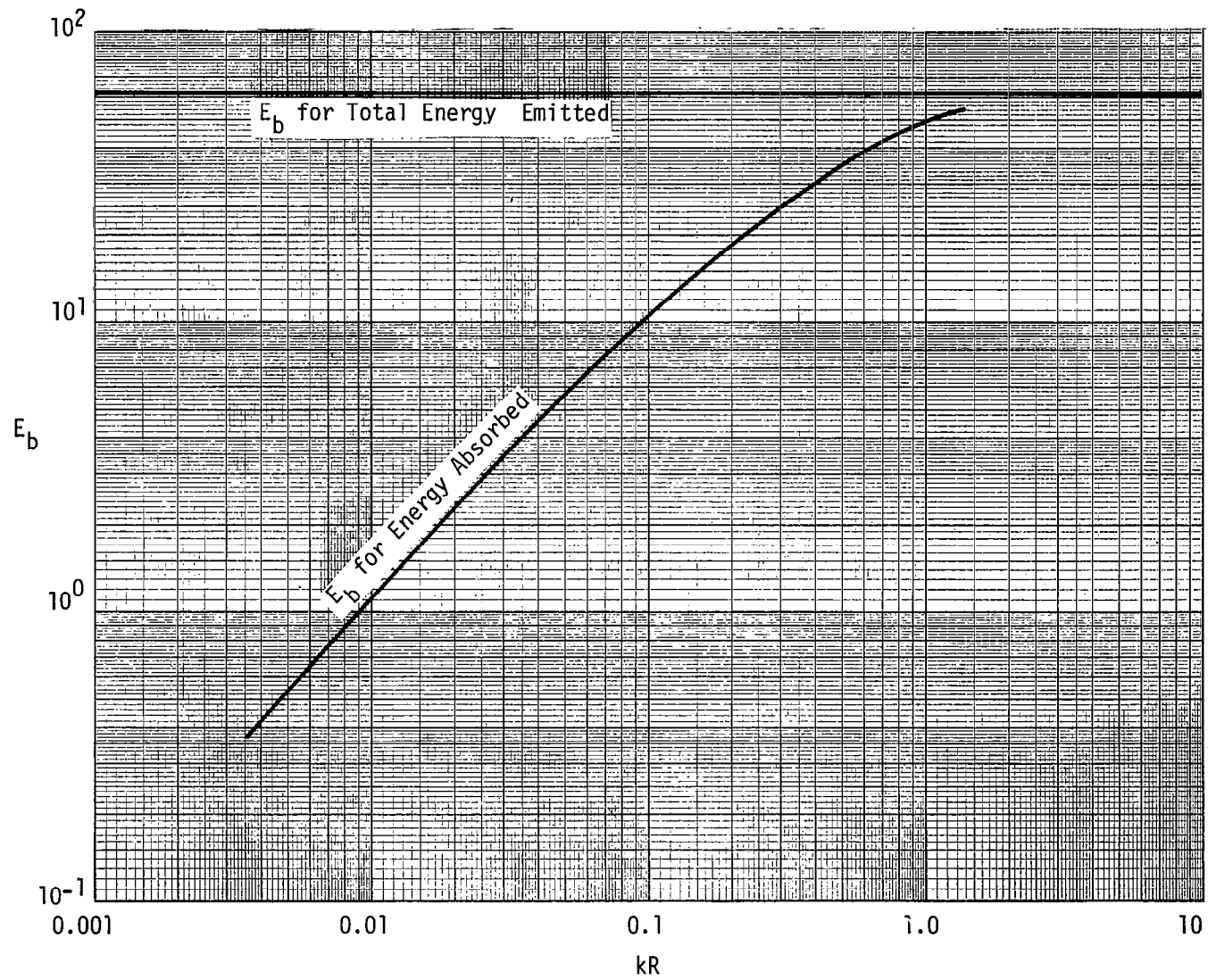
Figure 36. Generalized Results for a Length-to-Radius Ratio of 10.0.
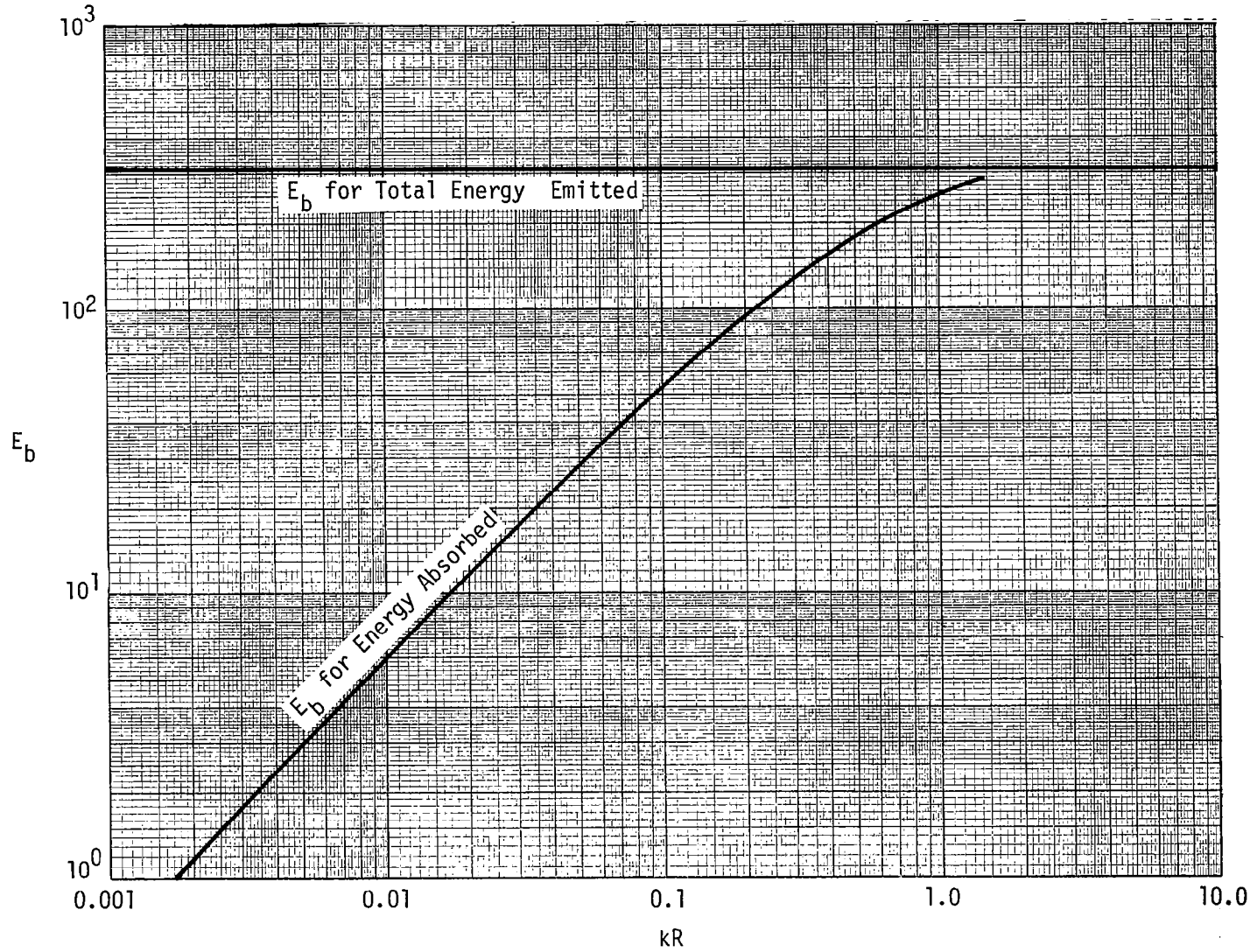
Figure 37. Generalized Results for a Length-to-Radius Ratio of 48.906.

This absorption may be significant in some systems, especially when the length-to-radius ratio is small. The increase in heat transfer is calculable from the basic radiation equation by changing the limits of integration and developing a calculation procedure similar to the one presented. The same result, however, is available from the generalized chart, but the following developments are required.

The absorption process in an unheated length can be described by first analyzing how absorption within a heated region is changed upon adding other heated increments. Consider two equal lengths of enclosure. If they are adjacent, the heat absorbed may be designated as E_{2x}; if they are separate the total for both is $2E_x$. The absorption is greater when the two lengths are adjacent because of mutual absorption from each other. It follows then that

$$E_{2x} - 2E_x = 2\Delta E_x^x \qquad (4.7)$$

where $2\Delta E_x^x$ is the increase in absorption when the lengths are placed together. The subscript on this quantity indicates the absorbing length and the superscript indicates the emitter. The factor 2 appears because of the reciprocal emission and absorption between the two lengths.

The next step is to consider three increments. The relationship for this case is

$$E_{3x} - 3E_x = 2\Delta E_x^{2x} + 2\Delta E_x^x \qquad (4.8)$$

where again the delta-quantities describe the effect of placing the three lengths together. They are derived by considering the radiation received by each length, taken individually, that is emitted from all

lengths on each side of it, taken separately. By way of explanation,
define the increments consecutively as A, B, and C. If A and B are
taken together radiating to C, the result is ΔE_x^{2x} (here 2x is the
emitting length and x the absorber). The lengths B and C radiate to
A, hence a second ΔE_x^{2x}. The total then is $2\Delta E_x^x$. Then A can radiate
to B and C to B; these combinations give $2\Delta E_x^x$.

If four increments (A, B, C, and D) are taken, a similar equa-
tion with an additional term is obtained. Again the radiation from
the entire neighborhood to each element is considered; a different
approach is clearer, however, when higher combinations are involved.
The notation may be employed:

$$ABCD \rightarrow A = (A \rightarrow A) + (BCD \rightarrow A) \qquad (4.9)$$

$$ABCD \rightarrow B = (B \rightarrow B) + (ACD \rightarrow B) \qquad (4.10)$$

$$ABCD \rightarrow C = (C \rightarrow C) + (ABD \rightarrow C) \qquad (4.11)$$

$$ABCD \rightarrow D = (D \rightarrow D) + (ABC \rightarrow D) \qquad (4.12)$$

and

$$(ABCD \rightarrow A) + (ABCD \rightarrow B) + (ABCD \rightarrow C) + (ABCD \rightarrow D) = E_{4x} \qquad (4.13)$$

where the arrow means "radiates to." If these results are added to-
gether the total radiation recieved by the elements in E_{4x}. When the
elements are separate the radiation interchange may be defined as

$$A \rightarrow A \qquad (4.14)$$

$$B \rightarrow B \qquad (4.15)$$

$$C \rightarrow C \qquad (4.16)$$

$$D \rightarrow D \qquad (4.17)$$

116

and

$$(A \rightarrow A) + (B \rightarrow B) + (C \rightarrow C) + (D \rightarrow D) = 4E_x \qquad (4.18)$$

Here the total radiation absorption is $4E_x$. Subtraction of the latter set of relations from the former gives

$$(ABCD \rightarrow A) - (A \rightarrow A) = BCD \rightarrow A \qquad (4.19)$$

$$(ABCD \rightarrow B) - (B \rightarrow B) = ACD \rightarrow B \qquad (4.20)$$

$$(ABCD \rightarrow C) - (C \rightarrow C) = ABD \rightarrow C \qquad (4.21)$$

$$(ABCD \rightarrow D) - (D \rightarrow D) = ABC \rightarrow D \qquad (4.22)$$

Following the development already given for equation (4.8) it may be shown that

$$BCD \rightarrow A = \Delta E_x^{3x} \qquad (4.23)$$

$$ABC \rightarrow D = \Delta E_x^{3x} \qquad (4.24)$$

$$ACD \rightarrow B = \Delta E_x^{2x} + \Delta E_x^{x} \qquad (4.25)$$

$$ABD \rightarrow C = \Delta E_x^{2x} + \Delta E_x^{x} \qquad (4.26)$$

Equations (4.9) through (4.26) may be shown to combine and give

$$E_{4x} - 4E_x = 2\Delta E_x^{3x} + 2\Delta E_x^{2x} + 2\Delta E_x^{x} \qquad (4.27)$$

If more increments are added, a series is established. In general then, it follows that

$$E_{(n+1)x} - (n+1)E_x = 2\Delta E_x^{nx} + 2\Delta E_x^{(n-1)x} + \ldots + 2\Delta E_x^{x} \qquad (4.38)$$

and

$$\dot{E}_{nx} - nE_x = 2\Delta E_x^{(n-1)x} + 2\Delta E_x^{(n-2)x} + \ldots + 2\Delta E_x^x \qquad (4.29)$$

These equations may be rearranged and solved to give

$$\Delta E_x^{nx} = \frac{1}{2}[\; E_{(n+1)x} - (n+1)E_x \;] - [\; \Delta E_x^{(n-1)x} + \Delta E_x^{(n-2)x} + \ldots$$

$$+ \; \Delta E_x^x \;] \qquad (4.30)$$

and

$$\Delta E_x^{nx} = \frac{1}{2}[\; E_{(n+1)x} - (n+1)E_x] - \frac{1}{2}(E_{nx} - nE_x) \qquad (4.31)$$

Since

$$(n+1)E_x = nE_x + E_x \; , \qquad (4.32)$$

$$\Delta E_x^{nx} = \frac{E_{(n+1)x} - E_{nx} - E_x}{2} \qquad (4.33)$$

The significance of ΔE_x^{nx} is that it arises from the end incre-
ment receiving radiation from all the n other elements. This amount
of energy is received regardless of whether or not the end element is
emitting. Hence, if nx is a heated length, the radiation from it to
x can be evaluated from equation (4.33).

When a length of enclosure radiates to a longer length it is
desirable to have ΔE_{nx}^x rather than ΔE_x^{nx}. The result is directly
available from

$$E_{(n+1)x} - E_{nx} - E_x = \Delta E_x^{nx} + \Delta E_{nx}^x \qquad (4.34)$$

which together with Equation (4.33) yields

$$\Delta E_{nx}^{x} = \frac{E_{(n+1)x} - E_{nx} - E_{x}}{2} \qquad (4.35)$$

It follows also that

$$\Delta E_{nx}^{x} = \Delta E_{x}^{nx} \qquad (4.36)$$

The derivations are restricted to n being an integer. It may be readily shown, however, that the derivation holds for any real value of n.

The utility of the extension formulas may be demonstrated by specific examples. Take, for instance, a cylinder with an L/R ratio of 3.0 containing a particle cloud with a kR value of 1.0. When an unheated extension equal to one half the heated length is involved, equation (4.33) is applicable and n is 2. The heat absorbed by particles while they are in the extension is

$$\Delta E_{x}^{2x} = \frac{E_{3x} - E_{2x} - E_{x}}{2} \qquad (4.37)$$

where E_{x} is the generalized ordinate for L/R of 1.5, E_{2x} for an L/R of 3.0, and E_{3x} for an L/R of 4.5, each being established on the curve, kR = 1. The points for the L/R ratios reflect the changes in cylinder length being considered, since the radius is the same for all cases. If there are extensions on both ends of the heated length, calculations are made for each separately. When both extensions are the same, the result for one length is doubled.

In the preceding example, if the unheated length were five times that of the heated section the result would be

$$\Delta E^x_{5x} = \frac{E_{6x} - E_{5x} - E_x}{2} \tag{4.38}$$

where again x is the L/R ratio of the basic heated length. The unheated-to-heated length ratio does not have to be integral. For instance, it may be 5.5 and the additional heat absorption would be

$$\Delta E^x_{5.5x} = \frac{E_{6.5x} - E_{5.5x} - E_x}{2} \tag{4.39}$$

For each example, ΔE^x_{nx}, or ΔE^{nx}_x, whichever is needed, is to be added to E_b for the heated length to obtain the total result for the system.

In performing the calculations for specific cases it may be found that the total absorption $(E + \Delta E)$ does not increase smoothly with increasing unheated length. This condition results from inaccuracies in reading the generalized graph. To obtain improved results, it may be necessary, in particular for L/R over unity, to construct a larger, more accurate graph by the use of Figures 33 through 37 as already described.

Application to Other Types of Radiation

While this investigation was concerned with thermal radiation, the basic equations and results are applicable to all forms of electromagnetic and field-emission radiation. One conceivable use might be the evaluation of the radiation dosage an aerosol receives while passing through a cylindrical enclosure with nuclear radiation coming into its interior. The calculation may be made directly if a radiation cross-section value for the suspended particles is known.

Other Important Variables

For many systems, the described calculations are adequate. Frequently, however, either the wall enclosure or the particle surfaces,

or both, are not perfect absorbers and adjustments in the calculations may be required. The emissivity of the wall is first taken into account when the radiation intensity is evaluated; the calculations as described, however, are unaffected at this point. If radiation crosses the enclosure and is intercepted by the wall surface, it is partly absorbed and partly reflected. The reflected energy is available for further absorption by the particles and the infinitely continuing process adds to the heat transfer as more reflections occur. Only the first few, perhaps two or three, need be considered in many cases.

If the energy intercepted by the wall from each emission is evaluated, these reflections may be traced and their contribution to the overall result calculated. It is feasible to attempt these calculations, but a detailed study is required before general conclusions can be stated. It is reasonable to expect, however, that situations with large wall emissivities should correspond very closely to the ideal solution. If, for example, the wall emissivity is 0.75 then only one-fourth of the radiation intercepted by the walls is reflected. If the aerosol is highly absorbing very little energy reaches the wall, hence the reflected energy may be neglected. If the aerosol is weakly absorbing, a large portion of the energy may be intercepted by the wall, the extent of interception being dependent on the wall-to-wall view factor. When the reflected energy traverses the aerosol, part of it is absorbed therein, and in terms of a percentage, this part is approximately the same as for the original direct emission. Since a maximum of 25 per cent of the direct emission can be reflected, the additional absorption is no more than about 25 per cent of the first-pass absorption. The

maximum absorption occurs only when the wall-to-wall view factor
approaches unity. Subsequent reflections may be considered but they
contribute little; the second reflection amounts only to about 6 per
cent of the absorption by direct radiation. Hence, it may be concluded
that, qualitatively, a maximum error due to imperfect wall emissivities
can be estimated if the first few reflection processes and the wall-to-
wall view factors are considered.

Imperfect absorption by the particles is more complicated. A
first approximation for absorptivities less than unity is to multiply
the ideal result by the absorptivity of the particles. The results
for particle absorptivities less than, but near, unity should be accur-
ate within a few per cent; they may be estimated as above. Further and
more precise adjustments are complicated by scattering patterns, changes
in attenuation coefficient, and view factor considerations, to mention
some of the more important variables. Additional study is recommended.
The problem should be considered along with back-radiation to which it
is closely related.

Still another area requiring further investigation is the effect
of aerosol temperature variations on back-radiation and attenuation
coefficients. It is believed that this work can readily be extended to
describe these more involved problems.

Experimental Results and Comparison with Theoretical Development

Previous investigators have dealt with the absorption of radiant
energy by particles clouds and have presented theoretical formulations
applying to their problem. Generally, however, the calculated results

served as corrections to other problems or as secondary but important factors rather than as a study of primary interest. Reliance was made almost completely on calculations because of the difficulties in obtaining experimental data for radiation to dispersed systems. This investigation sought to measure the absorptances of selected, well-characterized aerosols and to compare the results with theory as herein presented. A primary effort was also made to study specifically the effect of particle size on the absorptive characteristics of the aerosols. The heat transfer data obtained have already been presented graphically in Figures 26, 27, and 28 and tabulated in Appendix B. The results as shown were for the total increase in heat absorption due to the addition of particles to the aerosol stream. Further considerations were required before the heat absorption due to radiation could be evaluated.

The experimental approach was predicated on the enhancement of radiative heat transfer to the aerosol system and the reduction to a minimum of all other heat transfer processes. Not all the extraneous heat transfer effects were removed. From the experimental and calculated data of Appendix B it was established that when air alone was flowing in the aerosol system an average of 7.8 Btu/min was absorbed. This value ranged from 7.4 to 7.9 for practically all tests. This heat transfer was sufficiently small for radiation to contribute significantly to the result. Adjustments in the final result were required to account for changes in convection when particles were added to the system.

Particles in a flowing gas increase the convective heat transfer coefficient above that for the gas alone. This problem has been studied

and quantitative data have been derived. Results relating the Nusselt number to particle loading as derived from Tien[48] and Farber and Morley[49] are given in Figure 38. Data were available down to a Reynolds number of 13,500, but the aerosol systems in this investigation had a Reynolds number of 10,000. From generalized curves, however, the data could be extrapolated with acceptable accuracy to the required Reynolds number for aerosols with solids-to-gas weight ratios less than 1.5.

The heat transfer by convection to the aerosol system may be described by

$$(Q_c)_a = h_a A(t_w - t_a)_{mean} \tag{4.40}$$

and

$$(Q_c)_p = h_p A(t_w - t_p)_{mean} \tag{4.41}$$

where only the heat transfer inside the aerosol conduit is considered. The ratio of these two equations is

$$\frac{(Q_c)_p}{(Q_c)_a} = \frac{h_p A(t_w - t_p)_{mean}}{h_a A(t_w - t_a)_{mean}} \tag{4.42}$$

During heating, t_a was never different from t_p by more than 10° F and in many cases 5° F. The wall temperature, while not measured, was probably reduced slightly by the increase in heat transfer. It was assumed than that the mean temperatures were very nearly equal and the heat transfer with and without particles was essentially determined by
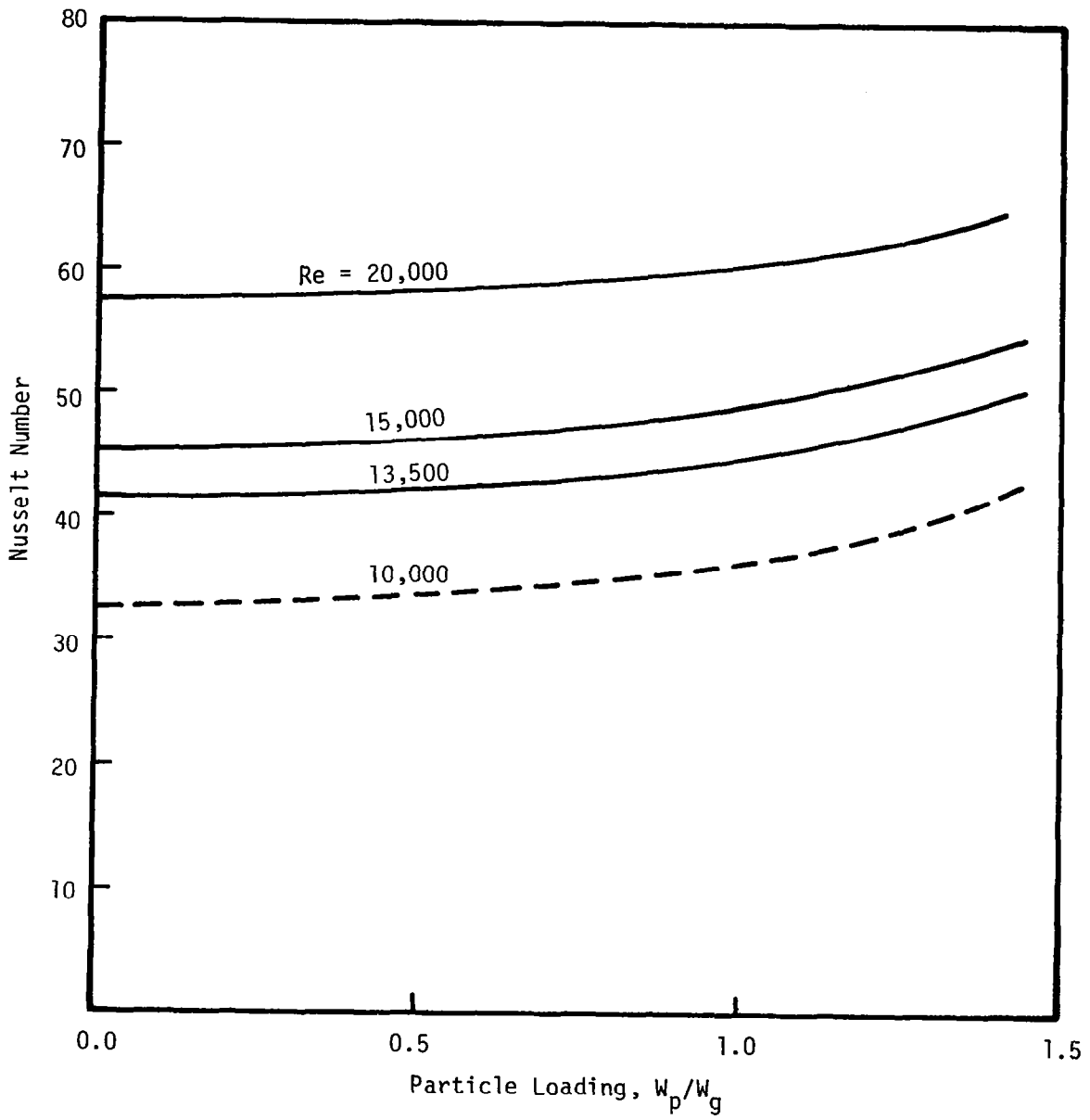
Figure 38. Nusselt Number for Particle-Gas Suspensions for Experimental System.

$$\frac{(Q_c)_p}{(Q_c)_a} = \frac{h_p}{h_a} \qquad (4.43)$$

The ratio of heat transfer coefficients was numerically equal to the ratio of Nusselt numbers given in Figure 38. Since $(Q_c)_a$ was found by experiment to be 7.8 Btu/min, $(Q_c)_p$ could be estimated. The amount of energy previously calculated by equations (3.6) and (3.15) represented the total heat absorption due to the addition of particles to the system with corrective heat transfer included. The heat absorbed by radiation alone was less by the amount $(Q_c)_p - (Q_c)_a$.

The data for total heat absorption and for radiant absorption alone are presented in Figures 39 and 40. The results were replotted versus k rather than particle cloud concentration because the latter presentation was more general and was useful in comparing the experimental with the theoretical results.

Particle Geometry, Attenuation Coefficient, and Associated Quantities

Of basic importance were particle sizes and size distributions. These data were required for the evaluation of such quantities as the particle surface and cross-sectional areas, S_v, and k, respectively. An attempt was made to derive the surface areas from low temperature gas adsorption isotherms but this approach was found to require much more study before it could yield reliable results. Surface area determinations, therefore, were calculated from direct measurements of statistical particle diameters. These size distributions are given in Appendix A. The size designations, the zinc powder excepted, are for the screen opening size employed in preparing the different fractions;
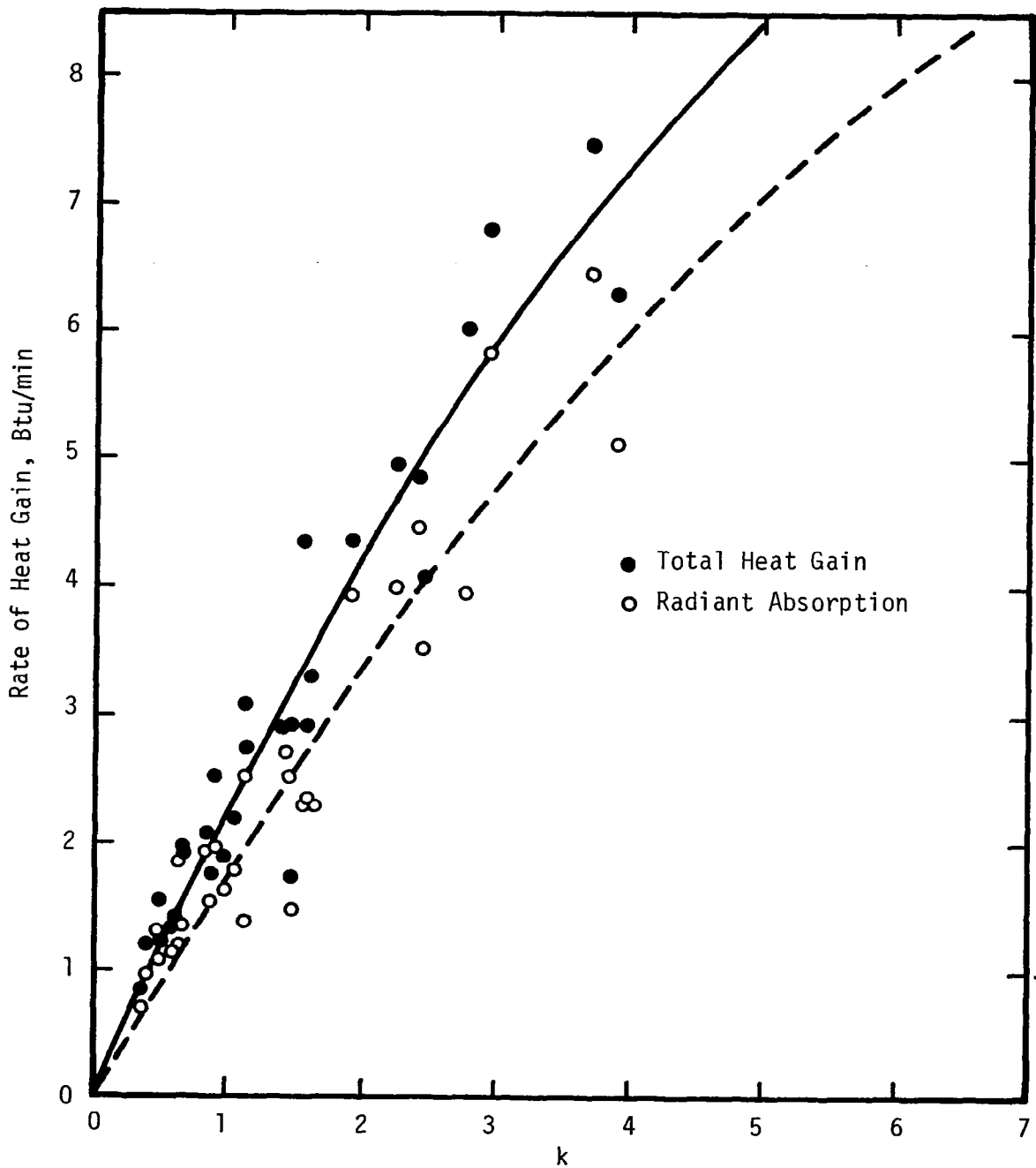
Figure 39. Rate of Heat Gain by Ferrous Sulfide and Cupric Oxide Aerosols as a Function of the Attenuation Coefficient Before and After Correction for Convective Heat Transfer.
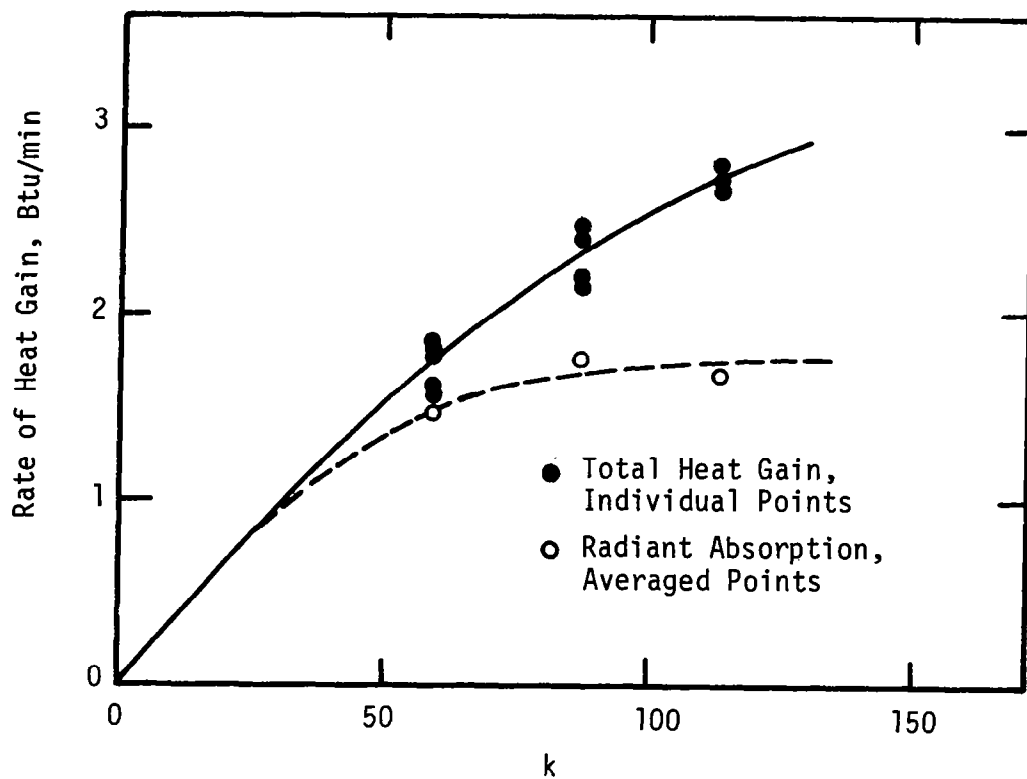
Figure 40. Rate of Heat Gain by Zinc Aerosols as a Function of the
Attenuation Coefficient Before and After Correction for
Convective Heat Transfer.

the quoted diameters are not the particle size limits for each powder. Imperfect separation and particle attrition during the tests produced broadened distributions. The mean particle sizes among the samples were significantly different.

The geometric quantity most significant in radiation heat transfer is S_v, the ratio of particle cross sectional area to particle volume. This parameter multiplied by the particle volume concentration gave the attenuation coefficient, k. The calculated results for S_v are summarized in Table 2. The computational procedure is described in the section headed Particle Geometry and Measurement of Chapter III.

While the attenuation coefficient is determined solely by the product of the quantity S_v and the particle volume concentration, two other parameters influenced its value. One was the decrease in concentration with increasing aerosol temperature; the other was the increase in hold-up concentration because of velocity slip. The temperature rise of the aerosols studied decreased the calculated flow concentration by about 10 per cent. The flow concentration as determined experimentally, however, was not a measure of the number (or volume) of particles actually within a given length of aerosol conduit, it is the hold-up concentration that is actually needed. Direct experimental data were not available for the particle sizes employed but from other studies with larger particles[50] it appeared that the hold-up concentration was about 10 per cent larger than the flow concentration. Since precise data were not available and the two effects were opposite and probably very nearly equal, these two variables were neglected.

Table 2. Surface Property, S_v, Calculated from
Particle Size Distributions

Material	Size Designation	$S_v \times 10^{-3}$ (1/ft)
FeS	53-88, micron	6.610
	44-53	10.55
	30-44	13.75
	20-30	15.08
CuO	53-88	4.670
	44-53	6.130
	30-44	10.67
Zn	20-30	18.03
	1-10	653.0

Radiation Properties of Quartz Enclosure and Particles

The quartz aerosol conduit could be regarded as behaving like a black enclosure, although the radiation passing through it was not black. Radiation within the furnace but outside the quartz tubes approached that of a perfect radiator because of the high emissivity of the furnace walls and because the furnace was nearly a complete enclosure. This energy, however, upon passing through the quartz tubes was screened, and, from the transmissive properties of the quartz given in Figure 20, the radiation reaching the center conduit appeared to have been principally between one and three microns in wave length for a black body furnace temperature of 2200° R. From the standpoint of energy distribution with respect to wave length, the radiation, then, was far from being black. The quartz, however, was over 90 per cent transparent to the radiation (one to three microns) reaching the inner concuit. Radiation crossing the tube without being absorbed continued through the wall and the overall effect was the same as if it were absorbed there by a black surface. The quartz then, because of its excellent transmissive properties, behaved as though it were black in that reflections from the wall back to the aerosol could be neglected.

The ferrous sulfide and cupric oxide aerosol particles were considered to be very nearly completely absorbing. They were black in appearance which meant that radiation in the visible range (0.3 to 0.8 micron) was largely absorbed. While this degree of absorption did not necessarily hold for longer wave length it is probable that a high degree of absorption prevailed up to three microns which is not very far in the infrared region; for most systems the infrared region must

be considered up to 15 microns. There were no experimental data for ferrous sulfide to indicate the absorptivity of this material; a value of approximately 0.8 was reported[51] for cupric oxide for very low-temperature radiation. This experimental number, however, does not correspond very well with the short wave lengths transversing the aerosol system.

The zinc particles had an absorptivity of approximately 0.045. Measured values of 0.04 to 0.05 have been reported for pure zinc surfaces and a value of 0.11 for surfaces oxidized at 750° F.[52] The zinc particles used in the experimental tests were smoothed and polished by extended circulation in the apparatus and should have had an emissivity very near the minimum for the pure material.

Comparison of Theoretical and Experimental Findings

The ferrous sulfide and cupric oxide aerosols were similar in particle size ranges, concentrations, and radiation properties. Their radiation absorption characteristics were likewise similar. A joint comparison, therefore, was made of the experimental results and the theoretical calculations. The correlation is given in Figure 41. The experimental data are corrected for convective heat transfer as previously described; without the adjustment the experimental results averaged about twenty per cent higher than the calculated values which were derived for totally absorbing particles. The absorption data are given as the fraction of energy absorbed over energy emitted since this ratio (or efficiency) is of more practical importance than merely the heat absorbed by the particular aerosols. The abscissa, k, of the plot also has general significance in that its value is jointly deter-

Figure 41. Theoretical Curve and Experimental Data for Ferrous Sulfide and Cupric Oxide Aerosols Relating Absorption Efficiency and Attenuation Coefficient.

133

mined by concentration and the parameter, S_v, which in turn is a function of particle size and size distribution.

The correlation between the experimental and the calculated data appears good. The data points for the two materials, however, group above the theoretical curve for the ferrous sulfide and below it for the cupric oxide. This grouping may be due to different convective heat transfer characteristics for the two aerosols because of particle shape. The ferrous sulfide particles were irregular and the cupric oxide particles were more nearly spherical or similar in shape to smoothed pebbles in a creek bed. It is believed that the experimental data establish that particle cloud radiation properties can be properly evaluated provided the particle emissivities are high, the particle size distributions are accurately determined, and scattering effects are insignificant. These conditions have been assumed in previous studies but were really never tested by direct experimentation.

The results should be applicable to processes where the particle dimension is equal to or greater than the wave length of the radiation impinging on the particle. For black body radiation from a 2000° F source, the particles should be around 15 microns and greater, the particle surfaces should be highly absorbant. If the radiation source has a black body temperature of $10,000^{\circ}$ F, or more, particle sizes down to around 0.5 micron may be reliably treated.

The data for the zinc aerosols were compared with the theoretical development in a manner similar to that for the ferrous sulfide and cupric oxide aerosols. There was the difference, however, that the theoretical curve had to be corrected for the zinc's very low absorpti-

vity; in the former comparison the particles were apparently very nearly black. While there are many factors to be considered for reflective particle surfaces, a first approximation was made by multiplying the theoretical result by the apparent emissivity of the zinc particles. The resulting curve is shown in Figure 42 with the experimental data points. The approximation seems good for the high k values. The agreement is uncertain for more dilute suspensions since experimental points were not obtained below k = 59.

General use of the theoretical approximation is by no means recommended. The agreement for the high k values is probably due to the fact that absorption took place principally at the outer region of the particle cloud, and the small metal spheres produced very pronounced back-scattering. Hence, where the incoming radiation encountered the particles near the outer limits of the aerosol it must have been reflected away from the aerosol without significant multiple particle scattering for each ray. The result then would be essentially that of a smooth zinc metal surface absorbing 0.043 of the incoming radiation and reflecting the balance.

While the estimated theoretical line may be incorrect by a large percentage, its use for a high concentration of metal spheres appears good. At lower k values, or more properly kR values, the result may be used for estimation purposes where no other more-refined approach is available. This should be the subject of further investigations in the future.
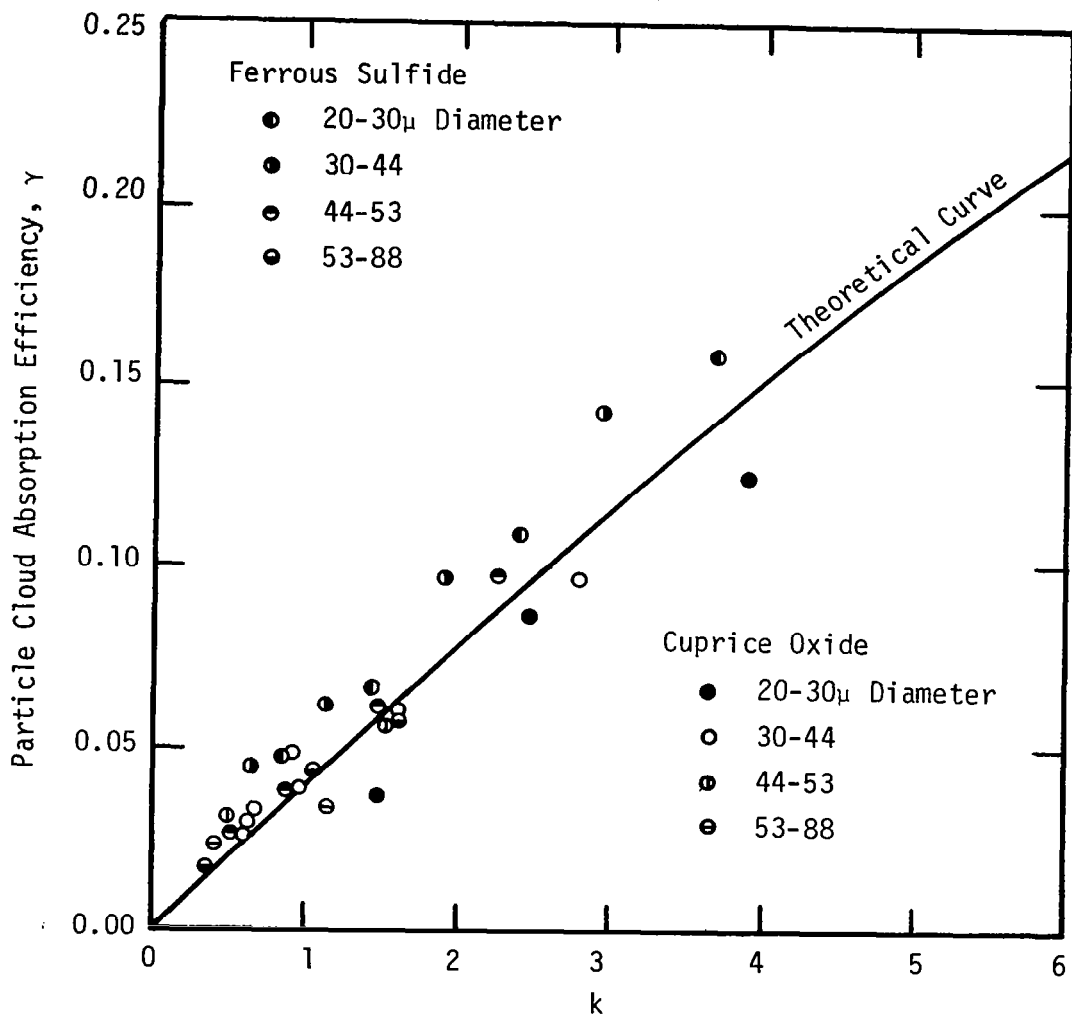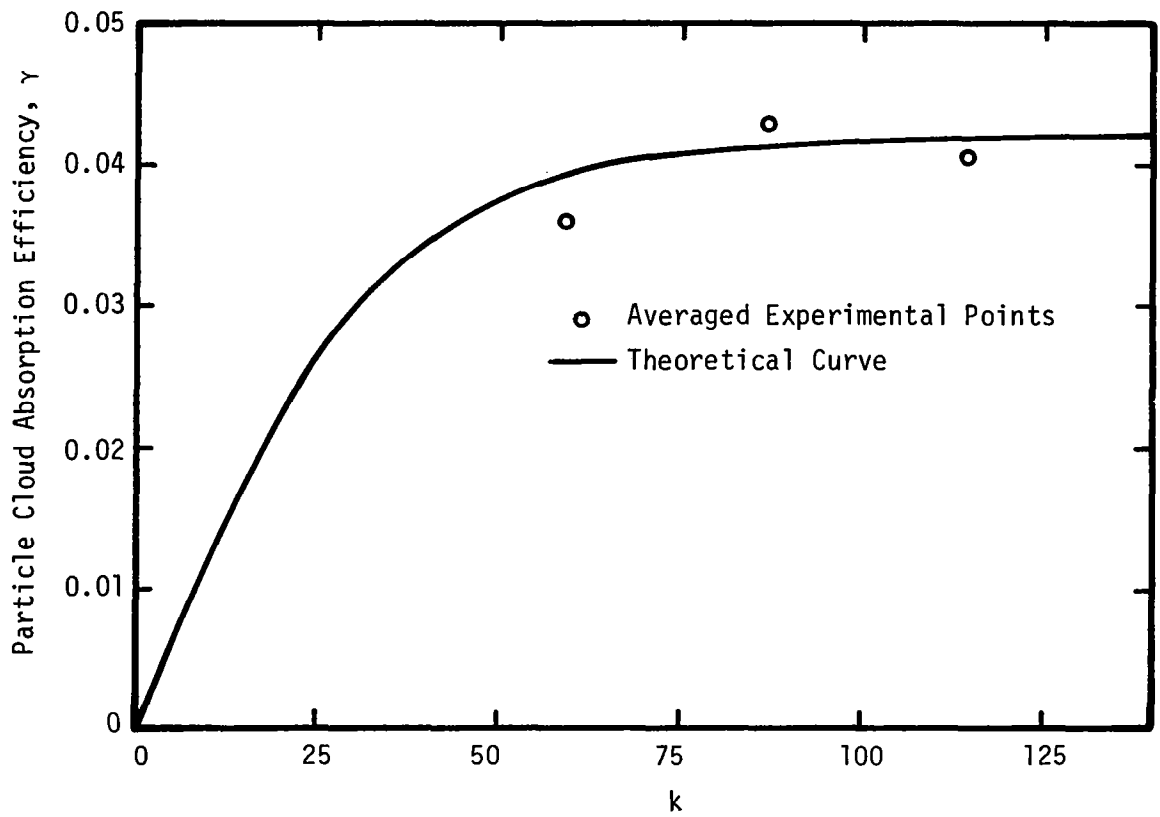
Figure 42. Theoretical Curve and Experimental Data for Zinc
            Aerosols Relating Absorption Efficiency and
            Attenuation Coefficient.

CHAPTER V

CONCLUSIONS AND RECOMMENDATIONS

The following statements summarize the more important results
of this investigation:

1. A combined analytical and numerical procedure was developed
to solve the basic radiation equation describing the radiant heat trans-
fer from a black cylindrical enclosure radiating uniformly to a black,
evenly dispersed particle cloud within from which back thermal radiation
and radiation scattering were negligible.

2. A generalized graph was prepared from theoretical concepts
which describes the rate of heat absorption by the particle cloud in
terms of cylinder wall radiation intensity, cylinder length and radius,
and particle cloud attenuation constant. The results were expressed as
non-dimensional quantities with $Q_b/(i_{bnw})(\pi R^2)$ as the ordinate, L/R
as the abscissa, and kR as a parameter.

3. The theoretical results for a given kR value may be extra-
polated to very large or very small L/R values since the curves in these
regions become very nearly linear.

4. Interpolation between kR curves may be accurately accomplished
by replotting the data on a log-log grid with L/R as a parameter. The
curves so obtained are smooth and for the most part are linear, except
near total absorption.

5. For L/R ratios greater than unity, the absorption efficiency

of a particle cloud is high for kR values of unity and larger.

6. The absorption efficiency decreases rapidly with decreasing L/R below unity.

7. All parametric curves approach a straight line with a slope of $45°$ at high L/R values because, for these conditions, the radiation system is behaving as though it were an infinitely long cylinder.

8. Equations were developed expressing the rate of heat absorption by an aerosol while in the entrance and exhaust sections adjoining a heated length.

9. An experimental method was developed for measuring the absorption of radiant energy by particle clouds when their temperatures are low relative to that of the source, normally convective heat transfer is dominant under these conditions compared with radiative heat transfer.

10. It was confirmed experimentally that the radiation properties of a dispersion may be characterized by its particle concentration, the total particle cross sectional area, and the total particle volume when the latter are determined from precise, statistical measurements from particle size histograms. Uncertainties arise, only when radiation scattering is significant and the particles are not black.

11. The theoretical development should be applicable in determining the dose rate for an aerosol being exposed to nuclear radiation provided the appropriate cross sections for the aerosol particles are known.

While the results of this investigation contribute to an understanding of thermal radiation to particle clouds, there are numerous other problems yet to be solved. Among the more important may be

listed the following:

1. An investigation of back radiation from the aerosol to the wall should be made using the approach initiated by this study. The results should be extended to include radiation scattering, and the effect of non-black particles.

2. The effects of axial temperatures variations should be investigated and extended to include radial temperature profiles.

3. A calculation of the effect of non-black enclosures on the radiation process should be made.

4. The experimental technique, perhaps with modifications, should be applied to systems of different length-to-radius ratios to test the theoretical work more thoroughly. For very short length-to-radius ratios a non-flow system with a radiation section constructed similarly to the one employed in this study would probably give most satisfactory results.

5. Radiation to translucent and partially transparent particles has been studied only briefly and should be investigated further.

A P P E N D I X - A

PARTICLE SIZE DISTRIBUTIONS
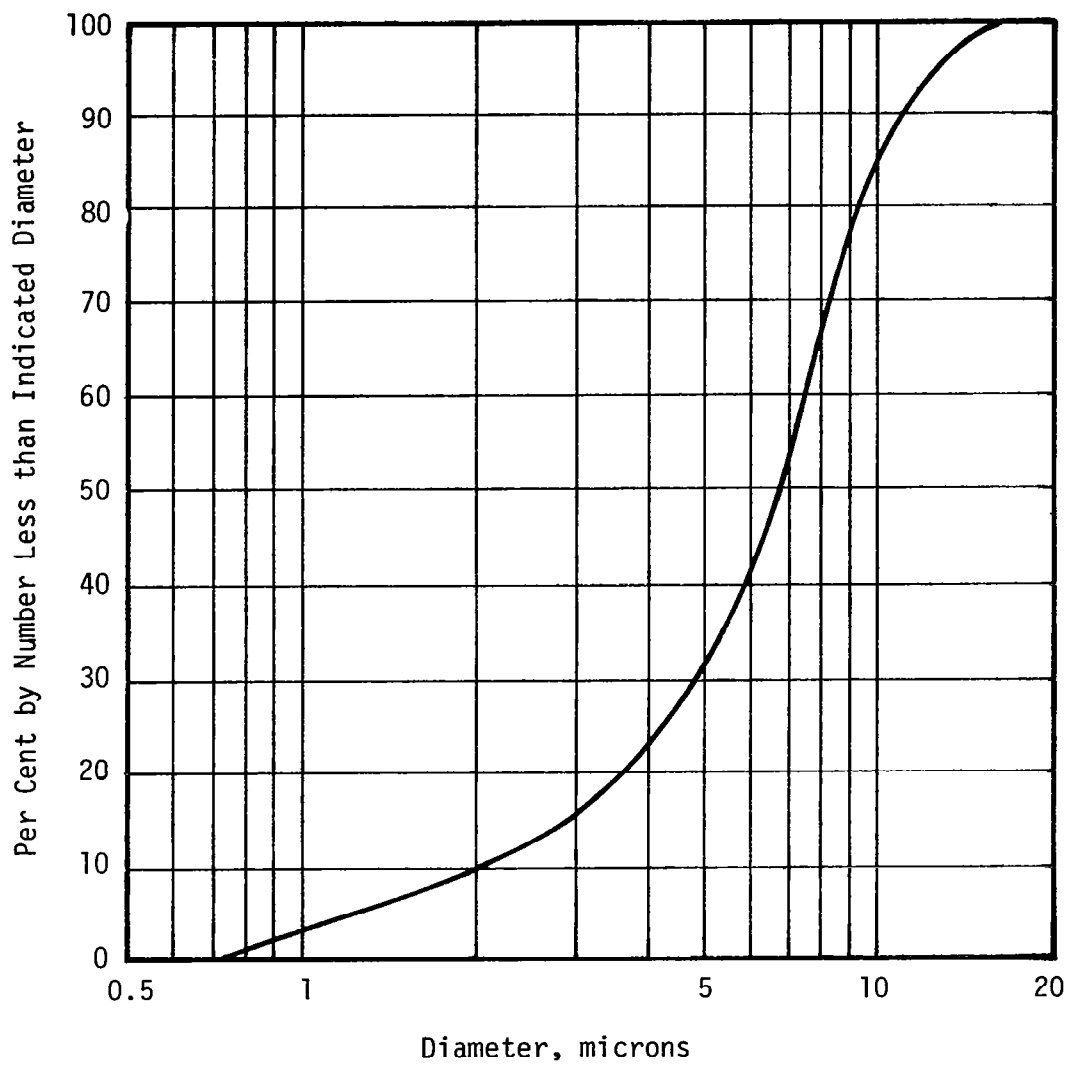
Figure 43. Particle Size Distribution of Zinc.
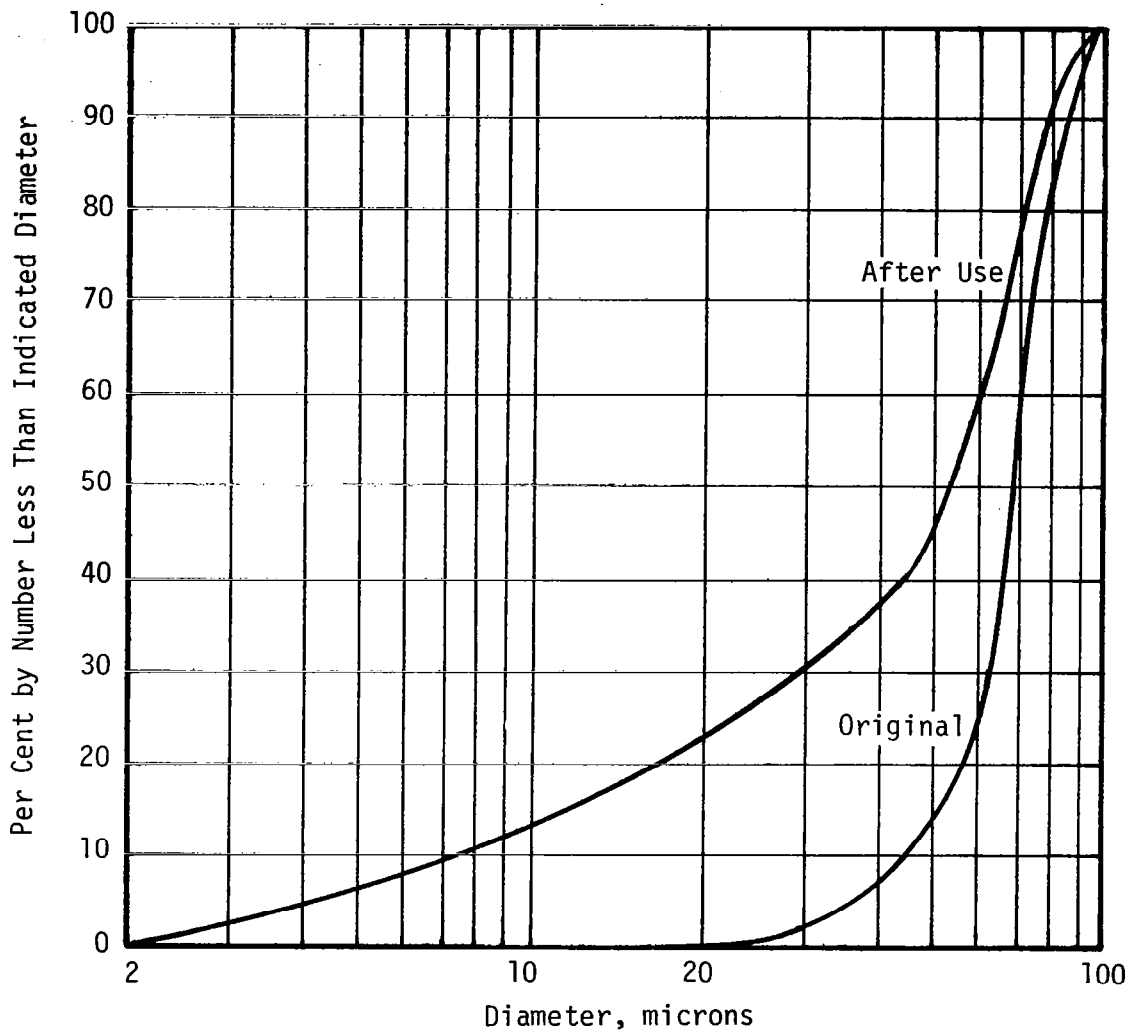
Figure 44. Particle Size Distributions for Ferrous Sulfide
Particles, 53-88μ Screen Size Fraction.
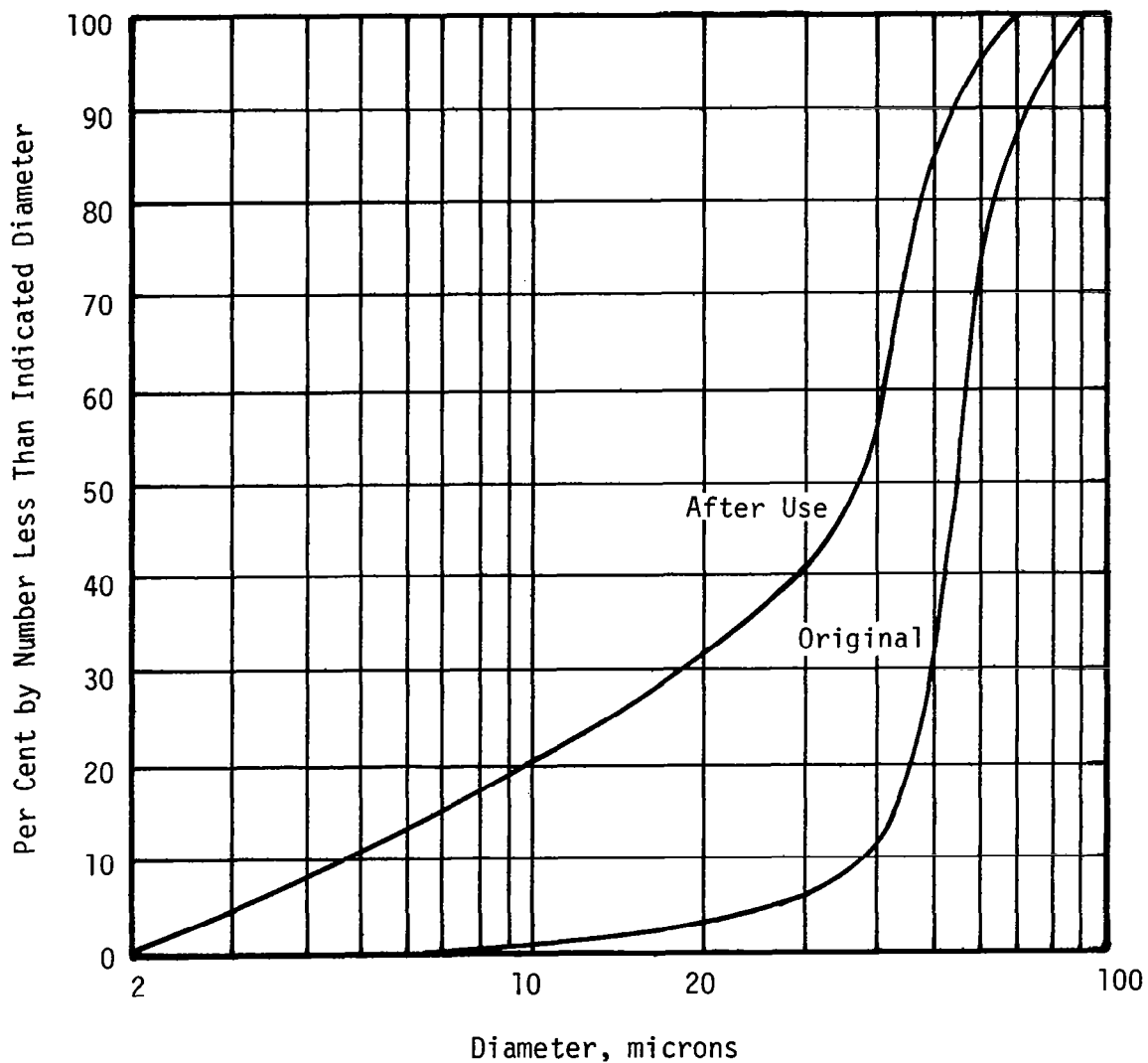
Figure 45. Particle Size Distributions for Ferrous Sulfide
Particles, 44-53μ Screen Size Fraction.
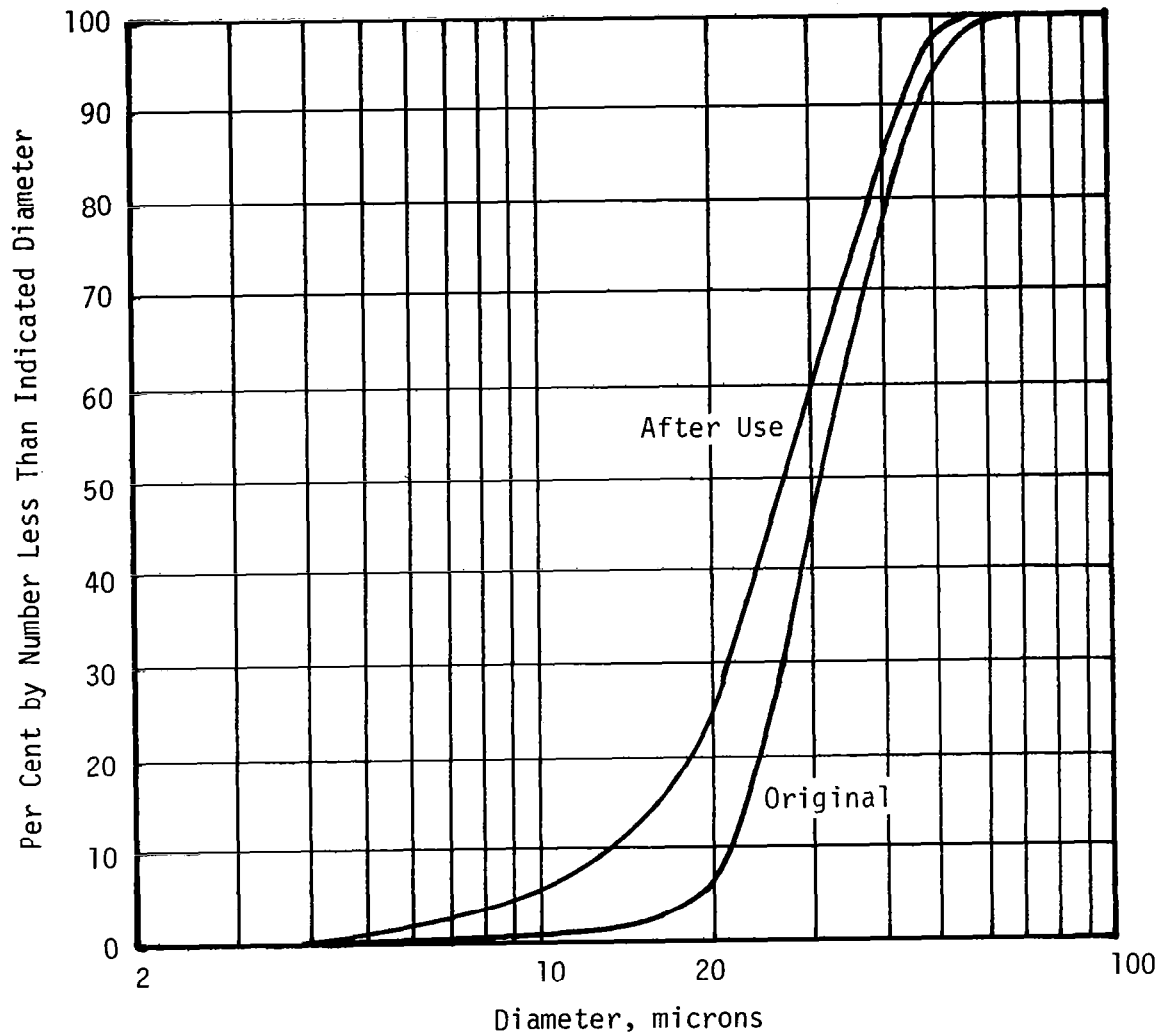
Figure 46. Particle Size Distributions for Ferrous Sulfide
Particles, 30-44μ Screen Size Fraction.
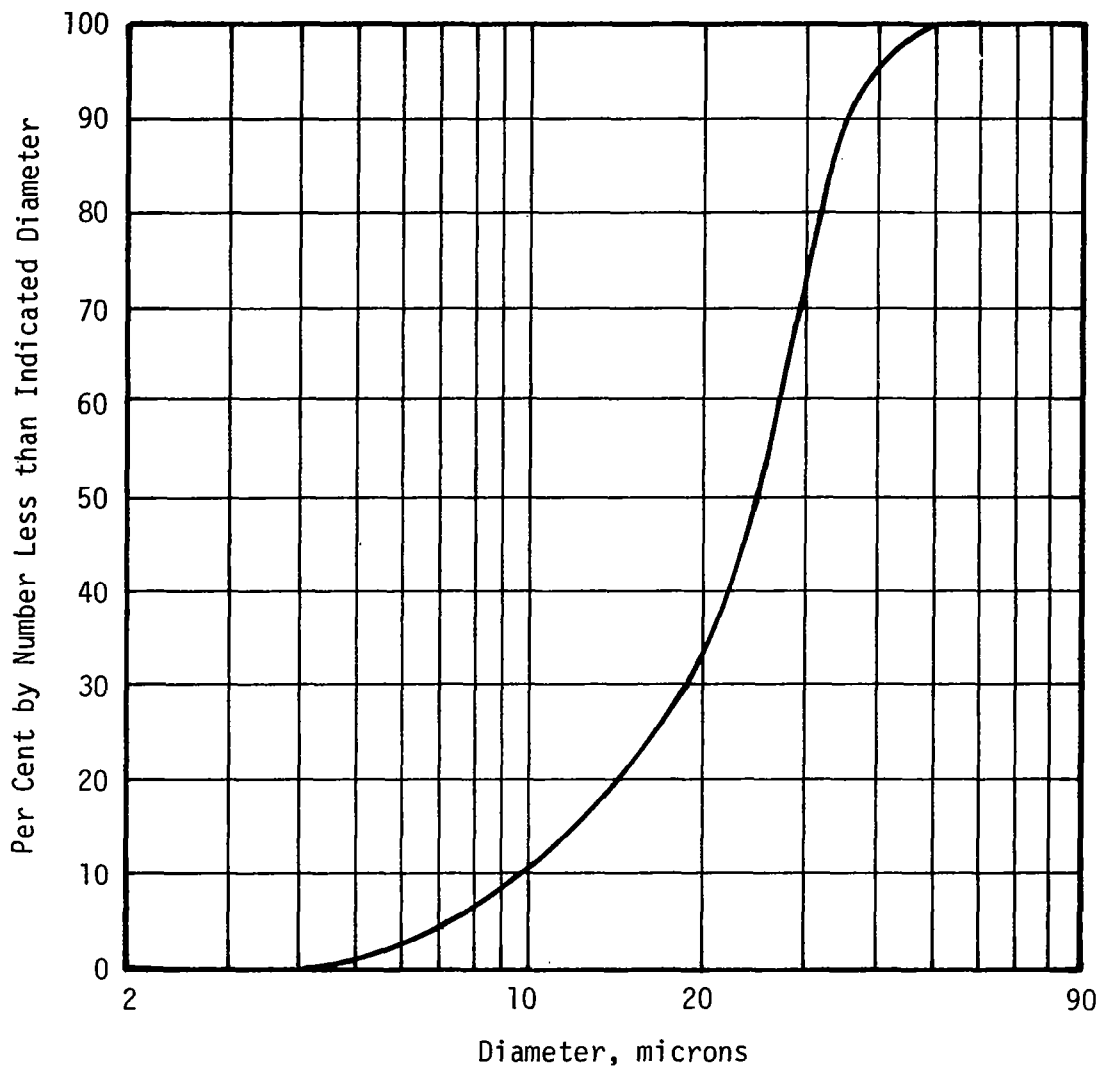
Figure 47. Particle Size Distribution for Ferrous Sulfide
Particles, 20-30 Screen Size Fraction.
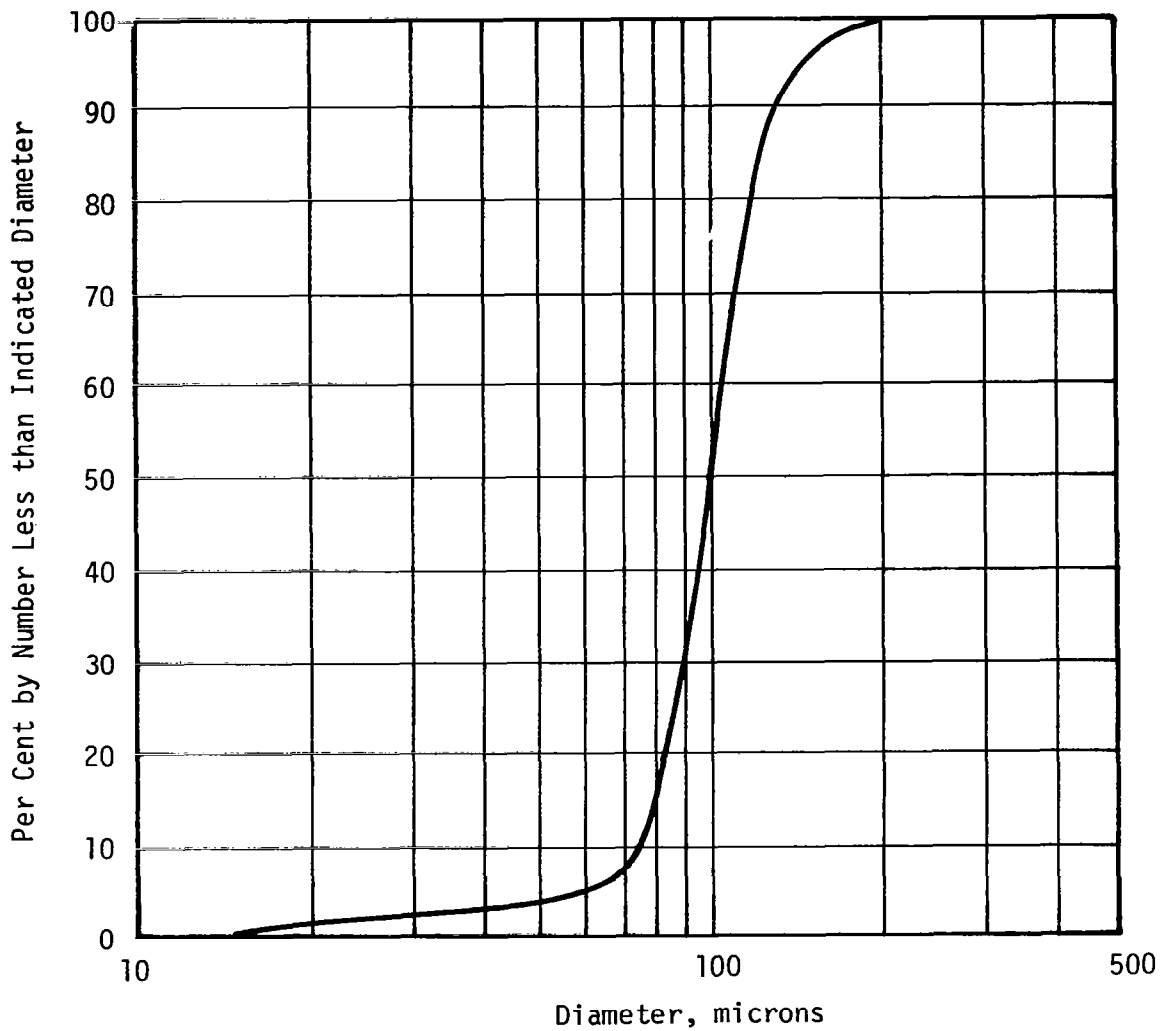
Figure 48. Particle Size Distribution for Cupric Oxide
Particles, 53–88μ Screen Size Fraction.
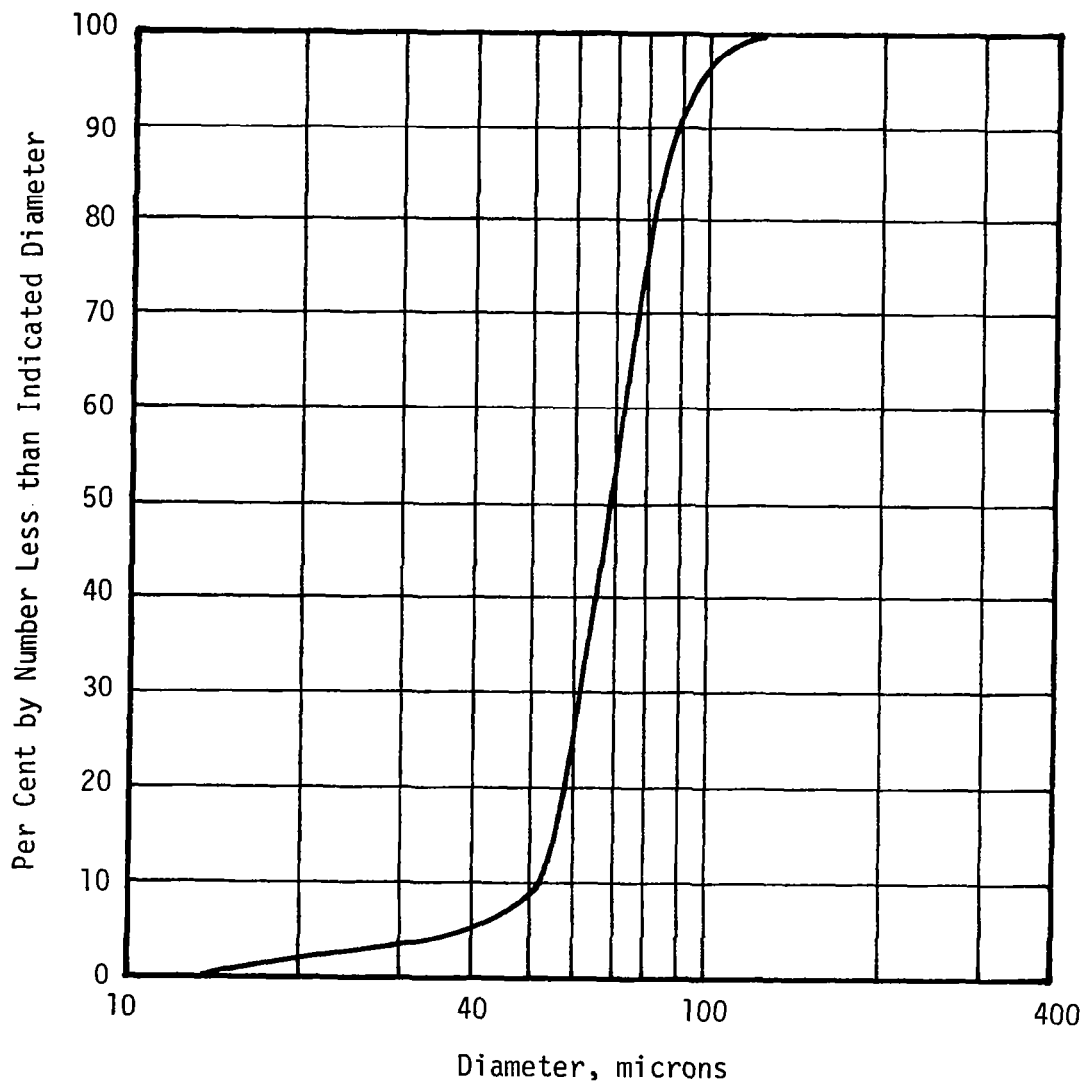
Figure 49. Particle Size Distribution for Cupric Oxide
Particles, 44-53μ Screen Size Fraction.

148
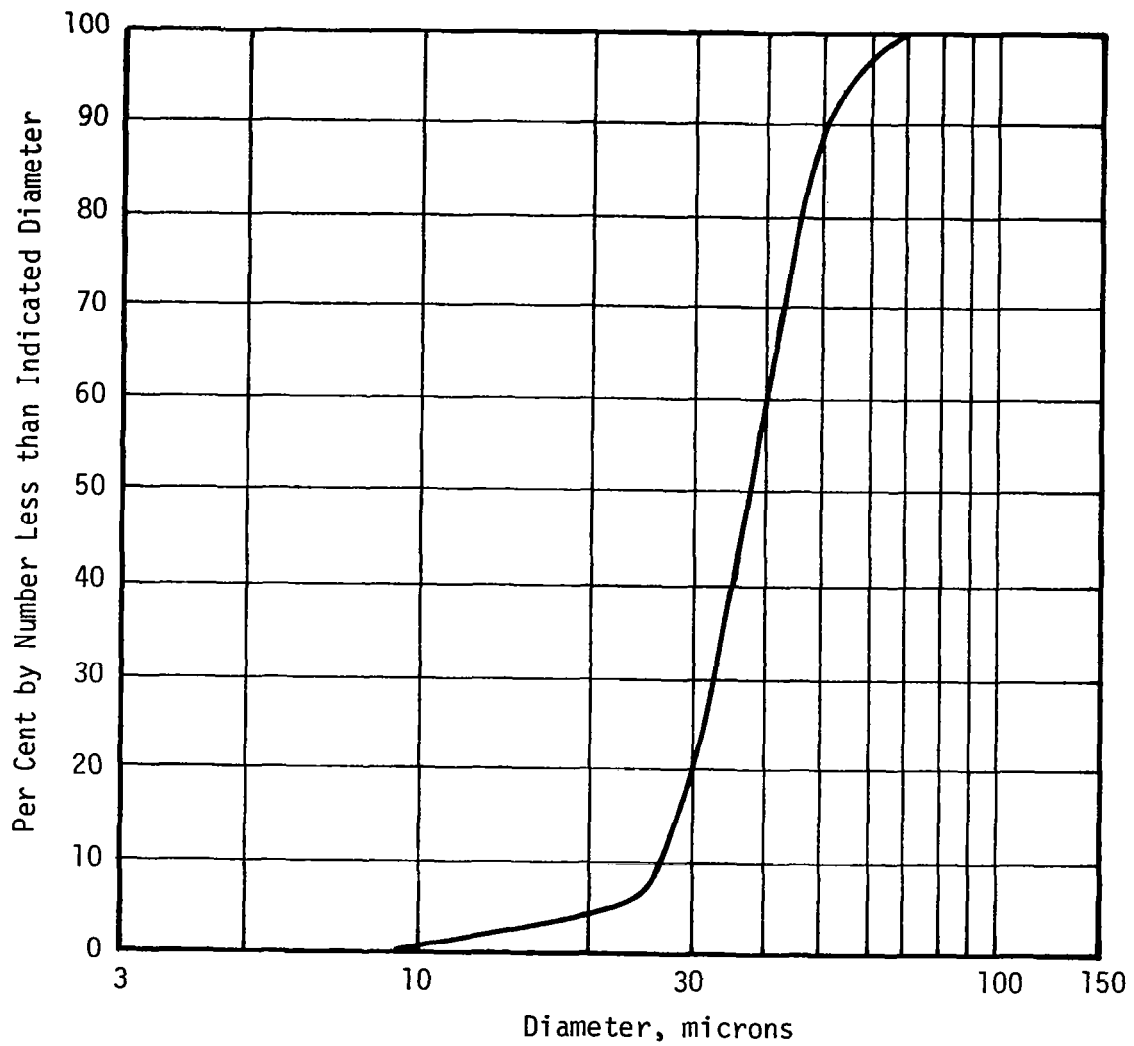
Figure 50. Particle Size Distribution for Cupric Oxide
Particles, 30-44μ Screen Size Fraction.
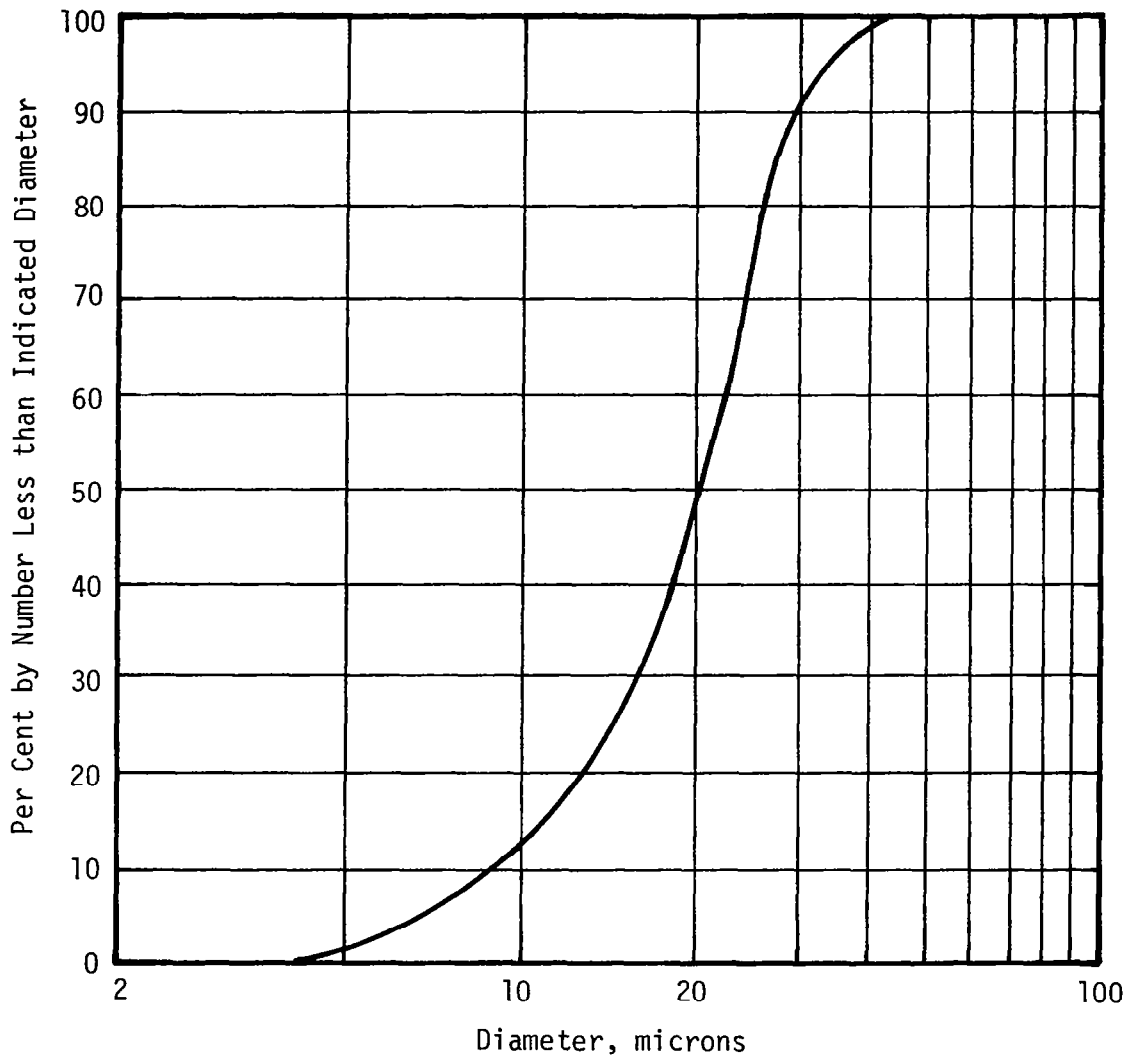
Figure 51. Particle Size Distribution for Cupric Oxide
Particles, 20-30μ Screen Size Fraction.

A P P E N D I X - B

EXPERIMENTAL AND

CALCULATED HEAT TRANSFER DATA

Table 3. Experimental and Calculated Data for Zinc[a]

Powder Feed Rate $\left(\frac{lb}{min}\right)$	Stream Temperature at: Deagglomerator Exit for Air or Aerosol (°F)	Heat Exchanger Exit for Air or Aerosol Air (°F)	Aerosol (°F)	Heat Exchanger Coolant Temperature Rise and Change in Rise when Aerosol Formed Δt_c (°F)	$\Delta(\Delta t_c)$ (°F)	Enthalpy Changes Resulting From Aerosol Formation Aerosol Air $\left(\frac{Btu}{min}\right)$	Particles $\left(\frac{Btu}{min}\right)$	Total[b] $\left(\frac{Btu}{min}\right)$
0.19	78.4	106.6	126.8	7.7	0.3	1.18	0.28	1.46
0.19	78.5	106.1	127.3	7.7	0.4	1.24	0.28	1.52
0.19	78.8	104.3	127.1	6.7	0.3	1.33	0.86	2.19
0.13	78.8	105.9	123.7	6.8	0.3	1.04	0.55	1.59
0.13	83.4	112.0	129.0	7.2	0.0	0.99	0.56	1.55
0.19	83.6	113.7	135.0	7.3	0.1	1.24	0.92	2.16
0.25	84.5	114.8	140.6	7.3	0.5	1.50	1.30	2.80
0.25	85.1	115.7	139.6	7.4	0.5	1.39	1.26	2.65
0.25	85.9	116.4	140.2	7.2	0.6	1.39	1.26	2.65
0.13	90.9	117.9	138.3	7.4	0.1	1.19	0.58	1.77
0.13	91.3	118.8	139.3	7.7	-0.1	1.20	0.59	1.79
0.19	91.8	118.8	144.0	7.7	0.3	1.47	0.93	2.40
0.19	91.5	119.0	144.8	7.9	0.3	1.50	0.95	2.45
0.13	89.8	111.6	133.0	3.9	0.2	1.25	0.53	1.78
0.13	90.5	112.9	133.8	4.4	0.0	1.22	0.53	1.75

[a] Experiment conditions: Heat exchanger coolant, water, 0.095 CFM, and 0.195 CFM for last two tests; air flow rate for aerosol, 3.22 CFM at 1 atm, 70°F; Indicated furnace temperature 2280°F.

[b] Total did not include heat calculated for coolant; see text.

Table 4. Experimental and Calculated Data for 53-88μ Ferrous Sulfide[a]

Powder Feed Rate $\left(\frac{lb}{min}\right)$	Stream Temperature at: Deagglomerator Exit for Air or Aerosol (°F)	Heat Exchanger Exit for Air or Aerosol Air (°F)	Aerosol (°F)	Heat Exchanger Coolant Temperature Rise and Change in Rise when Aerosol Formed Δt_c (°F)	$\Delta(\Delta t_c)$ (°F)	Enthalpy Changes Resulting From Aerosol Formation Aerosol Air $\left(\frac{Btu}{min}\right)$	Particles $\left(\frac{Btu}{min}\right)$	Total[b] $\left(\frac{Btu}{min}\right)$
0.24	83.3	105.7	127.1	8.3	1.3	1.25	1.82	3.07
0.24	81.9	127.1	137.7	6.7	0.6	0.62	2.32	2.94
0.24	83.0	129.3	138.8	8.0	0.5	0.55	2.32	2.87
0.16	82.6	130.2	140.1	7.3	0.2	0.58	1.52	2.10
0.16	82.6	132.1	140.3	7.5	0.3	0.48	1.53	2.01
0.089	82.2	134.2	141.1	8.1	-0.2	0.40	0.92	1.32
0.059	81.5	125.1	130.7	7.5	0.1	0.33	0.49	0.82
0.059	81.8	126.6	132.0	7.1	0.7	0.31	0.50	0.81
0.089	82.3	127.2	135.0	7.5	-0.2	0.45	0.83	1.28
0.16	82.5	129.3	140.2	7.4	0.1	0.64	1.53	2.17
0.24	82.5	130.2	144.0	7.5	0.1	0.80	2.55	3.35
0.089	82.6	132.0	140.8	8.1	-0.2	0.51	0.91	1.42
0.089	81.3	129.2	136.9	9.0	0.4	0.45	0.87	1.32
0.089	81.8	129.3	137.8	8.6	-0.5	0.50	0.88	1.38
0.16	82.6	130.2	141.7	8.9	0.1	0.67	1.57	2.24
0.16	82.9	132.9	143.8	9.2	0.2	0.64	1.61	2.25
0.24	83.4	133.3	147.3	8.6	0.2	0.82	2.65	3.47
0.24	83.7	134.3	149.0	9.0	0.2	0.86	2.71	3.57

(Continued)

Table 4. Experimental and Calculated Data for 53-88μ Ferrous Sulfide[a]
(continued)

Powder Feed Rate $(\frac{lb}{min})$	Stream Temperature at: Deagglomerator Exit for Air or Aerosol ($^{\circ}$F)	Heat Exchanger Exit for Air or Aerosol Air ($^{\circ}$F)	Aerosol ($^{\circ}$F)	Heat Exchanger Coolant Temperature Rise and Change in Rise when Aerosol Formed Δt_c ($^{\circ}$F)	$\Delta(\Delta t_c)$ ($^{\circ}$F)	Enthalpy Changes Resulting From Aerosol Formation Aerosol Air $(\frac{Btu}{min})$	Particles $(\frac{Btu}{min})$	Total[b] $(\frac{Btu}{min})$
0.059	82.9	133.2	139.3	8.9	0.1	0.36	0.56	0.92
0.059	78.8	127.3	133.5	10.2	0.2	0.36	0.55	0.91
0.089	79.2	128.7	137.7	11.2	0.5	0.53	0.92	1.45
0.16	79.3	129.9	142.7	11.0	0.8	0.75	1.68	2.43
0.24	79.9	130.2	146.0	10.2	0.5	0.92	2.15	3.67
0.16	79.9	130.3	142.6	10.4	0.0	0.72	1.66	2.38
0.089	79.8	129.8	138.8	9.7	0.5	0.53	0.93	1.46
0.059	79.6	130.3	137.1	9.9	0.3	0.40	0.58	0.98

[a] Experiment conditions: Heat exchanger coolant, water, 0.095 CFM, air flow rate for aerosol, 3.22 CFM at 1 atm, 70°F; furnace temperature 2280°F.

[b] Total did not include heat calculated for coolant; see text.

Table 5. Experimental and Calculated Data for 44-53μ Ferrous Sulfide[a]

Powder Feed Rate $(\frac{lb}{min})$	Deagglomerator Exit for Air or Aerosol ($^{\circ}$F)	Stream Temperature at: Heat Exchanger Exit for Air or Aerosol		Heat Exchanger Coolant Temperature Rise and Change in Rise when Aerosol Formed		Enthalpy Changes Resulting From Aerosol Formation			
		Air ($^{\circ}$F)	Aerosol ($^{\circ}$F)	Δt_c ($^{\circ}$F)	$\Delta(\Delta t_c)$ ($^{\circ}$F)	Aerosol Air $(\frac{Btu}{min})$	Particles $(\frac{Btu}{min})$	Coolant $(\frac{Btu}{min})$	Total $(\frac{Btu}{min})$
0.089	81.7	158.8	167.3	41.6	0.9	0.55	1.30	0.12	1.97
0.16	82.6	159.5	171.2	42.5	0.1	0.75	2.35	0.01	3.11
0.24	82.9	160.6	180.1	43.4	0.5	1.26	4.00	0.07	5.33
0.16	83.2	159.7	174.2	43.3	1.3	0.93	2.41	0.17	3.51
0.089	83.3	159.2	170.3	43.0	1.5	0.71	1.32	0.20	2.23
0.059	83.4	158.4	166.6	42.5	1.2	0.53	0.83	0.16	1.52
0.059	79.4	151.1	158.3	30.4	0.3	0.40	0.79	0.04	1.23
0.24	79.8	156.0	174.4	41.0	-0.3	1.19	3.90	-0.04	5.04
0.24	79.9	154.0	176.9	40.3	0.5	1.48	4.00	0.07	5.55
0.24	80.0	155.7	174.2	41.6	-0.7	1.19	3.88	-0.10	4.97
0.24	81.0	156.4	174.2	41.8	-0.8	1.15	3.84	-0.12	4.87
0.24	81.0	156.4	174.2	41.9	-1.1	1.15	3.84	-0.16	4.82
0.24	81.2	156.8	174.4	42.6	-1.1	1.13	3.84	-0.16	4.81
0.24	81.2	157.6	176.0	42.5	-1.2	1.19	3.91	-0.18	4.91
0.24	81.6	158.6	177.3	42.8	-1.2	1.20	3.94	-0.18	4.97
0.16	81.4	160.0	173.3	43.9	-0.1	0.86	2.44	-0.02	3.28
0.16	81.5	157.6	169.8	42.7	0.2	0.79	2.34	-0.03	3.10

(Continued)

Table 5. Experimental and Calculated Data for 44-53μ Ferrous Sulfide[a]
(continued)

Powder Feed Rate $(\frac{lb}{min})$	Deagglomerator Exit for Air or Aerosol (°F)	Stream Temperature at: Heat Exchanger Exit for Air or Aerosol		Heat Exchanger Coolant Temperature Rise and Change in Rise when Aerosol Formed		Enthalpy Changes Resulting From Aerosol Formation			
		Air (°F)	Aerosol (°F)	Δt_c (°F)	$\Delta(\Delta t_c)$ (°F)	Aerosol Air $(\frac{Btu}{min})$	Particles $(\frac{Btu}{min})$	Coolant $(\frac{Btu}{min})$	Total $(\frac{Btu}{min})$
0.16	81.6	157.6	167.2	42.2	-0.6	0.62	2.27	-0.09	2.80
0.16	81.7	158.3	168.9	42.5	-0.8	0.69	2.31	-0.12	2.88
0.16	81.7	158.8	169.3	42.5	-0.8	0.68	2.32	-0.12	2.88
0.16	81.8	158.3	167.7	42.1	-0.8	0.61	2.28	-0.12	2.76
0.16	81.9	159.2	168.4	42.5	-1.0	0.59	2.29	-0.15	2.74
0.16	82.0	160.5	170.4	43.2	-1.2	0.64	2.34	-0.18	2.80
0.16	82.1	160.7	170.4	43.3	-1.1	0.63	2.34	-0.16	2.80
0.16	82.2	160.0	160.3	43.1	-0.9	0.60	2.31	-0.13	2.78
0.089	82.5	160.9	168.9	43.7	-0.5	0.52	1.31	-0.07	1.75
0.089	82.7	162.2	169.8	44.2	-0.5	0.49	1.32	-0.07	1.74
0.089	82.5	160.9	168.1	43.6	-0.3	0.46	1.30	-0.04	1.72
0.089	82.7	161.3	168.9	43.6	-0.4	0.49	1.31	-0.06	1.74
0.089	82.7	161.3	168.9	43.2	0.6	0.49	1.31	-0.06	1.74
0.089	82.7	161.7	168.4	43.4	-0.5	0.43	1.30	-0.07	1.66
0.089	82.9	161.7	168.9	43.4	-0.2	0.46	1.31	-0.03	1.74
0.089	83.0	162.2	167.7	43.0	-0.5	0.35	1.29	-0.07	1.57

(Continued)

Table 5. Experimental and Calculated Data for 44-53μ Ferrous Sulfide[a]
(concluded)

Powder Feed Rate $(\frac{lb}{min})$	Stream Temperature at:			Heat Exchanger Coolant Temperature Rise and Change in Rise when Aerosol Formed		Enthalpy Changes Resulting From Aerosol Formation			
	Deagglomerator Exit for Air or Aerosol (^{O}F)	Heat Exchanger Exit for Air or Aerosol				Aerosol			
		Air (^{O}F)	Aerosol (^{O}F)	Δt_c (^{O}F)	$\Delta(\Delta t_c)$ (^{O}F)	Air $(\frac{Btu}{min})$	Particles $(\frac{Btu}{min})$	Coolant $(\frac{Btu}{min})$	Total $(\frac{Btu}{min})$
0.089	83.4	163.3	170.4	43.9	-0.9	0.46	1.32	-0.13	1.65
0.059	83.4	162.6	168.4	44.4	-0.1	0.37	0.85	-0.02	1.21
0.059	83.4	162.6	168.1	44.1	0.2	0.35	0.85	0.03	1.23
0.059	83.4	163.3	169.0	43.9	0.1	0.37	0.86	0.02	1.24
0.059	83.4	163.7	169.3	43.7	0.2	0.36	0.85	0.03	1.24
0.059	83.1	163.2	168.7	43.2	0.2	0.35	0.86	0.03	1.24
0.059	82.9	163.2	168.7	43.2	0.1	0.35	0.86	0.02	1.23
0.059	82.9	162.6	168.0	42.8	0.0	0.35	0.85	0.00	1.17
0.059	82.9	162.2	167.7	43.0	-0.2	0.35	0.85	-0.03	1.17

[a] Experiment conditions: Heat exchanger coolant, air, 6.70 CFM at 1 atm, 70° F; air flow rate for aerosol, 3.22 CFM at 1 atm, 70° F; furnace temperature 2280° F.

Table 6. Experimental and Calculated Data for 30-44μ Ferrous Sulfide

Powder Feed Rate $(\frac{lb}{min})$	Stream Temperature at: Deagglomerator Exit for Air or Aerosol (°F)	Heat Exchanger Exit for Air or Aerosol Air (°F)	Aerosol (°F)	Heat Exchanger Coolant Temperature Rise and Change in Rise when Aerosol Formed Δt_c (°F)	$\Delta(\Delta t_c)$ (°F)	Enthalpy Changes Resulting From Aerosol Formation Aerosol Air $(\frac{Btu}{min})$	Particles $(\frac{Btu}{min})$	Coolant $(\frac{Btu}{min})$	Total $(\frac{Btu}{min})$
0.059	79.3	165.8	183.5	44.7	3.3	1.26	1.06	0.49	2.80
0.059	79.3	167.7	187.2	46.8	2.7	1.26	1.08	0.40	2.73
0.059	79.3	168.6	189.8	47.3	3.8	1.37	1.11	0.56	3.03
0.24	79.4	168.6	229.3	47.1	7.8	3.91	6.18	1.15	11.2
0.24	79.5	169.3	228.7	47.5	6.2	3.83	6.15	0.91	10.9
0.24	80.3	171.3	230.6	48.2	6.8	3.82	6.19	1.00	11.0
0.16	80.3	175.2	225.6	50.3	7.0	3.25	3.85	1.00	8.13
0.16	80.0	178.9	227.6	52.5	5.0	3.14	3.91	0.74	7.78
0.16	80.0	181.7	228.7	50.0	8.2	3.03	3.94	1.2	8.18
0.16	80.0	179.9	224.5	52.0	5.0	2.87	3.83	0.77	7.48
0.089	80.0	180.4	211.7	52.5	4.9	2.02	2.00	0.72	4.74
0.089	8.0	181.0	211.0	52.2	4.8	1.93	1.99	0.71	4.63
0.089	80.0	182.0	210.0	53.0	4.4	1.80	1.98	0.65	4.42
0.089	80.0	186.3	216.7	54.4	4.7	1.96	2.08	0.69	4.73
0.089	80.0	186.1	207.9	54.9	3.8	1.40	1.28	0.56	3.25
0.059	80.0	188.1	209.7	54.8	4.4	1.39	1.30	0.65	3.34

(Continued)

Table 6. Experimental and Calculated Data for 30-44µ Ferrous Sulfide[a]
(continued)

Powder Feed Rate $(\frac{lb}{min})$	Stream Temperature at:			Heat Exchanger Coolant Temperature Rise and Change in Rise when Aerosol Formed		Enthalpy Changes Resulting From Aerosol Formation			
	Deagglomerator Exit for Air or Aerosol (°F)	Heat Exchanger Exit for Air or Aerosol				Aerosol			
		Air (°F)	Aerosol (°F)	Δt_c (°F)	$\Delta(\Delta t_c)$ (°F)	Air $(\frac{Btu}{min})$	Particles $(\frac{Btu}{min})$	Coolant $(\frac{Btu}{min})$	Total $(\frac{Btu}{min})$
0.089	79.6	190.6	219.4	56.5	4.1	1.86	2.13	0.60	4.58
0.16	81.4	193.7	235.3	59.0	3.9	2.86	4.08	0.57	7.33
0.24	81.0	196.6	245.1	60.4	3.8	3.12	6.76	0.56	10.4

[a] Experiment conditions: Heat exchanger coolant, air 7.51 CFM at 1 atm, 70° F; air flow rate for aerosol, 3.22 CFM at 1 atm, 70° F; furnace temperature 2280° F.

Table 7. Experimental and Calculated Data for 20-30µ Ferrous Sulfide[a]

Powder Feed Rate $\left(\frac{lb}{min}\right)$	Deagglomerator Exit for Air or Aerosol ($^\circ$F)	Heat Exchanger Exit for Air or Aerosol		Heat Exchanger Coolant Temperature Rise and Change in Rise when Aerosol Formed		Enthalpy Changes Resulting From Aerosol Formation			
		Air ($^\circ$F)	Aerosol ($^\circ$F)	Δt_c ($^\circ$F)	$\Delta(\Delta t_c)$ ($^\circ$F)	Aerosol Air $\left(\frac{Btu}{min}\right)$	Particles $\left(\frac{Btu}{min}\right)$	Coolant $\left(\frac{Btu}{min}\right)$	Total $\left(\frac{Btu}{min}\right)$
0.156	72.5	156.0	180.4	33.6	3.8	1.45	2.86	0.49	4.80
0.156	72.0	156.3	179.1	35.1	3.8	1.36	2.84	0.49	4.69
0.156	71.7	157.2	179.0	35.2	3.8	1.30	2.84	0.49	4.63
0.156	71.4	157.7	179.2	35.2	3.8	1.28	2.86	0.49	4.63
0.156	71.4	155.0	179.0	36.7	3.8	1.43	2.85	0.49	4.77
0.089	70.6	155.0	171.3	35.7	2.6	0.97	1.53	0.34	2.84
0.089	71.4	160.0	174.1	35.3	2.6	0.84	1.56	0.34	2.74
0.089	73.4	162.0	177.2	35.4	2.6	0.90	1.58	0.34	2.82
0.089	74.9	164.0	179.2	36.1	2.6	0.90	1.59	0.34	2.83
0.059	75.8	164.5	177.2	36.1	1.9	0.76	1.01	0.25	2.02
0.059	75.6	162.2	175.0	35.5	1.9	0.76	0.99	0.25	2.00
0.059	75.2	162.0	174.1	35.7	1.9	0.72	0.99	0.25	1.96
0.059	75.6	162.8	173.3	35.7	1.9	0.63	0.98	0.25	1.85
0.242	76.1	165.8	197.1	35.9	5.3	1.86	4.99	0.69	7.54
0.242	76.3	165.8	196.7	36.1	5.3	1.84	4.96	0.69	7.49
0.242	76.4	163.7	194.8	36.2	5.3	1.85	4.88	0.69	7.42

[a] Experiment conditions: Heat exchanger coolant, air 7.05 CFM at 1 atm, 70°F; air flow rate for aerosol, 3.22 CFM at 1 atm, 70°F; furnace temperature 2280°F.

Table 8. Experimental and Calculated Data for 20-30μ Ferrous Sulfide[a,b]

Powder Feed Rate $(\frac{lb}{min})$	Stream Temperature at: Deagglomerator Exit for Air or Aerosol (°F)	Heat Exchanger Inlet for Air or Aerosol Air (°F)	Aerosol (°F)	Enthalpy Changes Resulting From Aerosol Formation Aerosol Air $(\frac{Btu}{min})$	Particles $(\frac{Btu}{min})$	Total $(\frac{Btu}{min})$
0.156	84.3	218.1	231.0	0.77	3.89	4.66
0.089	84.5	221.4	233.2	0.70	2.26	2.96
0.089	85.0	223.5	236.4	0.77	2.30	3.07
0.089	85.0	223.9	238.8	0.89	2.34	3.23
0.156	84.5	227.5	244.0	0.98	4.23	5.21
0.156	85.8	221.9	242.3	1.21	4.15	5.36
0.156	88.4	225.1	243.2	1.08	4.10	5.18
0.089	88.4	226.8	240.6	0.82	2.31	3.13
0.059	88.4	225.7	239.0	0.79	1.51	2.30
0.059	88.4	226.7	238.0	0.67	1.50	2.17

[a] Experiment Conditions: Heat exchanger coolant, air 6.96 CFM at 70°F, 1 atm; air flow rate for aerosol 3.22 CFM at 70°F, 1 atm; furnace temperature, 2280°F.

[b] Energy balance between furnace inlet and heat exchanger inlet.

Table 8a. Experimental and Calculated Data for 20-30µ Ferrous Sulfide[a,b]

Powder Feed Rate ($\frac{lb}{min}$)	Stream Temperature at: Deagglomerator Exit for Air or Aerosol (°F)	Heat Exchanger Exit for Air or Aerosol Air (°F)	Aerosol (°F)	Heat Exchanger Coolant Temperature Rise and Change in Rise when Aerosol Formed Δt_c (°F)	$\Delta(\Delta t_c)$ (°F)	Enthalpy Changes Resulting From Aerosol Formation Air ($\frac{Btu}{min}$)	Particles ($\frac{Btu}{min}$)	Coolant ($\frac{Btu}{min}$)	Total ($\frac{Btu}{min}$)
0.156	84.3	142.8	174.2	33.6	2.9	1.87	2.38	0.37	4.62
0.089	84.5	145.2	166.2	35.1	2.3	1.25	1.24	0.30	2.79
0.089	85.0	146.6	169.0	35.2	2.8	1.33	1.28	0.36	2.97
0.089	85.0	146.8	169.8	35.2	3.7	1.37	1.29	0.48	3.14
0.156	84.5	150.0	185.1	36.7	3.3	2.09	2.67	0.42	5.18
0.156	85.8	146.8	184.6	35.7	3.8	2.25	2.62	0.49	5.36
0.156	88.4	150.0	186.1	35.3	3.9	2.15	2.59	0.50	5.23
0.089	88.4	150.0	172.2	35.4	3.3	1.32	1.27	0.42	3.01
0.059	88.4	150.2	166.2	36.1	2.9	0.95	0.78	0.37	2.10
0.059	88.4	150.0	165.8	36.1	2.9	0.94	0.77	0.37	2.08

[a] Experiment Conditions: Heat exchanger coolant, air 6.96 CFM at 1 atm, 70°F; air flow rate for aerosol 3.22 CFM at 70°F, 1 atm; furnace temperature 2280°F.

[b] Energy balance between furnace inlet and heat exchanger exit.

Table 9. Experimental and Calculated Data for 53-88μ Cupric Oxide[a,b]

| Powder Feed Rate $(\frac{lb}{min})$ | Stream Temperature at: | | | | Enthalpy Changes Resulting From Aerosol Formation | | |
| | Deagglomerator Exit for Air or Aerosol (°F) | Heat Exchanger Inlet for Air or Aerosol | | | Aerosol | | |
		Air (°F)	Aerosol (°F)		Air $(\frac{Btu}{min})$	Particles $(\frac{Btu}{min})$	Total $(\frac{Btu}{min})$
0.101	73.0	216.0	207.4		-0.52	1.83	1.31
0.101	72.8	216.0	204.9		-0.67	1.80	1.13
0.101	73.9	218.7	206.1		-0.76	1.81	1.05
0.101	74.0	219.4	206.8		-0.76	1.81	1.05
0.101	74.6	221.4	209.7		-0.71	1.83	1.12
0.101	74.9	223.2	210.5		-0.77	1.85	1.08
0.181	75.8	219.6	199.5		-1.21	3.01	1.80
0.181	75.9	220.5	201.8		-1.13	3.06	1.93
0.181	76.1	223.1	202.0		-1.27	3.06	1.76
0.181	77.3	224.3	202.9		-1.29	3.05	1.76
0.313	77.5	226.1	192.7		-2.02	4.84	2.82
0.313	78.3	228.5	193.2		-2.13	4.83	2.70
0.313	78.5	230.2	193.1		-2.24	4.81	2.57
0.313	78.5	231.2	195.7		-2.14	4.92	2.78
0.313	79.1	233.4	195.5		-2.29	4.88	2.59

[a] Experiment Conditions: Heat exchanger coolant, air 7.20 CFM at 70°F, 1 atm; air flow rate for aerosol, 3.22 CFM at 70°F, 1 atm; furnace temperature, 2280°F.

[b] Energy balance between furnace inlet and heat exchanger inlet.

Table 9a. Experimental and Calculated Data for 53-88μ Cupric Oxide[a,b]

Powder Feed Rate $\left(\frac{lb}{min}\right)$	Deagglomerator Exit for Air or Aerosol (°F)	Heat Exchanger Exit for Air or Aerosol		Heat Exchanger Coolant Temperature Rise and Change in Rise when Aerosol Formed		Enthalpy Changes Resulting From Aerosol Formation			
		Air (°F)	Aerosol (°F)	Δt_c (°F)	$\Delta(\Delta t_c)$ (°F)	Aerosol Air $\left(\frac{Btu}{min}\right)$	Particles $\left(\frac{Btu}{min}\right)$	Coolant $\left(\frac{Btu}{min}\right)$	Total $\left(\frac{Btu}{min}\right)$
0.101	73.0	136.9	145.0	34.1	0.1	0.49	0.96	0.01	1.46
0.101	72.8	137.0	144.4	32.8	-0.8	0.45	0.96	-0.10	1.31
0.101	73.9	137.9	145.2	34.5	-0.4	0.44	0.96	-0.05	1.30
0.101	74.0	139.4	145.9	35.2	-1.5	0.39	0.96	-0.20	1.15
0.101	74.6	141.1	147.9	35.8	-1.5	0.41	0.98	-0.20	1.19
0.101	74.9	141.3	149.3	35.5	-0.6	0.48	0.99	-0.08	1.39
0.181	75.8	140.9	149.0	34.8	-2.6	0.49	1.75	-0.35	1.89
0.181	75.9	140.5	150.3	35.0	-2.3	0.59	1.78	-0.31	2.06
0.181	76.1	142.1	151.4	36.0	-3.0	0.56	1.81	-0.41	1.96
0.181	77.3	142.5	152.0	35.8	-2.6	0.57	1.79	-0.34	2.02
0.313	77.5	138.6	152.5	36.0	-4.3	0.84	3.11	-0.58	3.37
0.313	78.3	140.6	153.5	36.0	-4.7	0.78	3.12	-0.63	3.27
0.313	78.5	140.9	154.4	36.0	-4.4	0.82	3.15	-0.59	3.38
0.313	78.5	141.4	156.0	37.1	-4.9	0.88	3.22	-0.66	3.44
0.313	79.1	143.4	155.1	37.1	-5.5	0.71	3.14	-0.75	3.10

[a] Experiment Conditions: Heat exchanger coolant, air 7.20 CFM at 70°F, 1 atm; air flow rate for aerosol, 3.22 CFM at 70°F, 1 atm; furnace temperature, 2280°F.

[b] Energy balance between furnace inlet and heat exchanger exit.

Table 10. Experimental and Calculated Data for 44-53μ Cupric Oxide[a,b]

Powder Feed Rate ($\frac{lb}{min}$)	Stream Temperature at: Deagglomerator Exit for Air or Aerosol (°F)	Heat Exchanger Inlet for Air or Aerosol Air (°F)	Aerosol (°F)	Enthalpy Changes Resulting From Aerosol Formation Air ($\frac{Btu}{min}$)	Aerosol Particles ($\frac{Btu}{min}$)	Total ($\frac{Btu}{min}$)
0.101	70.0	209.4	206.9	-0.14	1.86	1.72
0.181	70.9	210.0	200.9	-0.52	3.16	2.64
0.181	71.7	207.2	200.6	-0.38	3.13	2.75
0.181	72.5	209.4	201.3	-0.46	3.13	2.67
0.181	75.0	216.1	207.2	-0.51	3.23	2.72
0.181	75.4	216.8	206.6	-0.58	3.20	2.62
0.181	75.6	217.1	206.6	-0.60	3.20	2.60
0.181	76.2	216.2	206.3	-0.57	3.17	2.60
0.181	76.2	217.1	206.3	-0.62	3.17	2.55
0.313	77.1	218.7	203.0	-0.90	5.30	4.40
0.313	77.2	218.2	202.1	-0.92	5.26	4.54
0.313	77.3	219.3	201.8	-1.00	5.24	4.24
0.313	77.4	218.5	202.9	-0.89	5.38	4.39
0.313	77.5	219.2	202.9	-0.93	5.28	4.35
0.313	78.0	220.2	204.3	-0.91	5.32	4.41

(continued)

Table 10. Experimental and Calculated Data for 44-53μ Cupric Oxide[a,b]
(continued)

Powder Feed Rate $(\frac{lb}{min})$	Stream Temperature at: Deagglomerator Exit for Air or Aerosol (^{O}F)	Heat Exchanger Inlet for Air or Aerosol Air (^{O}F)	Aerosol (^{O}F)	Enthalpy Changes Resulting From Aerosol Formation Aerosol Air $(\frac{Btu}{min})$	Particles $(\frac{Btu}{min})$	Total $(\frac{Btu}{min})$
0.181	77.6	221.1	209.0	-0.69	3.21	2.52
0.181	77.5	223.0	208.9	-0.81	3.21	2.40
0.181	77.0	221.0	208.9	-0.69	3.22	2.55
0.101	76.9	219.4	214.5	-0.28	1.87	1.59
0.101	76.4	218.3	214.5	-0.22	1.88	1.66
0.101	75.8	219.5	213.7	-0.33	1.88	1.55
0.101	75.5	220.3	214.5	-0.33	1.89	1.56

[a] Experiment Conditions: Heat exchanger coolant, air 7.01 CFM at 70°F, 1 atm; air flow rate for aerosol, 3.05 CFM at 70°F, 1 atm; furnace temperature, 2280°F.

[b] Energy balance between furnace inlet and heat exchanger inlet.

Powder Feed Rate ($\frac{lb}{min}$)	Deagglomerator Exit for Air or Aerosol (°F)	Heat Exchanger Exit for Air or Aerosol		Heat Exchanger Coolant Temperature Rise and Change in Rise When Aerosol Formed		Enthalpy Changes Resulting From Aerosol Formation			
		Air (°F)	Aerosol (°F)	Δt_c (°F)	$\Delta(\Delta t_c)$ (°F)	Aerosol		Coolant ($\frac{Btu}{min}$)	Total ($\frac{Btu}{min}$)
						Air ($\frac{Btu}{min}$)	Particles ($\frac{Btu}{min}$)		
0.101	70.0	130.0	140.9	34.2	-0.1	0.62	0.93	-0.01	1.54
0.181	70.9	131.2	145.4	34.5	-0.8	0.81	1.70	-0.11	2.40
0.181	71.7	130.4	145.4	34.1	-0.6	0.86	1.71	-0.08	2.49
0.181	72.5	131.4	147.0	33.9	-0.4	0.61	1.73	-0.05	2.29
0.181	75.0	136.2	152.1	34.7	-0.6	0.91	1.80	-0.08	2.63
0.181	75.4	137.9	151.5	34.9	-0.8	0.78	1.81	-0.11	2.48
0.181	75.6	137.0	152.0	34.7	-0.6	0.86	1.81	-0.08	2.59
0.181	76.2	137.9	152.7	35.0	-0.9	0.84	1.83	-0.12	2.55
0.181	76.2	136.6	152.7	35.1	-1.0	0.92	1.82	-0.13	2.61
0.313	77.1	138.3	159.4	35.1	-2.5	1.21	3.20	-0.33	4.08
0.313	77.2	137.9	159.4	34.7	-1.5	1.23	3.20	-0.20	4.28
0.313	77.3	137.0	159.6	34.8	-1.7	1.29	3.21	-0.22	4.28
0.313	77.4	137.0	160.0	35.1	-2.1	1.32	3.21	-0.28	4.25
0.313	77.5	137.5	160.0	35.1	-1.9	1.29	3.22	-0.25	4.26
0.313	78.0	137.9	161.4	35.2	-1.9	1.34	3.25	-0.25	4.34
0.181	77.6	138.6	155.1	35.7	-0.6	0.94	1.86	-0.08	2.72
0.181	77.5	138.5	155.1	35.5	-0.7	0.95	1.86	-0.09	2.72

(continued)

Table 10a. Experimental and Calculated Data for 44-53μ Cupric Oxide[a,b]
(continued)

Powder Feed Rate $(\frac{lb}{min})$	Deagglomerator Exit for Air or Aerosol ($^\circ$F)	Stream Temperature at: Heat Exchanger Exit for Air or Aerosol		Heat Exchanger Coolant Temperature Rise and Change in Rise When Aerosol Formed		Enthalpy Changes Resulting From Aerosol Formation			
		Air ($^\circ$F)	Aerosol ($^\circ$F)	Δt_c $(^\circ F)$	$\Delta(\Delta t_c)$ $(^\circ F)$	Aerosol Air $(\frac{Btu}{min})$	Particles $(\frac{Btu}{min})$	Coolant $(\frac{Btu}{min})$	Total $(\frac{Btu}{min})$
0.181	77.0	139.5	154.9	35.7	-1.0	0.88	1.85	-0.13	2.60
0.101	76.9	137.5	150.0	35.1	+0.1	0.72	1.03	+0.01	1.76
0.101	76.4	137.0	150.3	35.4	-0.2	0.76	1.02	-0.03	1.75
0.101	75.8	136.2	149.7	34.9	-0.1	0.77	1.01	+0.01	1.79
0.101	75.5	137.5	150.0	35.3	0.0	0.72	1.01	0.00	1.73

[a] Experiment Conditions: Heat exchanger coolant, air 7.01 CFM at 70°F, 1 atm; air flow rate for aerosol, 3.05 CFM at 70°F, 1 atm; furnace temperature, 2280°F.

[b] Energy balance between furnace inlet and heat exchanger exit.

Table 11. Experimental and Calculated for 30-44μ Cupric Oxide[a,b]

Powder Feed Rate $(\frac{lb}{min})$	Stream Temperature at:			Enthalpy Changes Resulting From Aerosol Formation		
	Deagglomerator Exit for Air or Aerosol ($^{\circ}$F)	Heat Exchanger Inlet for Air or Aerosol			Aerosol	
		Air ($^{\circ}$F)	Aerosol ($^{\circ}$F)	Air $(\frac{Btu}{min})$	Particles $(\frac{Btu}{min})$	Total $(\frac{Btu}{min})$
0.181	80.8	226.1	212.3	-0.76	3.61	2.85
0.181	80.9	226.1	211.4	-0.81	3.59	2.78
0.181	81.0	226.2	210.6	-0.86	3.56	2.70
0.181	81.0	225.3	211.3	-0.77	3.58	2.81
0.181	81.1	226.1	211.3	-0.81	3.58	2.77
0.181	81.7	227.3	212.2	-0.83	3.59	2.76
0.181	81.8	227.2	213.0	-0.78	3.61	2.83
0.181	81.9	228.0	213.0	-0.83	3.60	2.77
0.181	81.7	228.0	213.5	-0.81	3.62	2.81
0.181	81.9	228.4	214.3	-0.78	3.64	2.86
0.181	81.9	228.9	213.0	-0.88	3.60	2.72
0.181	81.9	229.0	213.8	-0.84	3.63	2.79
0.103	81.9	227.1	221.8	-0.29	2.19	1.90
0.103	81.9	227.1	221.8	-0.29	2.19	1.90
0.103	81.9	226.5	220.6	-0.33	2.17	1.84
0.103	81.9	227.1	220.4	-0.37	2.17	1.80
0.103	82.8	227.1	221.6	-0.30	2.17	1.87

(continued)

169

Table 11. Experimental and Calculated Data for 30-44μ Cupric Oxide[a,b]
(continued)

| Powder Feed Rate ($\frac{lb}{min}$) | Stream Temperature at: | | | Enthalpy Changes Resulting From Aerosol Formation | | |
| | Deagglomerator Exit for Air or Aerosol (°F) | Heat Exchanger Inlet for Air or Aerosol | | Aerosol | | |
		Air (°F)	Aerosol (°F)	Air ($\frac{Btu}{min}$)	Particles ($\frac{Btu}{min}$)	Total ($\frac{Btu}{min}$)
0.103	82.8	227.7	221.6	-0.34	2.17	1.87
0.103	82.9	226.8	222.0	-0.27	2.18	1.91
0.103	83.0	227.7	222.0	-0.31	2.18	1.87
0.103	83.4	227.9	222.4	-0.31	2.18	1.87
0.103	83.6	227.7	223.6	-0.23	2.19	1.96
0.103	83.7	227.9	222.9	-0.28	2.18	1.90
0.103	83.6	227.9	222.0	-0.33	2.17	1.84
0.070	83.6	227.9	225.9	-0.11	1.51	1.40
0.070	83.9	227.8	226.4	-0.08	1.52	1.44
0.070	84.2	227.8	226.4	-0.08	1.51	1.43
0.070	84.5	228.7	227.3	-0.08	1.52	1.44
0.070	84.2	229.9	228.0	-0.11	1.53	1.42
0.070	84.2	230.3	228.5	-0.10	1.54	1.44
0.320	84.5	230.0	219.2	-0.60	6.56	5.96
0.320	84.9	228.7	219.2	-0.52	6.53	6.01
0.320	85.0	229.2	219.2	-0.55	6.53	5.98

(continued)

Table 11. Experimental and Calculated Data for 30-44μ Cupric Oxide[a,b]
(continued)

Powder Feed Rate ($\frac{lb}{min}$)	Stream Temperature at: Deagglomerator Exit for Air or Aerosol (°F)	Heat Exchanger Inlet for Air or Aerosol Air (°F)	Heat Exchanger Inlet for Air or Aerosol Aerosol (°F)	Enthalpy Changes Resulting From Aerosol Formation Aerosol Air ($\frac{Btu}{min}$)	Enthalpy Changes Resulting From Aerosol Formation Aerosol Particles ($\frac{Btu}{min}$)	Total ($\frac{Btu}{min}$)
0.320	84.7	230.0	218.3	-0.65	6.50	5.85
0.320	85.0	232.3	221.1	-0.62	6.62	6.00
0.320	85.4	232.9	222.4	-0.58	6.66	6.08
0.320	85.0	232.7	221.5	-0.62	6.64	6.02
0.320	85.0	232.7	222.3	-0.57	6.68	6.11
0.320	85.1	232.1	222.0	-0.56	6.67	6.11
0.320	85.8	234.5	222.3	-0.68	6.64	5.96
0.320	85.2	235.4	224.7	-0.59	6.78	6.19

[a] Experiment Conditions: Heat exchanger coolant, air 6.82 CFM at 70°F, 1 atm; air flow rate for aerosol, 3.04 CFM at 70°F, 1 atm; furnace temperature, 2280°F.

[b] Energy balance between furnace inlet and heat exchanger inlet.

Table 11a.   Experimental and Calculated Data for 30-44μ Cupric Oxide[a,b]

Powder Feed Rate ($\frac{lb}{min}$)	Stream Temperature at:			Heat Exchanger Coolant Temperature Rise and Change in Rise When Aerosol Formed		Enthalpy Changes Resulting From Aerosol Formation			
	Deagglomerator Exit for Air or Aerosol ($^{\circ}$F)	Heat Exchanger Exit for Air or Aerosol					Aerosol		
		Air ($^{\circ}$F)	Aerosol ($^{\circ}$F)	Δt_c ($^{\circ}$F)	$\Delta(\Delta t_c)$ ($^{\circ}$F)	Air ($\frac{Btu}{min}$)	Particles ($\frac{Btu}{min}$)	Coolant ($\frac{Btu}{min}$)	Total ($\frac{Btu}{min}$)
0.181	80.8	143.8	160.1	36.4	-1.3	0.89	2.17	-0.15	2.91
0.181	80.9	143.8	160.1	37.0	-2.3	0.89	2.17	-0.28	2.78
0.181	81.0	143.0	159.3	36.4	-1.6	0.89	2.14	-0.19	2.84
0.181	81.0	143.0	160.5	36.5	-1.6	0.96	2.17	-0.19	2.94
0.181	81.1	143.8	160.5	36.6	-1.7	0.91	2.17	-0.21	2.87
0.181	81.7	144.6	160.5	36.7	-1.6	0.87	2.16	-0.19	2.84
0.181	81.8	145.0	160.9	36.5	-1.3	0.87	2.17	-0.15	2.89
0.181	81.9	145.4	161.3	36.9	-1.7	0.87	2.17	-0.22	2.82
0.181	81.7	145.4	161.3	36.9	-1.6	0.87	2.18	-0.19	2.86
0.181	81.9	146.2	161.7	37.1	-1.7	0.84	2.18	-0.21	2.81
0.181	81.9	145.4	161.7	37.1	-1.8	0.89	2.18	-0.21	2.86
0.181	81.9	145.0	161.7	37.0	-1.5	0.91	2.18	-0.18	2.91
0.103	81.9	145.8	156.8	37.2	-0.5	0.60	1.17	-0.07	1.70
0.103	81.9	143.8	156.0	37.0	-0.5	0.67	1.15	-0.06	1.76
0.103	81.9	145.4	156.8	36.9	-0.4	0.62	1.17	-0.05	1.74
0.103	82.8	146.2	157.6	36.6	-0.4	0.62	1.17	-0.05	1.74
0.103	82.8	147.5	157.6	37.3	-1.1	0.56	1.17	-0.14	1.59

(continued)

Table 11a. Experimental and Calculated Data for 30-44μ Cupric Oxide[a,b]
(continued)

Powder Feed Rate $(\frac{lb}{min})$	Stream Temperature at:			Heat Exchanger Coolant Temperature Rise and Change in Rise When Aerosol Formed		Enthalpy Changes Resulting From Aerosol Formation			
	Deagglomerator Exit for Air or Aerosol (°F)	Heat Exchanger Exit for Air or Aerosol					Aerosol		
		Air (°F)	Aerosol (°F)	Δt_c (°F)	$\Delta(\Delta t_c)$ (°F)	Air $(\frac{Btu}{min})$	Particles $(\frac{Btu}{min})$	Coolant $(\frac{Btu}{min})$	Total $(\frac{Btu}{min})$
0.103	82.9	147.5	158.0	36.8	-0.3	0.58	1.17	-0.04	1.71
0.103	83.0	147.5	158.0	37.1	-0.6	0.58	1.17	-0.07	1.68
0.103	83.4	145.8	158.4	36.8	-0.3	0.69	1.17	-0.04	1.82
0.103	83.6	147.1	159.3	37.1	-0.6	0.67	1.18	-0.08	1.77
0.103	83.6	147.5	159.3	36.8	0.0	0.64	1.18	-0.01	1.81
0.103	83.7	146.2	158.4	36.9	-0.5	0.67	1.17	-0.06	1.78
0.103	83.6	146.2	158.4	36.9	-0.4	0.67	1.17	-0.05	1.79
0.070	83.6	146.2	156.4	37.1	-0.1	0.56	0.77	0.01	1.32
0.070	83.9	146.6	156.0	36.8	0.0	0.51	0.76	-0.01	1.26
0.070	84.2	146.6	156.0	36.8	-0.1	0.51	0.76	-0.01	1.26
0.070	84.5	147.1	156.0	37.3	-0.1	0.49	0.76	-0.01	1.24
0.070	84.2	147.9	157.2	37.2	0.0	0.51	0.77	0.00	1.28
0.070	84.2	148.3	156.8	37.3	-0.1	0.47	0.77	-0.01	1.23
0.320	84.5	147.5	179.3	37.0	-2.1	1.74	4.60	-0.26	6.08

(continued)

Table 11a. Experimental and Calculated Data for 30-44μ Cupric Oxide[a,b]
(continued)

Powder Feed Rate $(\frac{lb}{min})$	Stream Temperature at:			Heat Exchanger Coolant Temperature Rise and Change in Rise When Aerosol Formed		Enthalpy Changes Resulting From Aerosol Formation			
	Deagglomerator Exit for Air or Aerosol (°F)	Heat Exchanger Exit for Air or Aerosol					Aerosol		
		Air (°F)	Aerosol (°F)	Δt_c (°F)	$\Delta(\Delta t_c)$ (°F)	Air $(\frac{Btu}{min})$	Particles $(\frac{Btu}{min})$	Coolant $(\frac{Btu}{min})$	Total $(\frac{Btu}{min})$
0.320	84.9	147.1	178.9	36.4	-1.5	1.74	4.55	-0.17	6.12
0.320	85.0	147.1	179.3	36.7	-2.1	1.76	4.57	-0.26	6.07
0.320	84.7	147.1	178.9	36.4	-1.9	1.74	4.56	-0.23	6.07
0.320	85.0	149.5	181.3	36.6	-1.3	1.74	4.67	-0.16	6.25
0.320	85.4	148.7	181.7	37.9	-2.5	1.80	4.67	-0.30	6.17
0.320	85.0	149.5	181.3	37.2	-1.9	1.74	4.67	-0.24	6.17
0.320	85.0	149.9	182.1	37.6	-2.3	1.76	4.71	-0.28	6.19
0.320	85.1	147.9	186.4	37.4	-2.1	2.11	4.92	-0.25	6.78
0.320	85.8	149.5	182.1	37.6	-2.5	1.78	4.67	-0.31	6.14
0.320	85.2	149.9	183.6	37.9	-2.2	1.84	4.77	-0.26	6.35

[a] Experiment Conditions: Heat exchanger coolant, air 6.82 CFM at 70°F, 1 atm; air flow rate for aerosol, 3.04 CFM at 70°F, 1 atm; furnace temperature, 2280°F.

[b] Energy balance between furnace inlet and heat exchanger exit.

Table 12a. Experimental and Calculated Data for 20-30μ Cupric Oxide[a,b]

Powder Feed Rate ($\frac{lb}{min}$)	Deagglomerator Exit for Air or Aerosol (°F)	Heat Exchanger Exit for Air or Aerosol Air (°F)	Aerosol (°F)	Heat Exchanger Coolant Temperature Rise and Change in Rise When Aerosol Formed Δt_c (°F)	$\Delta(\Delta t_c)$ (°F)	Enthalpy Changes Resulting From Aerosol Formation Aerosol Air ($\frac{Btu}{min}$)	Particles ($\frac{Btu}{min}$)	Coolant ($\frac{Btu}{min}$)	Total ($\frac{Btu}{min}$)
0.092	88.1	150.7	165.7	36.2	-0.9	0.74	1.08	-0.11	1.72
0.092	88.1	149.1	164.9	36.3	-0.8	0.78	1.07	-0.09	1.76
0.092	88.1	151.1	165.7	36.3	-0.7	0.72	1.08	-0.08	1.72
0.092	88.1	152.0	166.5	36.3	-0.7	0.72	1.09	-0.08	1.73
0.092	88.1	152.0	166.9	36.0	-0.6	0.74	1.10	-0.07	1.77
0.092	88.1	152.4	166.9	36.4	-0.7	0.72	1.10	-0.08	1.74
0.092	88.1	151.1	166.7	36.2	-0.9	0.77	1.10	-0.11	1.76
0.153	88.1	151.3	194.6	35.7	-3.3	2.15	2.48	-0.41	4.22
0.153	88.1	152.0	192.7	36.0	-2.3	2.02	2.43	-0.29	4.17
0.153	88.1	153.2	193.9	36.3	-3.1	2.02	2.46	-0.39	4.09
0.153	88.1	154.4	191.5	36.8	-2.8	1.84	2.40	-0.35	3.90
0.153	88.1	153.6	192.3	36.8	-3.0	1.92	2.42	-0.37	3.99
0.153	88.9	152.8	192.7	36.4	-3.1	1.98	2.44	-0.38	4.04
0.243	88.9	154.4	191.5	36.8	-2.7	2.52	4.32	-0.34	6.50
0.243	89.5	153.8	202.1	36.6	-2.3	2.47	4.14	-0.28	6.34
0.243	89.3	154.0	201.3	36.6	-2.3	2.42	4.12	-0.27	6.27
0.243	89.3	154.0	201.3	37.2	-1.6	2.42	4.12	-0.19	6.35
0.243	89.3	154.4	202.9	37.6	-2.5	2.44	4.15	-0.30	6.29

Table 12a. Experimental and Calculated Data for 20-30μ Cupric Oxide[a,b]
(continued)

Powder Feed Rate $(\frac{lb}{min})$	Deagglomerator Exit for Air or Aerosol (°F)	Stream Temperature at: Heat Exchanger Exit for Air or Aerosol		Heat Exchanger Coolant Temperature Rise and Change in Rise When Aerosol Formed		Enthalpy Changes Resulting From Aerosol Formation			
		Air (°F)	Aerosol (°F)	Δt_c (°F)	$\Delta(\Delta t_c)$ (°F)	Aerosol Air $(\frac{Btu}{min})$	Particles $(\frac{Btu}{min})$	Coolant $(\frac{Btu}{min})$	Total $(\frac{Btu}{min})$
0.243	89.3	154.0	201.7	37.2	-2.0	2.44	4.13	-0.27	6.31
0.243	89.3	153.6	201.3	37.1	-2.6	2.44	4.12	-0.31	6.25
0.153	89.3	152.0	189.6	36.2	-2.6	1.92	2.33	-0.30	3.95
0.153	89.3	152.0	190.0	36.2	-3.0	1.94	2.34	-0.35	3.93
0.153	89.3	153.6	193.1	36.4	-3.0	2.02	2.41	-0.36	4.07
0.092	89.3	158.6	168.3	37.9	-1.0	0.75	1.10	-0.12	1.72
0.092	89.3	154.4	168.1	38.0	-0.8	0.70	1.10	-0.10	1.70
0.092	89.3	154.0	168.5	37.9	-0.5	0.74	1.10	-0.06	1.78

[a] Experiment Conditions: Heat exhchanger coolant, air 6.83 CFM at 70°F, 1 atm; air flow rate for aerosol 2.80 CFM at 70°F, 1 atm; furnace temperature, 2280°F.

[b] Energy balance between inlet and heat exchanger exit.

REFERENCES

1. Hottel, H. C., Cohen, E. S., "Radiant Heat Exchange in a Gas-filled Enclosure: Allowance for Non-uniformity of Gas Temperature," American Institute of Chemical Engineers Journal, 4, No. 1, 3-14 (1958).

2. Haslam, R. T., Hottel, H. C., "Combustion and Heat Transfer," Transactions of the American Society of Mechanical Engineers, FSP-50.-3, 9-19 (1928).

3. Hottel, H. C., "The Melchett Lecture for 1960: Radiative Heat Transfer in Combination Chambers," Journal of the Institute of Fuel, 34, 220-34 (1961).

4. Wohlenberg, W. J., Morrow, D. G., "Radiation in the Pulverized Fuel Furnace," Transactions of the American Society of Mechanical Engineers, 47, 127-76 (1925).

5. Haslam, op. cit.

6. McAdams, W. A., Heat Transfer, 3rd Edition, McGraw-Hill Book Co., Inc., New York, pp. 99-105 (1954).

7. Johnstone, H. F., Pigford, R. L., Chapin, J. H., "Heat Transfer to Clouds of Falling Particles," Transactions of the American Institute of Chemical Engineers, 37, 95-133 (1941).

8. Ibid.

9. Oktay, C. M., "The Effect of Particle Size, Concentration, and Temperature on Heat Transfer to Clouds of Small Particles," University of Florida, Ph.D. Thesis, 1955.

10. Schulderberg, D. C., Whitelaw, R. L., Carlson, R. W., "Gaseous Suspension - A New Reactor Coolant," Nucleonics, 19, 67, 68, 70, 72, 74, and 76 (1961).

11. Hoffman, T. W., Gauvin, W. H., "An Analysis of Spray Evaporation in a High Temperature Environment, I. Radiant Heat Transfer to Clouds of Droplets and Particles," Canadian Journal of Chemical Engineering, 39, 179-88 (1961).

12. Hottel, Cohen, op. cit.

13. Haslam, op. cit.

14. Einstein, T. H., "Radiant Heat Transfer to Absorbing Gases Enclosed in a Circular Pipe with Conduction, Gas Flow and Internal Heat Generation," NASA TR R-156, National Aeronautics and Space Administration, Washington, D. C., 1963.

15. Lanzo, C. D., Ragsdale, R. G.,"Heat Transfer to a Seeded Flowing Gas From an Arc Enclosed by a Quartz Tube," NASA TMX-52005, National Aeronautics and Space Administration, Washington, D. C., 1963.

16. McAdams, op. cit., pp. 63, 103.

17. Stull, V. R., Plass, G. N., "Emissivity of Dispersed Carbon Particles," _Journal of the Optical Society of America_, 50, 121-129 (1960).

18. Van de Hulst, H. C., _Light Scattering by Small Particles_, 1st Edition, John Wiley and Sons, Inc., New York, pp. 114-30, 1957.

19. Thring, M. W., Foster, P. J., McGrath, I. A., Ashton, J. S., "Prediction of the Emissivity of Hydrocarbon Flames," _International Heat Transfer Conference_, Boulder Colorado, American Society of Mechanical Engineers, New York, pp. 796-802 (1961).

20. Eckert, E. R. G., "Messung der Durchlassigkut electrischer Nichtleiter fur Warmestrahlunz," _Forshung auf dem Gebiete des Ingenieurevesens_, 7, 265-70 (1936).

21. _International Critical Tables of Numerical Data, Physics, Chemistry, and Technology_, Volume V., National Research Council, E. W. Washburn Editor, McGraw Hill Book Co., Inc. New York, pp. 268-70, 1929.

22. Thomas, P. H., "Absorption and Scattering of Radiation by Water Sprays of Large Drops," _British Journal of Applied Physics_, 3, 385-93 (1952)

23. Friedman, H. M., Churchill, S. M., "The Absorption of Thermal Radiation by Fuel Droplets," Preprint Sixth National Heat Transfer Conference, American Institute of Chemical Engineers, August, 1963.

24. Van de Hulst, op. cit.

25. Sleicher, C. A., Churchill, S. W., "Radiant Heating of Dispersed Particles," _Industrial and Engineering Chemistry_, 48, 1819-24 (1956).

26. Bird, R. B., Stewart, W. E., Lightfoot, E. N., _Transport Phenomena_, John Wiley and Sons, Inc., New York, pp. 407-10 (1960).

27. Carlson, D. J., "Static Temperature Measurements in Hot Gas-Particle Flows," _American Rocket Society Journal_, 1107-9 (1962).

28. Bird, op. cit.

29. *Temperature - Its Measurement and Control in Science and Industry*, Volume 1, American Institute of Physics, Reinhold Publishing Corporation, New York, pp. 813-18, 1941.

30. Van de Hulst, op. cit., pp. 110-11.

31. Hottel, op. cit.

32. *Handbook of Chemistry and Physics*, Hodgman, C. D., ed. in Chief, 42ed, The Chemical Rubber Publishing Co., Cleveland, Ohio, pp. 276-68 (1960).

33. Milne, W. E., *Numerical Calculus*, Princeton, New Jersey, Princeton University Press, pp. 122-25 (1949).

34. Ibid.

35. Johnstone, op. cit.

36. Hoffman, op. cit.

37. Themelis, N. J., Gauvin, W. N., "Heat Transfer to Clouds of Particles," Pulp and Paper Research Institute of Canada, Montreal, Canada, 1962.

38. Catalog Q7A, General Electric Corporation, Willoughby Quartz Plant, Willoughby, Ohio.

39. Edwards, O., Lewis Research Center, personal communication.

40. Orr, C., Dalla Valle, J. M., *Fine Particle Measurement Size, Surface, and Pore Volume*, The Macmillan Co., New York, pp. 172-86 (1960).

41. Ibid, pp. 257-76.

42. *Catalysis*, Volume II, Emmett, P. H., editor, Reinhold Publishing Company, New York, pp. 109-33 (1955).

43. Orr, C., Op. Cit, p. 191.

44. Herdan, G., *Small Particle Statistics*, Elsevier Publishing Co., New York, p. 115, 1953.

45. Tien, C. L., "Heat Transfer by a Turbulently Flowing Fluid-Solids Mixture in a Pipe," *Journal of Heat Transfer, Transactions of the American Society of Mechanical Engineers*, 83, 183-88 (1961).

46. *Chemical Engineers' Handbook*, 3rd Edition, Perry, J. H., editor, McGraw-Hill Book Co., Inc., New York, p. 485, 1950.

47. Ibid.

48. Tien, op. cit.

49. Farber, L., Morley, M. J., "Heat Transfer to Flowing Gas-Solids Mixtures in a Circular Tube," Industrial and Engineering Chemistry, 49, 1143-50 (1957).

50. Iinoya, K., Kyoto University, Kyoto, Japan, personal communication.

51. Eckert, E. R. G., Drake, R. M., Heat and Mass Transfer, McGraw-Hill Book Co., Inc., New York, p. 380 (1959).

52. Chemical Engineers' Handbook, op. cit.